ENVIRONMENTALLY FRIENDLY RHODIUM(I) MODEL CATALYSTS

by

ZANELE GIFT MORERWA

ENVIRONMENTALLY FRIENDLY RHODIUM(I) MODEL CATALYSTS

by

ZANELE GIFT MORERWA

A dissertation submitted to meet the requirements for the degree of

MAGISTER SCIENTIAE

in the

DEPARTMENT OF CHEMISTRY
FACULTY OF NATURAL AND AGRICULTURAL SCIENCES

at the

UNIVERSITY OF THE FREE STATE

Supervisor: PROF. ANDREAS ROODT
Co-Supervisor: DR. GERTRUIDA JACOBA SUSANNA VENTER

February 2019

Jeremiah 29:11(NIV) “For I know the plans I have for you,” declares the Lord, “plans to prosper you and not to harm you, plans to give you hope and a future”

Acknowledgement

First of all, Lord Jesus thank you. Your grace and mercy truly have no bounds. The glory all belongs to you.

Prof. Roodt, I want to thank you for all the opportunities you have given me, along with the guidance, patience and humility you have shown me. It is a privilege to be known as your student. I pray the Lord continues blessing you because you are a blessing.

Thank you, Dr Truidie Venter, for all your hard work and thank you to all my colleagues in the Inorganic group for all your help.

To my mom (Dolly Mable Morerwa), I love you so much, I would not be here today if it were not for you. I thank you for your sacrifices, and for always pushing for me to have the best. I thank you for the prayers mom. Waking up in the middle of the night to find you kneeling at my bed, praying for me is something I have never taken for granted. You have never sought praise for anything you did for me and my siblings, even when we disappointed you, you always saw the good in us. Seeing you smile and knowing that you are proud of me is the only thing that makes this worth it.

To my siblings (Mark, Nomi, Lebo, Smangaliso, and Zandile), my nieces and nephews thank you for all the scarifies, laughter and prayers.

The financial assistance from the University of the Free State and the South African National Research Foundation (NRF) towards this research is hereby gratefully acknowledged. Opinions expressed and conclusions arrived at, are those of the author and are not attributed to the NRF.

Table of Contents

Abbreviations and Symbols

A_{obs}	Observed absorbance
ATR	Attenuated total reflectance
Å	Angstrom
Arom	Aromatic
C_6D_6	Deuterated benzene
$CDCl_3$	Deuterated chloroform
CD_2Cl_2	Deuterated dichloromethane
°	Degrees
°C	Degrees Celsius
d	Doublet in NMR spectra
d(…)	Distance
δ	Chemical shift
DMF	Dimethylformamide
Fig.	Figure
FID	Free induction decay
FT-NMR	Fourier transform nuclear magnetic resonance
g	Gram
Hz	Hertz
IR	Infra-red
J	Coupling constant
K	Kelvin
k_{obs}	Observed rate constant
k_1	the rate constant for the forward reaction
k_{-1}	the rate constant for the reverse reaction
L	Ligand
L,L'-Bid	Bidentate ligand
M	$mol.dm^{-3}$
m	Multiplet in NMR spectra
mg	Milligram
mmol	Millimol
nm	Nanometre

NMR	Nuclear Magnetic Resonance Spectroscopy
N,O-bid	Derivatives of 4-(phenylamino)pent-3-en-2-one
Par.	Paragraph
PGM	Platinum group metals
PhonyH	4-(phenylamino)pent-3-en-2-one
ppm	(Unit of chemical shift) parts per million
PR_3	Tertiary substituted phosphine
RMS	Quadratic mean(root-mean-square)
s	Singlet in NMR spectra
$t_{1/2}$	Half-life
TOF	Turn over frequency
TON	Turn over number
ν_{CO}	C=O IR stretching frequency
λ	UV/Vis wavelength
θ	Angle
Θ_E	Effective cone angle
UV/Vis	Ultraviolet/visible
Z	Number of molecules in unit cell

ABSTRACT

The aim of this study was to investigate model rhodium(I) complexes as environmentally friendly water-soluble homogeneous catalysts for processes such as the carbonylation of methanol, a process that is important in industry due to its role in i.e. the production of liquid fuels and bulk chemicals. The flexibility of manipulating tertiary phosphines in terms of bulkiness and Lewis basicity are factors which render them attractive candidates in the modification of square-planar complexes towards applied chemical processes. If the latter are utilized in homogeneous catalytic applications, different fundamental and bench-marking reactions are of importance such as substitution reactions and oxidative addition.

A range of 4-(phenylamino)pent-3-en-2-onate (PhonyH) derivatives with various electron withdrawing and donating substituents on the *para* position on the N-phenyl ring were synthesized and characterised with infrared and NMR spectroscopy. The uncoordinated compounds were then used to synthesis a range of dicarbonyl-[4-(phenylamino)pent-3-en-2-onato]-rhodium(I) complexes. Following the synthesis of the dicarbonyl-rhodium(I) complexes, tertiary phosphines, PR_3 (PR_3 = triphenylphosphine (PPh_3) and 1,3,5-triaza-7-phosphaadamantane (PTA)) were employed to substitute a CO from the parent complexes, forming carbonyl-[4-(phenylamino)pent-3-en-2-onato]-PR_3-rhodium(I) [Rh(N,O-bid)(CO)-(PR_3)] complexes. Single crystal X-ray crystallographic determinations of the [Rh(4-CH_3-Phony)(CO)(PPh_3)] and [Rh(4-F-Phony)(CO)(PPh_3)] complexes were successfully completed and compared with literature. [Rh(4-CH_3-Phony)(CO)(PPh_3)] crystalized in the triclinic ($P\bar{1}$) crystal system, whilst [Rh(4-F-Phony)(CO)(PPh_3)] crystalized in the monoclinic space group ($P2_1/c$).

A preliminary kinetic study of the CO substitution reaction and equilibrium studies were undertaken to evaluate how changes at the rhodium(I) centre could affect the reactivity of the rhodium(I) complex. Similarly, a preliminary kinetic study of the iodomethane oxidative addition to [Rh(4-CH_3-Phony)(CO)(PPh_3)] and [Rh(4-CH_3-Phony)(CO)(PTA)] was undertaken to evaluate the reactivities of these Rh(I) model complexes.

Through the substitution kinetic studies it was discovered that a large equilibrium constant (K_1) was present favouring the formation of the [Rh(4-CH_3-Phony)(CO)(PTA)] as product, but

further investigation was identified to clarify some uncertainties due to the presence of other preliminarily identified but unknown species also present.

The preliminary kinetic study of the iodomethane oxidative addition showed that the Rh(III) alkyl species which forms from the first product from the [Rh(4-CH_3-Phony)(CO)(PTA)] species exhibits a larger equilibrium constant value (K_1) than that obtained for the corresponding–[Rh(4-CH_3-Phony)(CO)(PPh_3)], although not that significant. Nevertheless, similar experiments when evaluating the [Rh(4-CH_3-Phony)(CO)(PTA)] as reactant confirmed its reactivity similar to the PPh_3 analog and hence the potential application for the design of future water-soluble catalyst models.

Keywords; catalysis, green chemistry, rhodium(I), homogeneous catalysts, XRD, substitution kinetics, oxidative addition.

1 INTRODUCTION & AIM OF STUDY

1.1 INTRODUCTION

The development of science is an important concept that cannot be overlooked or replaced. With every development, however, there are drawbacks. The aspiration of "green chemistry" is to sustain development while manufacturers meet the needs of the present without compromising future generations' ability to meet their own needs, whilst preserving the environment. Other factors such as the increasing cost of waste disposal, recycling, energy requirement and investment costs also contribute to industrial process developments and research. The concept of green chemistry aims to reduce waste, yield safer products, reduce the consumption of energy and resources, and avoid the use of toxic and/or hazardous reagents and solvents in the manufacturing and application of chemical products. The benefits of green chemistry include improving human health, the environment, and the economy and businesses as discussed in Par. 2.2.1.

The need for more environmentally friendly processes within the chemical industry has thus become essential. With catalysis being one of the fundamental pillars of green chemistry, the environment is protected by reducing the energy requirement, providing a new reaction pathway that has a lower barrier of activation, and decreasing the quantity of the reagents required due to the enhancement of selectivity and reduction of waste. Catalysis is relevant in multiple industrial processes i.e. the production of liquid fuels and bulk chemicals.[1] In this regard, the carbonylation of methanol is a process that highlights the importance of homogeneous catalysis.[2] Through coordination chemistry metal centres can be manipulated by modified ligands in order to synthesize tailor-made complexes that can be used to form desired products.[3] The substitution of cobalt as the primary metal catalyst[4] $[HCo(CO)_4]$ (BASF process) with rhodium $[RhI_2(CO)_2]^-$ (Monsanto process) and then further development to the

[1] J.J. Bravo-Suarez, R.V. Chaudhari, B. Subramaniam, *ACS Symp. Ser.*, **2013**, 1132, 3.
[2] Q. Qian, J. Zhang, M. Cui, B. Han, *Nat. Commun.*, **2016**, 11481, 1.
[3] B. Cornils, W.A. Herrmann, *Applied Homogeneous Catalysis with Organometallic Compounds*, VCH Publishers, New York, **1996**.
[4] D. Forster, M. Singleton, *J. Mol. Cat.*, **1982**, 17, 299.

iridium complex $[IrI_2(CO)_2]^-$ (Cativa process) resulted in milder reaction conditions that formed the desired product at a better yield.[5,6,7] Although the benefits of catalysts are vast, i.e. they have had a large role in pollution control (reduction of automotive emission and reduction of hydrocarbon emissions from vent streams in chemical operations), they too pose an environmental problem in the form of waste disposal if not managed properly.

The synthesis of a good (most often organometallic) catalyst is defined by the ease of catalyst modification by altering or changing the reaction conditions. The rate of the reaction and selectivity towards certain products are directly associated with the characteristics of the ligands attached to the metal centre.

Rhodium exhibits remarkable catalyst activity and selectivity in many chemical transformations in comparison to other metals,[8] giving a reason for its outstanding application in the hydrogenation of olefins and arenes, hydroformylation of olefins, olefin diene co-dimerization, and carbonylation of methanol to acetic acid.[9,10] Although there are various heterogeneous catalysed processes, homogeneous catalysis has more advantages and has gained more interest in the industry. However, the separation and recycling of the product from the homogeneous catalyst is a large contributing drawback,[11] which might be counteracted by less-polluting solvent systems such as water.

Thus, the synthesis of e.g. water-soluble homogeneous catalysts is an important avenue to pursue greener chemistry. A water-soluble catalyst is often based on two-phase catalysis (biphasic). A disadvantage of this two-phase catalyst is that the reaction rate may be low due to the low solubility of the substrate in water and/or phase transfer limitations.[12,13,14] Biphasic (aqueous/organic) catalysts however potentially simplify the separation of the catalyst from the product and aids in the recycling of the catalyst. The replacement of organic solvents which are toxic, volatile, and expensive is a contributing factor to the formation of a green catalyst.

---

[5] P.M. Maitlis, A. Haynes, G.J. Sunley, M.J. Howard, *J. Chem. Soc., Dalton Trans.*, **1996**, 2187.
[6] F.E. Paulik, J.F. Roth, *J. Chem. Soc., Chem. Commun.*, **1968**, 1578.
[7] G.J. Sunley, D.J. Watson, *Cat. Tod.*, **2000**, 58, 293.
[8] Y. Yuan, N. Yan, P.J. Dyson, *ACS Cat. Tod.*, **2003**, 77, 419.
[9] J. Halpern, *Chem. Eng. News*, **2003**, 81, 114.
[10] J.D. Lee, *Concise Inorganic Chemistry 4th Ed.*, Chapman & Hall, United Kingdom, London, **1991**.
[11] O. Deutchmann, H. Knozinger, K. Kochloefl, T. Turek, *Heterogeneous Catalysis and Solid Catalysts*, Wiley-VCH Verlag GmbH & Co. KGaA, **2009**.
[12] D.C. Bailey, S.H. Langer, *Chem. Rev.*, **1981**, 81, 109.
[13] F. Ciardelli, G. Braca, C. Carlini, G. Sbrana, G.J. Valentini, *Mol. Cat.*, **1982**, 14, 1.
[14] F.R. Hartley, P.N. Vezey, *Adv. Organ. Chem.*, **1977**, 14, 1.

Water as a solvent serves to the advantage of the environment, safety, and more economical reactions,[15] and may be even an example of combining homogeneous and heterogeneous systems. Reactions performed in a biphasic system result in the aqueous phase containing the water-soluble catalyst and the organic phase containing the dissolved product. This allows for potentially improved recycling and recovery of the catalyst through simple phase separation.[5]

With water being abundantly available, cheap, non-volatile, less harsh, and environmentally friendly,[5] benefits of using it as a solvent include improving reactivity and selectivity, simplifying the workup procedure, enabling the recycling of the catalyst, and allowing mild reaction conditions.[16,17,18] Due to the polar character of water new reactivity and selectivity may be expected for organometallic catalysis therein also provides an opportunity to overcome some shortcomings of a homogeneous catalyst, mainly recycling and recovery.

Platinum group elements (Ru, Ir, Pd, Pt, and Rh) are rare and expensive, hence recovery in industrial processes is extremely important. Rhodium complexes are the most prevalent industrial homogeneous catalysts for organic raw material processing, for example, the Monsanto process. Rhodium is a rose coloured precious metal that was discovered around 1804 by English chemist and physicist, William Hyde Wallaston who isolated the metal from crude platinum. The symbol of rhodium is a rose that is associated with the saying 'data rosa mel apibus' that means "the rose gives the bees honey".[19] Commercially rhodium is mostly obtained as a by-product of the extraction of nickel and copper from their ores. The element is the only transitional metal in group 9 that has one electron in its outer shell. Although rhodium is relatively inactive, two special properties include high electrical and heat conductivity. According to Cotton and Wilkinson *et.al.*[20] the main oxidation states of rhodium are I, III and IV, with the oxidation state III the most stable.

---

[15] H. Chen, Y. Li, J. Chen, P. Chen, Y. He, X. Li, *J. Mol. Cat. A: Chem.*, **1999**, 149, 1.
[16] R. Breslow, U. Maitra, *Tetra. Lett.*, **1984**, 25, 1239.
[17] W.A. Herrmann, *Aqueous Phase Organometallic Catalysis-Concept and* Application, Wiley-VCH, Weinheim, **1998**.
[18] J.J. Gajewski, *Acc. Chem. Res.*, **1997**, 30, 219.
[19] J. Emsley, *Nature's Building Blocks: An A-Z Guide to the Elements, 2nd Ed.*, Oxford University Press, New York, **2011**.
[20] F.A. Cotton, G. Wilkinson, P.L. Gaus, *Basic Inorganic Chemistry, 3rd Ed.*, John Wiley & Sons, Inc., New York, **1995**.

The selective hydrogenation of alkynes and alkenes occur through the usage of the so-called Wilkinson's catalyst[21] $[Rh(Cl)(PPh_3)_3]$, whereas $[RhH(PPh_3)_3(CO)]$ on the other hand is an effective hydroformylation catalyst.[22] These serve as examples of catalysts that requires both rhodium and phosphorous ligands in a catalytic system.

The concept of designing a water-soluble catalytically active species revolves around the design of a ligand that contains hydrophilic properties that allow it to separate into the aqueous phase whilst contributing the necessary steric and electronic properties to acquire the desired catalyst stability, activity, and selectivity. Ionic substituents, i.e. sulfonates, carboxylate, phosphonates, and ammonium, are commonly used to modify hydrophobic ligands into hydrophilic ligands.[23]

1.2 THE AIM OF THIS STUDY

The mentioned factors regarding the increasing cost of PGM and the effect of the industrial chemistry on the environment constantly inspires the search for new catalysts, in particular the synthesis of (more) environmentally friendly rhodium(I) entities. Par. 1.1 provided some background on different facets of homogeneous catalysis.

The importance of not only phosphorus donor ligands in homogeneous catalysis, although very important, can in principle be augmented with other donor atom ligand systems. One such an avenue to pursue is to combine the P-donor ligands with other ligand architectures, which is specifically the overarching aim of this MSc study.

Typically, although many O,O-donor ligand systems are known, N,O-bidentate ligand architectures in the form of enaminoketones are considered convenient and indeed forms the focus of this MSc investigation.

By using various ligands, the difference in electronegativity will result in changes in the geometric parameters of the molecule which in turn influences the reactivity of the molecule.

[21] J.F. Young, J.A. Osborn, F.H. Jardine, G. Wilkinson, *Chem. Comm.*, **1965**, 131.
[22] F.H. Jardine, J.A. Osborn, G. Wilkinson, J.F. Young, *Chem. Ind. (London)*, **1965**, 560; *J. Chem. Soc. (A)*, **1966**, 1711.
[23] K.H. Shaughnessy, *Chem. Rev.*, **2009**, 109, 2.

This feature will be utilized in the aim of synthesising an environmentally friendly water-soluble homogeneous rhodium(I) catalyst.

The various coordinating ligands were systematically chosen based on their electron withdrawing and donating properties but as mentioned above, focusing specifically on the N,O-enaminoketonato as bidentate ligand architecture. Since the chosen system displays a prominent phenyl ring substituent directly linked to the coordinating N-donor atom, the question as to how a subtle change on the R group on the *para* position of the bidentate N-phenyl will affect the complex's behaviour. Electronic or steric effects are induced at the Rh(I) centre through 6-membered coordination of the N,O-bidentate ligand. This was done to better understand the influence of using different substituents on the *para*-position in the Rh(I) complex.

Fig 1.1 illustrates the general complexes synthesized in this study, with R representing the electron withdrawing/donating group.

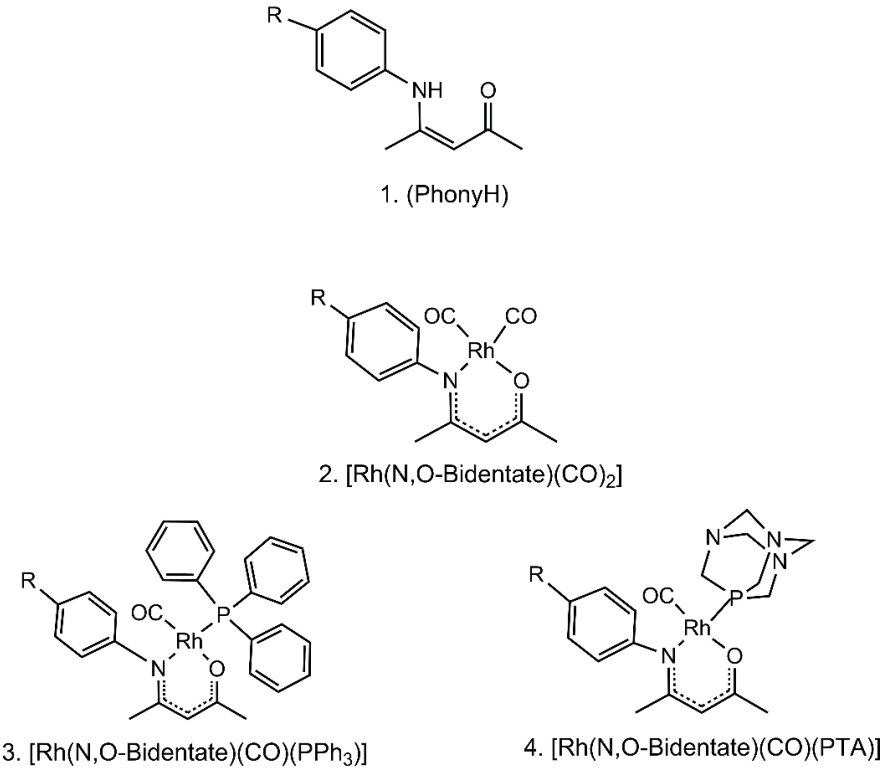

Figure 1.1: The various ligand and complexes studied.

With the above mentioned in mind, the following step-wise aims of this study are summarized as follows:

a) Literature evaluation of aspects of importance in ligand design and ligand synthesis and the selection of appropriate ligand architectures based on enaminoketones.

b) The synthesis and investigation of various enaminoketones as ligand systems containing different substituents on the periphery of the catalyst, in particular the *para* position of the phenyl moiety in rhodium complexes of the type [Rh(N,O-bid)$(CO)_2$], where N,O-bid$^-$ = derivatives of 4-(phenylamino)pent-3-en-2-onate.

c) Further functionalization of the metal complexes by introducing selective P-donor ligands, in particular *water-soluble* phosphine ligands such as PTA (1,3,5-triaza-7-phosphaadamantane), and the synthesis of [Rh(N,O-bid)(CO)(PR_3)] with various of these tertiary phosphines (PR_3) ligands.

d) To characterise the said complexes with IR (infrared), ^{1}H, ^{13}C and ^{13}P NMR (nuclear magnetic resonance) and UV/Vis.

e) Evaluation of the solid-state structures of the above-mentioned rhodium(I) complexes using single crystal X-ray diffraction.

f) Preliminary kinetics and equilibrium investigation into carbonyl substitution reaction of [Rh(N,O-bid)$(CO)_2$] with PTA (1,3,5-triaza-7-phosphaadamantane).

g) Preliminary kinetic mechanistic investigation of the oxidative addition of iodomethane to [Rh(N,O-bid)(CO)(PR_3)] complexes.

h) Analysis of results with respect to phosphine reactivity and coordinating ability and comparison to other phosphine systems available in the literature.

2 THEORETICAL & LITERATURE OVERVIEW

2.1 INTRODUCTION

In this chapter, literature regarding green chemistry, catalysis, and basic fundamental coordination chemistry will be discussed. Included is also motivation for the use of a homogeneous rhodium catalysis framework. Emphasis on rhodium features and versatility, along with water-soluble phosphines application in catalysis will be discussed. The investigation of kinetics is a focal point, hence the investigation of both oxidative addition and substitution reactions is included in this study, with general theory relating to reactions of square planar complexes. Background on basic ligand architectures and the influence on Rh(I) complexes described in literature will also be discussed.

2.2 GREEN CHEMISTRY

2.2.1 HISTORY

The development of new technology that is more sustainable and cost-effective and preserves the environment is of great interest in chemical transformation and the re-evaluation of more 'green' methodologies.[24] The protection and improvement of the environment is a concept that dates back as far as the 1960's when the modern day environmental movement began in the United States.[25] Through the publications of Anastas,[26] Clark,[27] Sheldon,[28] Trost,[29] and Warner[25] in the 1990's, the concept of "green chemistry" came into being. The aspiration of

[24] P.T. Anastas, M.M. Kirchhoff, *Acc. Chem. Res.*, **2002**, 35, 686.
[25] P. Krutko, S. Kelley, 'The American Center for Mobility', *American Centre*, **2012**.
[26] P.T. Anastas, J.C. Warner, *Green Chemistry Theory and Practice*, Oxford University Press, Oxford, **1998**.
[27] J.H. Clarke, *Green Chem.*, **1999**, 1, 1.
[28] a) R.A. Sheldon, *Chem. Ind.*, **1992**, 903.
b) R.A. Sheldon, *Green Chem.*, **2007**, 9, 1273.
[29] B. Trost, *Science*, **1991**, 254, 1471.

green chemistry is to sustain development while manufacturers meet the needs of the present without compromising the ability of future generations to meet their own needs. Current emphasis also lies on deviating from waste treatment, cleaning up regulations, and moving towards preventing pollution at its source and using/designing technologies and methodologies that are cleaner and economically competitive.[30] The benefits of green chemistry include reduced impact on human health and the environment, as well as a positive contribution towards the economy and businesses in the following three ways:[31]

(a) Human Health:

1. Cleaner air as there is a decrease in hazardous gases during production.
2. Cleaner water due to a decrease in the release of hazardous chemical waste to water.
3. Fewer personal protective clothing necessary and safer environments for employees in the industry due to the use of less toxic chemicals.
4. Consumers are offered products that are made with less waste and less toxic chemicals.
5. Safer, target specific pesticides that degrade rapidly are used to produce safer food.

(b) Environment:

1. Use of green chemicals counteracts the intentional/unintended release of toxic chemicals to the environment and can be recovered for further use.
2. Plants and animals suffer less.
3. A decreased impact on climate change.
4. Ecosystems are less interrupted by chemicals.
5. A decrease in hazardous landfills.

[30] J.H. Clark, *Part 1: Green Chemistry for Sustainable Development*, Wiley-VCH GmbH & Co, Weinheim, **2005**, 3.
[31] B.A. de Marco, B.S. Rechelo, E.G. Totoli, A.C. Kogwa, H.R.N. Salgado, *Sau. Pharm. J.*, **2019**, 27, 1.

(c) Economy and Business:

1. Less feedstock is consumed to obtain the same amount/higher yield of product.
2. A reduction in the number of synthetic steps results in faster manufacturing of products that increases the plant's capacity to save energy and water.
3. The decrease in waste reduces waste elimination costs.
4. Fewer products are required to achieve the same function, which saves on running costs.
5. Improves competitiveness between manufacturers.
6. Reduction in manufacturing plant size and carbon footprint.
7. Reduces the use of petroleum products, reducing depletion and price fluctuations.

Green chemistry research has been incorporated into a wide variety of areas such as polymers, bio-based/renewable chemicals/products, the design of safer chemicals, solvents and catalysis.[12] Catalysis serves as a fundamental pillar of green chemistry as set out in the principles below.[32] It reduces the energy requirement by providing a new reaction pathway that has a lower barrier of activation, increases selectivity, decreases the use of processing and separation agents, and allows for the use of less toxic material.

2.2.2 WATER AS A SOLVENT

75 % of the earth's surface and 65 % of the human body consists of water. In the production of fine chemicals and in the pharmaceutical industry, solvents contribute largely towards waste.[33,34] A large volume of solvent is used for processing, synthesis and separation. Although solvents are an important component in reactions, they can be toxic or flammable, and contribute significantly to chemical process waste and production cost. Some of the important features of organic solvents include their ability to be easily removed and dissolved in a wide range of compounds, hence the perspective of water as a solvent is an attractive alternative. Water is polar, pervasive, non-volatile, environmentally friendly, cost-effective, and a

[32] P.T. Anastas, M.M. Kirchhoff, T.C. Williamson, *Applied Catalysis A: General*, **2001**, 221, 3.
[33] B.W. Cue, J. Zhang, *Green Chem. Lett. Rev.*, **2009**, 2, 193.
[34] T. Welton, *Proc. R. Soc. A.*, **2015**, 2183, 471.

chemically selective and reactive solvent.[35,36,37] Although there are various benefits to using water as a solvent, there are disadvantages that could affect low solubility of some compounds, as well as moisture sensitive catalysts and reagents which result in deactivation. Utilization of water as a solvent has gathered increasing interest, especially in homogeneous transition metal catalysed processes.[38]

2.3 CATALYSIS

2.3.1 DISCOVERY

The term catalysis was first introduced over 100 years ago by J.J. Berzelius.[39] J. Roebuck used a catalyst in industry for the first time in 1746 in the manufacture of lead chamber sulfuric acid, but only in 1895 did Ostwald formulate the definition of a catalyst to be "a substance that accelerates the rate at which a chemical reaction approaches equilibrium without affecting the position of the equilibrium or permanently becoming involved in the reaction".[40] Catalysts provide new reaction pathways that have lower barriers of activation which may involve intermediates and the mechanism of the reaction.[41] Over 90 %[39] of industrial processes require catalysis which is applied in various fields such as pharmaceuticals, polymers, and petroleum processing.[42] There are two forms of catalysis: homogeneous and heterogeneous catalysis. Today the importance of designing a catalyst lies in optimizing stability and solubility, and increase the ease of separation from the product whilst being cost-effective and environmentally friendly.

The selection of a catalyst is based on several characteristics such as selectivity, amount of waste produced, amount of resources required, robustness of the catalyst, and the rate influence

[35] B. Cornils, E. Wiebus, *Environmental and Safety Aspects in Multiple Homogeneous Catalysis*, Wiley-VCH Verlag, Weinheim, **2005**.
[36] R. Braslow, U. Maitra, *Tetrahedron Lett.*, **1984**, 25, 239.
[37] J.J. Gajewski, *Acc. Chem. Res.*, **1997**, 30, 219.
[38] I.T. Hornvath, F. Joo, *Aqueous Organometallic Chemistry and Catalysis*, Kluwer Dodrecht, **1995**.
[39] J. Wisniak, *Educ. Quim.*, **2010**, 21, 60.
[40] A.J.B. Robertson, *Plat. Met. Rev.*, **1975**, 19, 64.
[41] P.W.N.M. Van Leeuwen, *Homogeneous Catalysis: Understanding the Art*, Springer, Netherlands, **2004**.
[42] M. Doble, A.K. Kruthiventi, *Green Chemistry and Processes*, Elsevier, USA, California, **2007**.

of the catalyst on the desired product.[43] The properties of the (homogeneous) catalyst are determined by both the metal and the ligand coordinated to it. In catalysis, ligands play a key role in the manipulation of the activity and selectivity of the catalyst through ligand optimization strategies. An organometallic catalyst consists typically of a metal centre surrounded by organic or inorganic ligands. Features of a good organometallic catalyst include the relative ease of catalyst modification by altering or changing the environment. This, in turn, influences the rate of the reaction and the selectivity towards certain products. When a catalyst is introduced into a chemical reaction, it binds with reactants in the catalytic cycle to form the product, and then regenerates to its original state. The catalyst does change and depletes during the reaction, hence needs to be renewed and changed over time. The activity of a catalyst is measured by the turnover number (TON) which is the number of times the catalytic agent goes through a cycle before becoming inactive, and turnover frequency (TOF) which is the TON/h.

2.3.2 HOMOGENEOUS VS HETEROGENEOUS

As mentioned already, catalysed reactions can be categorised into heterogeneous or homogeneous catalysis. Heterogeneous catalysis reactions normally involve solid state support with the reactants in the liquid or gas state whilst homogeneous catalysis reactions are those where the catalyst and the substrate are in the same phase, commonly a liquid phase.[44,45] Table 2.1 provides a comparison between homogeneous and heterogeneous catalysis.

[43] G. Rothenberg, *Catalysis: Concept and Green Application*, Wiley-VCH Publisher, Weinheim, **2008**.
[44] G.C. Bond, *Heterogeneous Catalysis*, Oxford, Clarendon Press, **1974**.
[45] T. Richardson, *Principles of Catalyst Development*, Plenum Press, New York, **1989**.

Table 2.1: Important aspects of Homogeneous vs heterogeneous catalysis.[46,47,48]

	Homogeneous	**Heterogeneous**
Understanding the mechanism	Better understanding of the mechanisms	Less understanding of the mechanisms
Selectivity	Yes	No
Reaction conditions	Milder	Harsh/strict
Thermal stability	Low	High
Diffusion limitations	None	Limited
Separations and recycling	Expensive	Easier
Flexibility	More flexibility in variability of steric and electronic properties of a ligand	Less flexibility and predictability
Heat transfer	Efficient heat transfer	Heat transfer problems
Processing	Not easily adapted to continuous processing	Continuous processing
Active centres	All metal centres	Only the surface site
Concentration	Low	High
Structure	Definite	Indefinite
Activity	High	Low
Determination of catalyst composition	Complicated	Easy
Catalyst regeneration	Complicated	Easy
Cost of catalyst loss	High	Low

Although the benefits of a heterogeneous catalyst outweigh those of a homogeneous catalyst, homogeneous catalysis is easier to study and the performance of the catalyst is easier to understand, unlike in heterogeneous catalysis. A range of homogeneously catalysed processes

[46] S. Bhaduri, D. Mukesh, *Homogeneous Catalysis: Mechanism and Industrial Application, 2nd Ed.*, John Wiley & Sons, Inc., New Jersey, **2014**.
[47] J. Hagen, *Industrial Catalysis: A Practical Approach, 3rd Ed.*, Wiley-VCH Verlag GmbH & Co. KGaA, Weinheim, **2005**, 1.
[48] B. Cornils, W.A. Herrmann, *Applied Homogeneous Catalysis with Organometallic Compounds, 2nd Ed.*, Wiley-VCH, Germany, Weinheim, **2002**, 1493.

are listed below[49] and can be performed at high selectivity through the utilization of homogeneous catalysts and well-chosen metal centres and ligand systems.[50,51]

- Alkene metathesis (Schrock's and Grubb's catalyst)[52,53,54]
- CO Hydrogenation[55]
- Co-oligomerization [56]
- Co-polymerisation[57]
- Methanol carbonylation (BASF, Monsanto, and Cativa processes)[58,59]
- Methanol homologation[60]
- Methoxycarbonylation[61]
- Hydrocarbonylation[62]
- Hydrocyanation (nickel phosphite complex)[17,63]
- Hydroformylation (cobalt and rhodium catalysts)[64]
- Hydrogenation (Wilkinson's catalyst)[65]

[49] D.V. Kama, *MSc. Phosphorus Bidentate Ligand Interaction at Platinum Group Metals: A Catalytic and Solid State Study*, University of the Free State, Bloemfontein, Free State, **2009**.
[50] C.C. Tzschucke, C. Markert, W. Bannwarth, S. Roller, A. Hebel, R. Haag, *Angew. Chem. Int. Ed.*, **2002**, 41, 3964.
[51] D.J. Cole-Hamilton, *Science,* **2003**, 299, 1702.
[52] R.R. Schrock, J.S. Murdzek, G.C. Bazan, J. Robbins, M. DiMare, O'Regan, *J. Am. Chem. Soc.,* **1990**, 112, 3875.
[53] R.H. Grubbs, S. Chang, *Tethedron,* **1988**, 54, 4413.
[54] R.H. Grubbs, *Tethedron,* **2004**, 60, 7117.
[55] J. Wang, Y. Kawazoe, Q. Sun, S. Chan, H. Su, *J. Cat.*, **2016**, 336, 94.
[56] W. Strohmeir, F.J. Muller, *Chem. Ber.*, **1967**, 100, 2812.
[57] C. Wulf, U. Doering, T. Werner, *RSC Adv.*, **2018**, 8, 3673.
[58] C.E. Hickey, P.M. Maitlis, *J. Chem. Soc. Chem. Commun.*, **1984**, 1609.
[59] R.H. Crabtree, *The Organometallic Chemistry of the Transition Metals,* John Wiley & Sons, New York, **1988**.
[60] M. Roper, H. Loevenich, *The Homologation of Methanol in W. Keim (Eds) Catalysis in C1 Chemistry,* **1983**, 405.
[61] O.V. Gusev, A.M. Kalsin, M.G. Peterleitner, P.V. Petrovskii, K.A. Lyssenko, N.G. Akhmedov, C. Bianchini, A. Meli, W. Oberhauser, *Organometallics,* **2002**, 21, 3637.
[62] W.H. Chiou, Y.W. Wang, C.L. Kao, P.C. Chen, C.C. Wu, *Organometallics*, **2014**, 33, 16, 4240.
[63] A. Falk, A.L. Goderz, H.G. Schmalz, *Angew. Chem. Int. Ed.*, **2013**, 52, 1576.
[64] W.A. Herrmann, B. Cornils, *Angew. Chem. Int, Ed.*, **1997**, 36, 1048.
[65] R.H. Crabtree, *The Organometallic Chemistry of the Transition Metal*, John Wiley & Sons, New York, **1988**.

2.3.3 BIPHASIC CATALYSIS

Biphasic catalytic systems facilitate the separation of the substrate (often) contained in the organic phase and the aqueous phase containing the product. The benefit of this system combined with a homogeneous catalyst includes the recycling of the catalyst in the aqueous phase without attenuation of the catalyst, hence preventing/reducing the separation problem encountered in homogeneous catalysis, and allowing reuse giving a high turnover number (TON) while reducing waste. The aqueous-biphasic catalytic system incorporated with a water-soluble catalyst results in easier separation and lower costs.[66] Through vigorous stirring of the water-soluble homogeneous catalysis and the substrate/product, interaction at the interphase region occurs. At the end of the reaction, the catalyst and the product then simply separate into their respective phases.

2.3.4 LIGAND SYSTEMS IN HOMOGENEOUS CATALYSIS

A ligand coordinates to the central metal through the donation of the ligand electron(s), and the steric and electronic properties thereof have a direct influence on the reactivity and selectivity of a transition metal catalyst. The importance of the behaviour of coordination and organometallic compounds have been emphasized by Braunschwieg, Damme, and Dewehurst[67] whose experiment gave conclusive evidence of the role played by strengthening π-back donation in transition metal complexes. Sigman and co-workers[68] went on to emphasize the structural and electronic influence of various phosphine ligands on the mechanistic pathway and reaction of the Suzuki reaction. Ligand modification is critical in the modification of catalysts as made evident in 1996 when Shell reported that the addition of a tertiary phosphine leads to improved selectivity and stability.[69] Having a good knowledge of ligand characterisation increases the understanding of the catalyst.

Critically important for a homogeneous catalyst's behaviour is the electronic and steric effects as induced by the ligands; these will be evaluated next.

---

[66] W.A. Herrmann, C.W. Kohlpaintner, *Angew. Chem. Int. Ed. Engl.*, **1993**, 32, 1524.
[67] H. Braunschweig, A. Damme, R.D. Dewehurst, A. Vargas, *Nat. Chem.*, **2013**, 115.
[68] Z.L. Niemeyer, A. Milo, D.P. Hickey, M.S. Sigman, *Nat. Chem.*, **2016**, 8, 610.
[69] R. Meijboom, M. Haumann, A. Roodt, L. Damoense, *Helv. Chim. Acta.*, **2005**, 88, 676.

2.3.4.1 ELECTRONIC EFFECTS

The electronic properties of phosphine ligands can be indirectly measured using infrared (IR) spectroscopy as introduced by Tolman some 50 years ago.[70] In the IR spectrum, terminal carbonyl ligands in a metal-ligand complex (such as the [Ni(CO)3L] complexes used by Tolman) can be identified in the wavenumber range 2125 to 1850 cm^{-1}. The electronic properties of other coordinated ligands in the same complex can then be determined from this information.[56,71] Electron density on the metal is increased by strong σ donor ligands, resulting in a back donation to the CO ligand. This causes shorter, CO bonds, stronger M-C bonds and a lower CO IR stretching frequency. The strong π acceptor ligands compete for the electrons responsible for back donation, which results in higher ν_{CO} frequencies, whilst weak π acceptor ligands result in lower ν_{CO} frequencies.

For tertiary phosphines ($PR_1R_2R_3$ with aryl groups R_1, R_2 and R_3) Eq. 2.1[72,73] can be used to determine an estimate for the electronic parameter (ν) for a range of ligands. χ_i is the individual substituent contribution which is calculated for a large number of substituents, R_1, R_2, and R_3.

$$\nu = 2056.1 + \sum_{i=1}^{3} \chi_i \qquad \text{..Eq. 2.1}$$

Ligands which may be considered as π acids are well described through the carbonyl ligand (Fig. 2.1.1) which illustrates how a filled σ orbital (i) overlaps with the (ii) empty dsp^2 orbital. Fig. 2.1.2 illustrates back bonding through the flow of electron density from the metal (i) to the carbonyl (ii). In a square planar complex, the increased electron density on the metal centre allows for more electron donating abilities from the metal's d orbital to the π^* orbital of CO.

[70] D. Setiawan, R. Kalescky, E. Kraka, D. Cremer, *Inorg. Chem.*, **2016**, 2332.
[71] W.D. Horrocks Jr., R.C. Taylor, *Inorg. Chem.*, **1963**, 2, 273.
[72] O. Kuhl, *Coord. Chem. Rev.*, **2005**, 249, 693.
[73] W. Strohmeier, F.J. Muller, *Z. Naturforschg*, **1967**, 22b, 451.

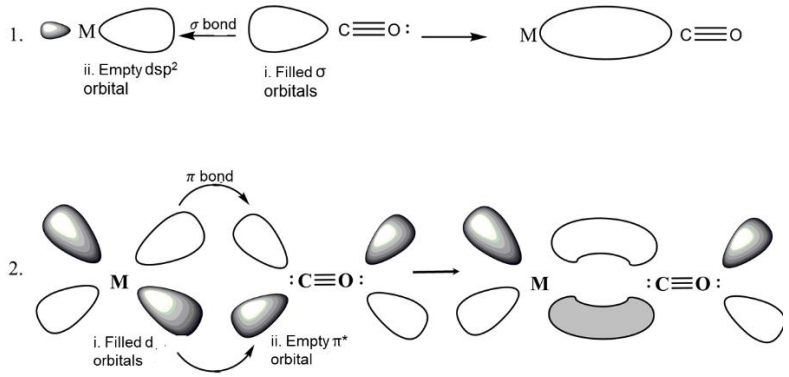

Figure 2.1: Molecular orbital view of metal carbonyl bonding.

Electron withdrawing and donating properties of molecules produce electronic effects via chemical bonds. For example, the donation of electrons from an R group on a phosphorous atom forms a σ bond. When the R group is electron withdrawing, the phosphine will be a weak σ donor while an electron donating R group will result in an increase in the σ donor ability. Fig. 2.2 indicates the formation of a σ bond by donation of an electron pair from the phosphorous atom to the metal, whilst the π bond is formed by the back acceptance from a filled d orbital to that of a vacant phosphorous 3d orbital in typical electron-rich late transition metals. In transition metal complexes where phosphines are the ligands, the density on the metal will be affected by the electron donating properties.

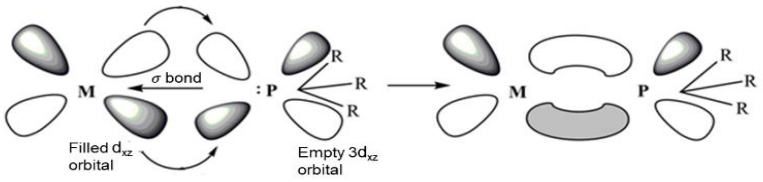

Figure 2.2: Molecular orbital view of tertiary phosphine metal bonding. The directions of the arrows indicate the flow of electrons.

2.3.4.2 STERIC EFFECT

Tolman cone angle was developed in 1977[74] to obtain a parameter to measure the steric bulk (size) of phosphine ligands. The steric effect is the result of nonbonding forces that cause repulsion and steric strain on the bonds. The interference between the R groups causes steric

[74] Z. Freixa, M.M. Pereira, J.C. Bayon, A.M.S. Silva, J.A.R. Salvador, A.M. Beja, J.A. Paixao, M. Ramos, *Tethedron: Asym.*, **2001**, 12, 1083.

effect due to electron clouds that may overlap. The bulkiness from $P(Me)_3$ to $P(t\text{-}Bu)_3$ increases causing steric strain, which in turn decreases the binding ability of the ligands in their respective orders.[75] The cone angle for tertiary phosphines was defined as a parameter of bulkiness by Tolman. For symmetrical ligands (all R are the same, Fig. 2.3.a) the apex of the cylindrical cone is centred 2.28 Å from the centre of the P atom which touches the Van der Waals radii of the outermost atom of the model. For unsymmetrical ligands (Fig. 2.3.b, $PR^iR^{ii}R^{iii}$), the cone angle is determined by using a model that minimizes the sum of the cone half angle as indicated by Eq. 2.2.[44]

$$\theta = \frac{2}{3}\sum_{i=1}^{3}\frac{\theta_i}{2} \qquad \text{..Eq. 2.2}$$

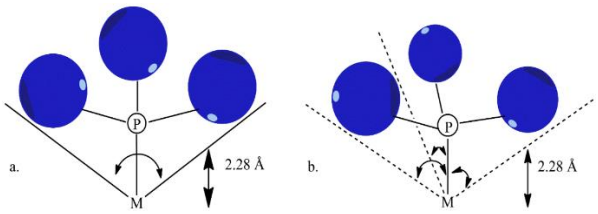

Figure 2.3: (a) Cone angle for symmetrical tertiary phosphines PR_3 (M = metal). (b) Method for measuring an unsymmetrical tertiary phosphine $PR^iR^{ii}R^{iii}$.

2.3.4.3 PHOSPHINES

The ability of neutral tertiary phosphines to stabilize low metal oxidation states and influence the steric and electronic properties of a metal centre[76] allows them to be common ligands in the design of model catalysts. Modification of the catalyst with a water-soluble ligand is important. Modified phosphines include sulfonated phenyl groups i.e. TPPTS (triphenylphosphine 3,3',3''-trisulfonic acid trisodium salt), TPPMS (monosulfonated triphenylphosphine) and PTA (1,3,5-triaza-7-phosphaadamantane), which are commonly used ligands in the design of water-soluble complexes.[77]

---

[76] A. Roodt, G.J.J. Steyn, *Res. Devel. Inorg. Chem.*, **2000**, 2, 1.
[77] F. Mohr, S. Sanz, E.R.T. Tiekink, M. Laguna, *Organometallics*, **2006**, 25, 3084.

PTA is a cage-like water-soluble tertiary phosphine that has gained interest due to its ability to form stable transition metal complexes. Daigle *et al.* first synthesised PTA in 1974 and it has since been improved.[78] Application in catalysis,[79] electrochemical properties and medical (i.e. for the development of anticancer metallodrugs[80]) has been investigated. PTA has water solubility comparable to sulfonated Phosphine m-TPPTS,[81] except that it has a higher resistance towards oxidation. PTA is also soluble in acetone, chloroform, dichloromethane and DMSO and its small cone angle (103°) may result in the formation of a transition metal complex containing more than one PTA entity. In addition, this ligand coordinates either at the phosphorous atom with soft transition metals or at the nitrogen atom with hard metals.[82,83,84]

Fig. 2.4 illustrates some of the water-soluble tertiary phosphines that have been investigated.

As indicated above, the purpose in designing a water-soluble homogeneous catalyst lies not only in the need to create an environmentally friendly complex that can be utilized in industrially important chemical processes but also aims at improving effective separation of the catalyst and the product. This has served as the driving force for water-based reactions and water-soluble catalysts.[85,86,87]

---

[78] D.J. Daigle, A.B. Pepperman Jnr., S.L. Vail, *J. Hetrocycl. Chem.*, **1974**,11, 407.

[79] a) S. Bolano, L. Gonsalvi, F. Zanobini, F. Vizza, V. Bertolasi, A. Romerosa, M. Peruzzini, *J. Mol. Cat. A.*, **2004**, 224, 61.

b) H. Horvath, G. Laurenczy, A. Katho, *J. Organomet. Chem.*, **2004**, 689, 1036.

c) B. Korthals, I. Gottker-Scnetmann, S. Mecking, *Organometallics*, **2007**, 26, 1311.

[80] M.V. Babak, S.M. Meier, K.V.M. Huber, J. Reynisson, A.A. legin, M.A. Jakupec, A. Roller, A. Stukalov, M. Gridling, K.L. Bennett, J. Colinge, W. Berger, P.J. Dyson, G.S. Furga, B.K. Keppler, C.G. Hartinger, *Chem. Sci.*, **2015**, 6, 2449.

[81] E.G. Kuntz, *CHEMTECH*, **1987**, 17, 570.

[82] a) A.D. Phillips, L. Gonsalvi, A. Romerosa, F. Vizza, M. Peruzzini, *Coord. Chem. Rev.*, **2004**, 248, 955.

b) J. Bravo, S. Bolano, L. Gonsalvi, M. Peruzzi, *Coord. Chem. Rev.*, **2010**, 254, 555.

[83] a) D.J. Daigle, *J. Inorg. Synth.*, **1998**, 32, 40.

b) M. Caporali, L. Gonsalvi, M. Peruzzini, F. Zanobini, e-EROS Encyclopaedia of reagents for Organic Synthesis, John Wiley & Sons, Ltd, **2010**.

[84] a) A.D. Philips, L. Gonsalvi, A. Romerosa, F. Vizza, M. Peruzzini, *Coord. Chem. Rev.*, **2004**, 248, 955.

b) J. Bravo, S. Bolano, L. Gonsalvi, M. Peruzzini, *Coord. Chem. Rev.*, **2010**, 254, 555.

[85] B. Cornils, *Org. Process Res. Dev.*, **1998**, 2, 121.

[86] B. Cornils, W.A. Herrmann, *Aqueous-Phase Organometallic Catalysis Concept and Application*, Wiley-VCH, Weinheim, **1998**.

[87] F. Joo, *Aqueous Organometallic Catalysis:* Kluwer Academic Publishers, Dordrecht, **2001**.

Thus, the days of keeping water out of reactions by creating anhydrous reactions conditions have taken a turn. Alterations in the ligand design and/or metal selection can provide improvement in selectivity, energy consumption and utilization of solvent. In the design of a homogeneous water-soluble catalyst, the electronic and steric properties of known organometallic complexes in water need to be considered, along with the recovery of the catalyst from the hydrophobic product through phase separation.

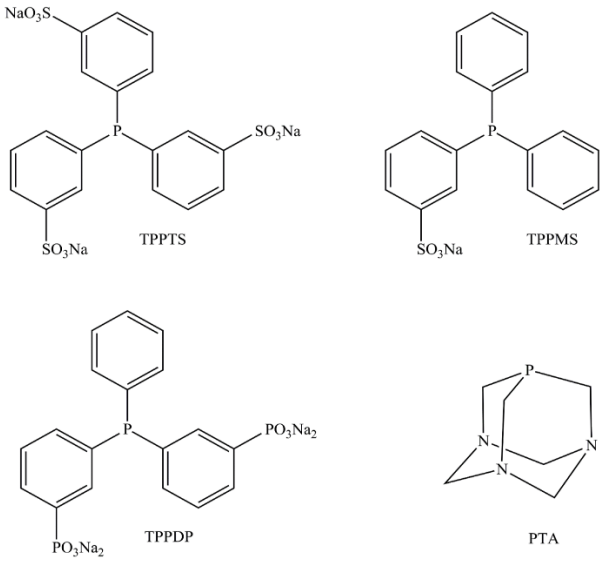

Figure 2.4: Various water-soluble phosphines and the cage-like structure of PTA.

With the increasing cost and scarceness of PGM (platinum group metals) which include Ru, Ir, Pd, Pt, and Rh, recovery of these metals is important in industrial applications of homogeneous catalysts. For the successful design of a water-soluble catalyst, the synthesised catalyst needs to be restricted to the aqueous phase through either using a supported aqueous-phase catalyst (SAP) or including organometallic catalysts into the pores of aluminosilicates or aluminophosphates, then using them in the water phase reactions of a water-solvent organic reagent.[88]

[88] M.W. Anderson, J. Shi, D.A. Leigh, A.E. Moody, F.A. Wade, B. Hamilton, S.W. Carr, *J. Chem. Soc. Chem. Commun.*, **1993**, 533.

2.4 RHODIUM

2.4.1 PRINCIPLE OXIDATION STATES

The main oxidation states of rhodium are I, III, and IV. From the mentioned oxidation states, III is the most stable and is the most common of rhodium complexes. The cationic and neutral complexes are generally kinetically inert.[89] Rhodium(I) complexes exist in square planar, tetrahedral, and 5 geometric species that are generally bonded to π-bonding ligands. These rhodium complexes generally undergo oxidative addition that is used in catalytic reactions.[90] Examples of rhodium(I) complexes are discussed in Table 2.2.

Table 2.2: Oxidative states of rhodium(I)

Coordination number	Geometry	Examples
3	Trigonal planar	$[RhCl(PCy_3)_2]$
4	Square planar	$[Rh(PPh_3)_2(CO)(Cl)$
	Tetrahedral	$[Rh(PMe_3)_4]^+$
5	Trigonal bipyramidal	$[Rh(SnCl_3)_5]^{4-}$

2.4.2 INDUSTRIAL USES

Due to its inertness against corrosion and general aggressive chemicals too, rhodium is used as a corrosive resistive coating material e.g. jewellery. A characteristic feature of transition metal atoms is their ability to form complexes with a variety of neutral ligands such as substituted phosphines, carbon monoxides, various molecules that have delocalized π orbitals.[54]

2.4.2.1 CATALYTIC CONVERTER

The ability of rhodium and other late transitional metals to act as catalysts is related to their electron-rich metal centres that have lower coordination numbers, which in turn allows substrate molecules to interact more easily at the metal centre.[91]

[89] F.A. Cotton, G. Wilkinson, *Advanced Inorganic Chemistry 4th Ed.*, John Wiley & Sons Inc., London, **1980**.

[90] F.A. Cotton, G. Wilkinson, *Advanced Inorganic Chemistry: A Comprehensive Text, 3rd Ed.*, John Wiley & Sons Inc., New York, **1972**.

[91] F.R. Hartley, *Chemistry of the Platinum Group Metals: Recent Development*, Elsevier Science Publishers, United States of America, New York, **1991**.

Before the formation of catalytic converters, toxic and harmful gasses were emitted from car engines through the exhaust pipe and would end up in our atmosphere. An automobile catalyst is the main part of an automobile catalyst converter which is used for decreasing harmful gasses. This is accomplished by the catalyst splitting the molecules into smaller fragments whereafter these are recombined into relatively harmless substances. CO is converted to CO_2 and NO is converted to N_2 by reduction with CO/H_2, which are the desired reactions in automobile catalytic converters.[92] Rhodium catalysts tend towards high catalytic activity but also great selectivity towards N_2 production.[93] These catalytic converters became compulsory in 1987. Rhodium reduces nitrogen oxides in exhaust gasses and is also a catalyst in the chemical industry for producing: nitric acid and enhancing hydrogenation reactions. [94]

2.4.2.2 HOMOGENEOUS CATALYSIS CHEMICAL BUILDING BLOCKS

Transition metal catalysts have excellent industrial application ranging from manufacture of bulk and fine chemicals. Homogeneous catalysts have high activity and product selectivity which allows them to be extensively used in industry, despite the fact that some are hard to separate from the product.[46] As mentioned earlier, Organometallic compounds of rhodium have shown to be good catalysts; successful homogeneous processes involving rhodium based systems are the hydroformylation[95] of alkenes using $[RhH(CO)(PPh_3)_3]$,[96] the asymmetric hydrogenation[97] of ALPHA-amidocinnamic acid,[98] and the carbonylation of methanol [99,100] using $[Rh(CO)_2(I)_2]^-$. Fig. 2.5 illustrates the basic chemical building blocks that are obtained through heterogeneous and homogeneous catalysis treatment of crude oil to obtain higher commodity products.

[92] E.E. Donath, *Catalysis-Science and Technology*, Springer-Verlag, New York, **1982**, 1.
[93] G. Comelli, V.R. Dhanak, M. Kiskinova, K.C. Prince, R. Rosei, *Surface Science Reports*, **1998**, 32, 65.
[94] H.J. Jung, E.R. Becker, J. Matthey, *Plat. Met. Rev.*, **1987**, 31, 4, 162.
[95] P.W.N.M. Van Leeuwen, C. Claver, *Rhodium Catalysed Hydroformylation*, Kluwer Academic Publishers, New York, **2002**.
[96] F.H. Jardine, *Polyhedron*, **1982**, 1, 569.
[97] J. Luo, A.G. Oliver, J. S. McIndoe, *Dalton Trans.*, **2013**, 42, 11312.
[98] J.M. Brown, *Angew. Chem. Int. Ed.*, **1987**, 26, 190.
[99] J. Zakzeski, *Phys. Chem. Chemi. Phys.*, **2009**, 11, 9903.
[100] M.J. Howard, M.D. Jones, M.S. Roberts, S.A. Taylor, *Cat. Today*, **1993**, 18, 325.

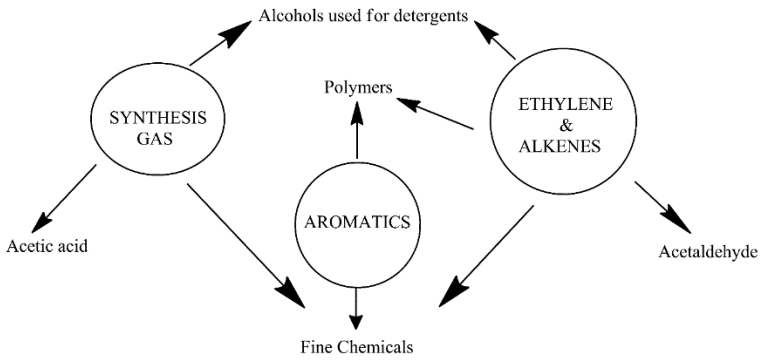

Figure 2.5: High commodity products that can be produced from homogeneous catalysis using these chemical building blocks.[73]

2.4.3 RHODIUM IN HOMOGENEOUS CATALYSIS-METHANOL CARBONYLATYION

The (catalytic) introduction of carbon monoxide into an organic or inorganic compound is known as a catalytic carbonylation reaction. For example, acetic acid is produced by transition metal compounds in processes such as cobalt BASF, iridium Cativa and the rhodium Monsanto process. 80 % of the over 10 million tons of acetic acid is based on carbonylation of methanol. Acetic acid is an important chemical that is used for a wide range of processes such as the production of vinyl acetate monomer, acetic anhydride, and esters production.[101] The Monsanto process replaced the BASF cobalt-catalysed process since its commercialization in the 1960s with rhodium. Reaction conditions are milder (30-60 atm pressure and 150-200 ºC) and selectivity is greater which contributes to reduced manufacturing costs, using less energy, producing higher yields, enabling faster reactions, and increasing the lifetime of the catalyst. Fig. 2.6 illustrates the catalytic cycle of the Monsanto process.

[101] H. Ryssel, *Burns*, **2009**, 35, 695.

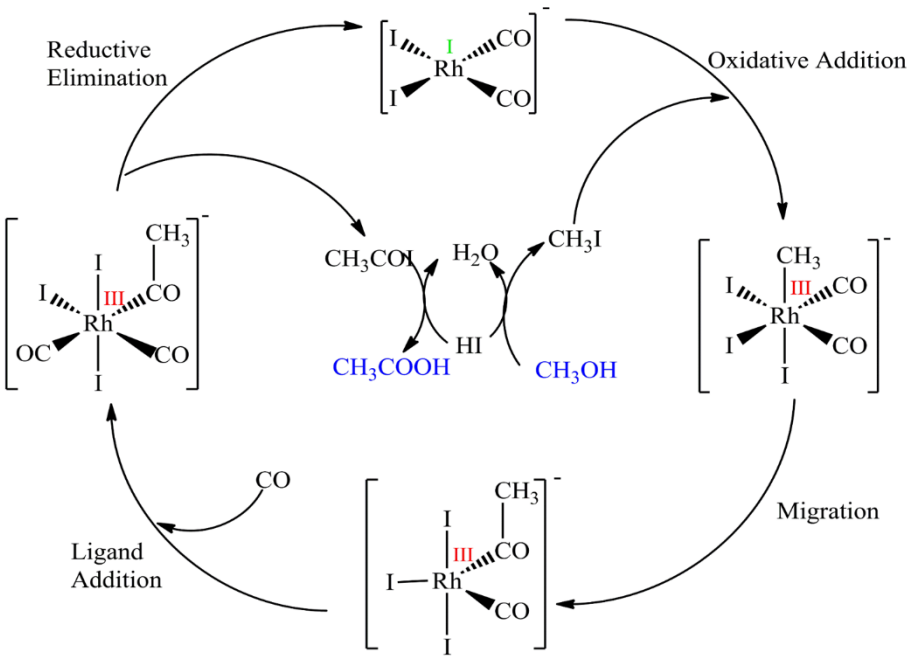

Figure 2.6: Monsanto process: catalytic cycle for the carbonylation of methanol using a rhodium catalyst.

The first step in the Monsanto process, which is also the rate determining step of the cycle, is the oxidative addition of iodomethane to $[Rh(CO)_2I_2]^-$. The alkyl rhodium(III) intermediate then undergoes migratory insertion of the oxidative addition product, forming the rhodium(III) acyl species $[(MeCO)Rh(CO)I_3]^-$. Ligand addition of carbon monoxide forms a 6 coordinated dicarbonyl $[(MeCO)Rh(CO)_2I_3]^-$ complex. The final step of the cycle is the reductive elimination of acetyl iodide, CH_3COI, which results in the regeneration of the starting complex, $[Rh(CO)_2I_3]^-$.

The understanding of the catalytic system certainly aided in designing a catalyst that produces the highest yield and provides a basic understanding of the catalyst in terms of reactivity such as when eventually rhodium was replaced by iridium.

Thus, knowledge on reactivities of different reactions of a catalytic cycle is very important for the continuous running at optimum conditions. Hence substitution kinetics and oxidative addition kinetics was included in this study, focusing on the ligand exchange reaction for the square planar type systems, and some aspects are briefly discussed below.

2.4.4 REACTION KINETICS

Chemical kinetics describe the reaction rate and associated parameters, focusing on the rate of change in the concentration of reactants and products.[102] The obtained information includes the speed at which the reaction occurs, the time taken for the transition,[103] and the intimate reaction mechanism.[104,105] Reactivity, stability, and mechanistic behaviour of the formation of metal complexes can also be established. In particular, oxidative addition and substitution reactions are two vital steps that are important in industrial catalytic processes and biological related investigations.[106,107,108,109] It is therefore imperative that a knowledge of these reactions and the underlying theory on it is considered and also utilised within this study to obtain a broader vision on aspects of importance.

2.4.4.1 SUBSTITUTION

As indicated, when attempting to design a catalytic system that might produce high selectivity and high yields, basic insight into the catalyst in terms of reactivity is required. Through the study of substitution reactions, information regarding the reactivity of a complex and its metal centre can be obtained.[110] Nucleophilic substitution on square-planar compounds of rhodium will be considered in this case. The two common stoichiometric mechanisms that occur in substitution reactions are known as dissociative or associative.

In an associative mechanism, which is the most common mechanism for a square planar complex, the M-Y bond is formed by Y occupying the vacant site on the metal before the M-

[102] A.F. Frost, R.G. Pearson, *Kinetics and Mechanism*, John Wiley and Sons, New York, **1953**.
[103] K.A. Connors, *Chemical Kinetics: Study of reaction rates in solution, 1st Ed*., VCH Publishers, Inc., New York, **1990**.
[104] J.H. Espenson, *Chemical Kinetics and Reaction Mechanism, 2nd Ed*., McGraw-Hill, New York, **1995**.
[105] C. Capellos, B.H.J. Bielski, *Kinetic Systems*, Wiley-Interscience, New York, **1972**.
[106] F.A Carey, R.M. Giuliano, *Organic Chemistry, 8th Ed*., McGraw-Hill, New York, **2011**.
[107] W.H. Brown, B.L. Iverson, E.V. Anslyn, C.S. Foote, *Organic Chemistry*, 7th Ed., Brooks/Cole: Belmont, CA, **2013**.
[108] E. Alessio, *Bioinorganic Medicinal Chemistry,* Wiley-VCH Verlag & Co. KGaA: Germany, **2011**.
[109] A.L. Noffke, A. Habtemariam, A.M. Pizarro, P.J. Sadler, *Chem. Comm.*, **2012**, 48, 5219.
[110] R. Van Eldik, K. Bowman-James, *Advances in Inorganic Chemistry*, Academic Press, United Kingdom, London, **2007**, 296.

X bond breaks; this mechanism favours the change in the entering of the ligand. The reaction is described in Scheme 2.1 and rate for this mechanism is calculated with Eq. 2.3:

Scheme 2.1: Schematic illustration representing the associative mechanism, for a square planar complex.

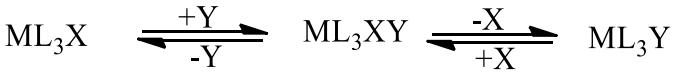

Rate = $k[L_nMX][Y]$ ..Eq. 2.3

The size and charge on the metal centre may be used to distinguish these two mechanisms and also influence the rate of substitution reactions. In an associative mechanism, a nucleophilic attack in square planar complexes is generally favoured and can occur in either the direct (k_{12}) or solvent (k_{13}) pathway, as illustrated in Scheme 2.2.

Scheme 2.2: Schematic representation of a square-planar substitution reaction, the direct and solvent pathway for the associative mechanism of a ligand substitution reaction.

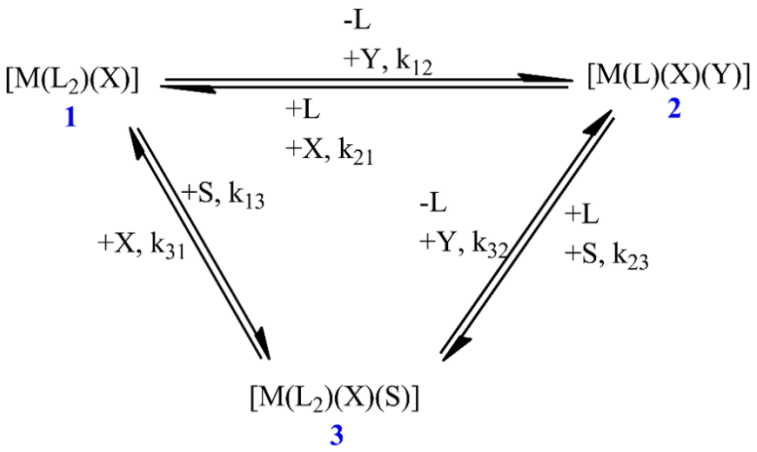

In the first pathway, the direct attack of the entering nucleophile on the metal produces a five-coordinated intermediate. The second pathway involves the attack of the solvent producing a labile solvent intermediate that is followed by the immediate attack of the entering nucleophile yielding the final product. From the reaction mechanism in Scheme 2.2, an expression for the

pseudo-first order rate constant (k_{obs}) which proceed under *equilibrium* conditions (not complete conversion to the substituted product) can be derived as given in Eq. 2.4.[111,112]

$$k_{obs} = k_{12}([Y] + \frac{[X]}{K_{eq}}) + \frac{\frac{k_{13}k_{32}}{K_{eq}k_{31}}[X] + k_{13}\frac{k_{32}}{k_{31}}[Y]}{[X]+\frac{k_{32}}{k_{31}}[Y]} \quad \text{..Eq. 2.4}$$

In cases where the reaction is non-reversible/ or under non-equilibrium (large K_{eq}), the common two-term rate law (Eq. 2.5) is used for square planar substitution.

$$k_{obs} = k_{12}[Y] + k_{13} \quad \text{..Eq. 2.5}$$

From a linear plot of the pseudo-first-order rate constant (k_{obs}) against concentration of the incoming ligand, the slope (k_{12}) and the intercept (k_{13} solvent assisted pathway) can be determined. Alternatively, under equilibrium conditions (small K_{eq}) the concentration of the leaving group needs to be considered in the overall rate, as given in Eq. 2.4.

The *trans* influence is a thermodynamic phenomenon that is defined by the weakening of the metal-ligand bond due to the ligand *trans* to it. This influence directs the substitution of either X or *trans* L. The shorter the bond length, the stronger the bond. The *trans* effect is a kinetic phenomenon that is defined as the effect of a coordinated ligand on the rate of substitution of the ligand *trans* thereto.[113] Strong π-acceptors stabilize the transition state by accepting electron density that is donated by the entering nucleophile donates to the metal centre and hence aids substitution at the site *trans* to it by lowering the activation barrier. The ligand *trans* to the leaving ligand in a square planar substitution reaction plays an important role.[114] Other factors also have an influence on the rate of the substitution reaction:

a) The entering ligands.[115]

b) The leaving/labile ligand.[103]

[111] S. Otto, *PhD. Structural and Reactivity Relationships in Platinum(II) and Rhodium(I) Complexes*, University of the Free State, **1999**, 13.
[112] C. Pretorius, *PhD. Structural and Reactivity Study of Rhodium(I) Carbonyl Complexes as Model Nano Assemblies*, University Of The Free State, Bloemfontein, South Africa, **2015**.
[113] A.V. Babkov, *Polyhedron*, **1988**, 7, 13, 1203.
[114] A. Werner, *Anorg. Allg. Chem.*, **1893**, 3, 267.
[115] F.A. Cotton, G. Wilkinson, P.L. Gause, *Basic Inorganic Chemistry*, John Wiley & Sons, United States of America, New York, **1995**, 192.

c) The central metal atom.[116]

d) The ligand *trans* to the leaving group.[117]

2.4.4.2 OXIDATIVE ADDITION REACTIONS

Addition of a neutral entity (usually bimolecular) to a transition metal centre and oxidizes the metal by 2 electrons simultaneously during the process of adding itself to the metal, is called oxidative addition. This often occurs in catalytic conversions. Two electrons are transferred from the metal to the entering entity, which may break the bond therein, often forming 2 new anionic ligands.

Oxidative addition (see Scheme 2.3) is a fundamental process in inorganic and organometallic chemistry.[118,119] It also plays a vital role in the Monsanto process, as seen in Par. 2.4.3, as it is the rate-determining step.

Scheme 2.3: Schematic illustration of the oxidative addition mechanism.

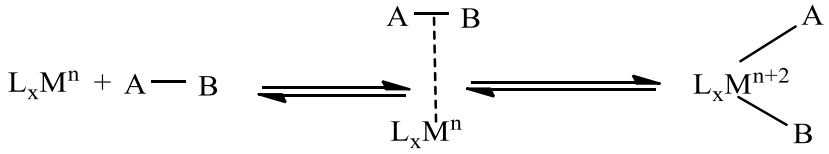

The more electron rich the metal centre is, the easier it is for the oxidation addition reaction to occur. Hence the most reactive metal towards a certain substrate for oxidative addition will be determined by the metal centre with the:

a) Strongest donor ligands

b) Fewest π-acceptor ligands

[116] G. Wulfsberg, *Inorganic Chemistry*, University Science Books, United States of America, Sausalito, **2000**.

[117] P.W. Atkins, T.L. Overton, J.P. Rourke, M.T. Weller, F.A. Armstrong, *Shriver & Atkins Inorganic Chemistry*, Oxford University Press, United Kingdom, Oxford, **2010**, 515.

[118] J.J. Hartwig, *Organotransition Metal Chemistry, from Bonding to Catalysis*, University Science Books, Sausalito, CA, **2010**, 1160.

[119] J.A. Labinger, *Organometallic*, **2015**, 34, 4784.

c) Most negative charge

Due to the covalent bond breaking in the substrate, the oxidative addition is commonly the slowest, the rate-determining step in the Monsanto catalytic cycle. The requirements for oxidative addition to occur are:

a) Availability of non-bonded electron density on the metal.

b) Two vacant coordination sites on the reacting complex (L_nM), that is, the complex must be coordinatively unsaturated.

c) A metal with stable oxidation states separated by 2 units; the higher oxidation state must be energetically accessible and stable.

The oxidative addition of iodomethane to complexes of the type [Rh(L,L'-bid)(CO)(PR_3)], (where L,L'-bid = monoanionic bidentate ligands; PR_3 = tertiary phosphines) has been investigated over the years by Roodt and co-workers due the ongoing interest in the development of novel catalytic species for rhodium supported catalytic carbonylation of methanol to acetic acid and methyl acetate.[120,121,122,123,124,125,126,127] Oxidative addition, since it is a key step in many catalytic systems, is therefore considered a bench-mark reaction to evaluate some aspect of a prospective new catalyst system.

It is therefore included in this MSc study as part of the basic evaluation criteria of a new catalyst model.

[120] J.G. Leipolt, E.C. Steynberg, R. Van Eldik, *Inorg. Chem.*, **1987**, 26, 3068.
[121] S.S. Basson, J.G. Leipoldt, A. Roodt, J.A. Venter, T.J. Van Der Walt, *Inorg. Chim. Acta.*, **1986**, 119, 35.
[122] S.S. Basson, J.G. Leipoldt, A. Roodt, J.A. Venter, *Inorg. Chim. Acta.*, **1987**, 128, 31.
[123] S.S. Basson, J.G. Leipoldt, J.A. Venter, *Acta. Cryst.*, **1990**, 1324.
[124] G.J.J. Steyn, A. Roodt, I. Poletaeva, Y.S. Varshavsky, *J. Organomet. Chem.*, **1997**, 536.
[125] A. Brink, A. Roodt, G. Steyl, H.G. Visser, *Dalton. Trans.*, **2010**, 39, 5572.
[126] S. Warsink, F.G. Fessha, W. Purcell, J.A. Venter, *J. Organomet. Chem.*, **2013**, 726, 14.
[127] G.J.S. Venter, *PhD. A Crystallographic, Computational and Mechanistic Study of Rhodium Enaminoketonato Complexes*, University of the Free State, Bloemfontein, Free State, **2013**.

2.5 CONCLUSION

In this chapter, some general aspects of green chemistry, catalysis and related reactions were discussed in terms of the journey to design and synthesize a new model homogeneous water-soluble rhodium(I) catalyst. A comparison between homogeneous and heterogeneous catalysis was included, the importance of water as a solvent and its importance towards green chemistry has also been mentioned in addition to the versatility of phosphines. Special focus was placed on substitution kinetics.

The literature covered serves as a background for this MSc study, wherein rhodium(I) complexes containing an N,O-bidentate ligand was prepared and the coordination of these ligands to rhodium in the presence of carbonyl and phosphines were investigated. The effect of the electronic and steric properties of certain ligands on the selectivity and stability of complexes were investigated through XRD, IR, and NMR characterization techniques. This was followed by the investigation of the mechanism and kinetics behaviour of these complexes using IR, NMR and UV-Vis spectroscopic methods.

More detail on the synthetic methodology, techniques employed, structures of model systems and solution behaviour is found and detailed in the following chapters.

3 BASIC THEORY OF SOLID AND SOLUTION STATE CHARACTERISATION AND SYNTHESIS CHARACTERISATION OF LIGAND AND METAL COMPLEXES

3.1 INTRODUCTION

Characterisation techniques are vital in identifying the starting materials, possible intermediates, and final products of a reaction mixture. Non-destructive methods identify the components without destroying the sample during the characterisation process. Infrared (IR), ultraviolet/visible (UV/Vis), and nuclear magnetic resonance (NMR) spectroscopy as well as X-ray diffraction crystallography (XRD) make up some of the non-destructive techniques that play a major role in determining the mechanism of reactions in chemical kinetic studies. In this chapter the basic theories of these characterisation techniques will be discussed along with the synthesis and characterisation of:

4-R-PhonyH

[Rh(4-R-Phony)$(CO)_2$]

[Rh(4-R-Phony)(CO)(PPh_3)]

[Rh(4-R-Phony)(CO)(PTA)]

R represents the electron withdrawing or donating group at the *para* position of the phenyl moiety bonded to the nitrogen atom with PhonyH = 4-(phenylamino)pent-3-en-2-one; $Phony^-$ = 4-(phenylamino)pent-3-en-2-onate.

The various ligands chosen in this study for coordination to Rh(I) offer unique electronic and steric characteristics that could potentially alter the electronic/steric environment at the rhodium(I) centre which could, in turn, may affect the kinetic results. These ligands were then

coordinated to the rhodium(I) dicarbonyl chloride dimer to form complexes of the type [Rh(N,O-bid)$(CO)_2$], where N,O-bid$^-$ = derivatives of 4-(phenylamino)pent-3-en-2-onate. The carbon monoxide in [Rh(N,O-bid)$(CO)_2$] was then substituted with PR_3 to form [Rh(N,O-bid)(CO)(PR_3)] complexes that were investigated in the kinetic studies to be discussed in Chapter 5; PR_3 = triphenylphosphine (PPh_3) and 1,3,5-triaza-7-phosphaadamantane (PTA).

3.2 NUCLEAR MAGNETIC RESONANCE (NMR) SPECTROSCOPY

Nuclear magnetic resonance (NMR) spectroscopy, developed in 1946,[128,129] is an important tool used by chemists and biochemists to provide information about the molecular structure as well as the number of magnetically distinct atoms in a compound. Moreover, it may also be used for quantitative determination of absorbing species in a non-destructive manner within a short period of time. In 1924 W. Pauli proposed that certain nuclei possess spin and magnetic momentum properties which, when exposed to a magnetic field result in a splitting of their energy levels.[130] NMR is similar to magnetic resonance imaging (MRI)[131] in the sense that it is based on the measurements of the absorption of electromagnetic radiation in the radio frequency region (*ca.* 60-900 MHz) by the nuclei of certain types of atoms (isotopes) in a molecule under the influence of a strong magnetic field (*ca.* 1-18 Tesla). The molecular environment influences the absorption of radio frequency radiation by a nucleus in a magnetic field and this effect then be correlated with the molecular structure. A nucleus has a nuclear spin that is characterized by a spin quantum number (*I*) that is dependent on the atomic number (*Z*) and the atomic mass (*A*). Subatomic particles (protons, neutrons, and electrons) can be viewed as spinning on their own axes, and when the spins are paired, the nucleus does not have a spin quantum number. Table 3.1 below gives an indication of how to determine the spin quantum number.

[128] A. Rahman, *Nuclear Magnetic Resonance*, Springer-Verlag, New York, **1986**.
[129] Bruker, *What is NMR? Nuclear Magnetic Resonance*, **2013**.
[130] A. Skoog, F.J. Holler, S.R. Crouch, *Principles of Instrumental Analysis, 7th Ed.*, Cengage Learning, **2017**.
[131] J.C. Kotz, P.M. Treichel, J.R. Townsend, *Chemistry and Chemical Reactivity*, Thomson Brooks/Cole Publishers, Canada, **2009**.

Table 3.1: Spin quantum number (*I*) due to atomic mass and number.[132]

Atomic mass (*A*)	**Atomic Number (*Z*)**	**Spin quantum number (*I*)**
Odd	Even / Odd	$^1/_2$, $^3/_2$, $^5/_2$ . . .
Even	Even	0
Even	Odd	1, 2, 3, . . .

According to quantum mechanics, a nucleus with spin *I* will have (2*I* + 1) possible orientations. Hence, a nucleus with spin ½ has orientations of +½ and -½. +½ is parallel to the applied field whilst -½ is anti-parallel to the applied field, but both these orientations have equal energy in the absence of a magnetic field. Application of a magnetic field results in the splitting of energy levels with each level being assigned a quantum number (m) as shown in Fig. 3.1. The positively charged nucleus generates its own magnetic field. When the nucleus, with magnetic momentum (μ), is aligned with the magnetic field (m = +½), it has lower energy. Should the spin quantum number (*I*) = ½ the nucleus is dipolar, and when greater than 1 it's quadrupolar. The main difference between the two nuclei is the spin-lattice relaxation times. The relaxation times of dipolar nuclei are generally greater than those of quadrupolar nuclei, resulting in high-resolution measurements whilst quadrupolar nuclei samples have broader lines due to the energy levels.

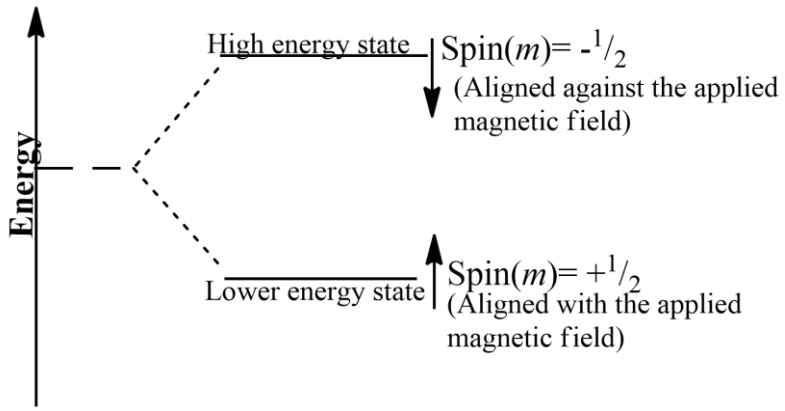

Figure 3.2: Two possible orientations of the magnetic momentum (μ) of a spinning proton in an external magnetic field.

[132] R.M. Lynden-Bell, R.K Harris, *Nuclear Magnetic Resonance Spectroscopy*, Thomas Nelson and Sons, South Africa, Cape Town, **1969**.

When the spin (I) quantum number of ½ is introduced into an external magnetic field (B_0) its magnetic momentum becomes orientated in one of the two directions. The spin states are degenerate in the absence of an external magnetic field. The energy of the spin state (*E*) is directly proportional to the value of *m* and the magnetic field strength, *B,* as indicated in Eq. 3.1.

$$\mathrm{E} = \frac{-\gamma m h B}{2\pi} \qquad \text{..Eq. 3.1}$$

The difference in energy (ΔE) between the two spin states is given by Eq. 3.2;

$$\mathrm{E} = \frac{\gamma h B}{2\pi} \qquad \text{..Eq. 3.2}$$

Here γ is the gyromagnetic ratio and *h* is Planck's constant (6.63×10^{-34}). When a nucleus gets radiated with a suitable frequency, absorption occurs due to the excess of lower energy state nuclei present in the strong magnetic field. The radio frequency absorbed by a nucleus is affected by the chemical environment of the electrons and nuclei that are near the nucleus being studied. The nuclei absorb electromagnetic radiation due to the energy level splitting induced by the magnetic field. Nuclei possessing spin ½ have only two spin states i.e. + ½, -½. Nuclei with anti-parallel spin (-½) to the applied field will possess greater energy compared to the spin that's parallel to the field. The chemical shift and the spin-spin splitting are two effects that are important in the structural analysis. The molecular environment influences the absorption of radio frequency radiation by these nuclei and this effect can be correlated to molecular structure.

The electrons that surround the nucleus form a magnetic field that shields the nucleus against the externally applied field. This results in lower Larmor frequencies and introduces the concept of shielding and deshielding of nuclei.[133] The shielding and deshielding affect the chemical shift. When a proton experiences an external magnetic field, lower frequency is required to achieve resonance resulting in the chemical shift shifting up-field (lower ppms) this is the shielding effect. Deshielding results in the chemical shift shifting downfield (higher ppm) due to protons experiencing a higher external magnetic field.

[133] G. Solomons, C. Fryhle, *Organic Chemistry, 7th Ed.*, Wiley & Sons, **2000**, 366.

3.3 ULTRAVIOLET/VISIBLE (UV/VIS) SPECTROSCOPY

Ultraviolet/visible spectroscopy is a quantitative analysis tool that is based on the absorption of energy in order to determine the reaction mechanism by following the formation and disappearance of a coloured reaction mixture.[134] The technique utilizes electromagnetic radiation between 190 and 800 nm which is subdivided into the ultraviolet (UV, 190-400 nm) and visible (Vis, 400-800 nm) range. The absorption of electromagnetic radiation results in the transition of electrons within a molecule between electronic energy levels (from lower to higher level). As a molecule is irradiated with energy, the absorbed energy excites the valence electron from a HOMO (Highest Occupied Molecular Orbital) to LUMO (Lowest Unoccupied Molecular Orbital).[135] Electrons in the HOMO of a sigma bond (σ) is excited to the empty antibonding σ * orbital (LUMO) of said bond. This is represented by $\sigma \rightarrow \sigma^*$ transition. Electrons from the π bonding orbital can be converted to the anti-bonding π^*-orbital. Non-bonding orbitals (n) (lone pair electrons) have their own transitions. The following molecular electronic transitions are found:

$\sigma \rightarrow \sigma^*$

$\pi \rightarrow \pi^*$

$n \rightarrow \sigma^*$

$n \rightarrow \pi^*$

The absorbed electromagnetic radiation possesses an energy that is equivalent to the energy difference between the excited and ground state. The strength with which the valence electrons are bound to the atoms determines the wavelength at which the molecules absorb energy. In double and triple bonds electrons are not strongly held, but are easily excited producing useful absorption peaks.

From the measured UV spectrum, structural information of a compound can be determined i.e. the nature of conjugated π or σ electron system present in a molecule. This information, however, needs to be used in collaboration with other analytical tools. In addition to the already mentioned uses of UV/Vis spectroscopy, applications include detection of impurities,

[134] C.N.R. Rao, *Ultra-Violet and Visible Spectroscopy, Chemical Application, 2nd Ed.*, Butterworth and Co. Publishers Ltd, England, **1967**.
[135] D.L. Pavia, G.M. Lampman, G.S. Kriz, *Introduction to Spectroscopy, 3rd Ed.*, Thomson Learning Inc., New York, **2001**.

qualitative analysis, quantitative analysis (following a reaction profile), and indicating the relationship between different groups conjugation of the compound. Beer's law is discussed in Par. 3.6.

3.4 INFRARED SPECTROSCOPY

Infrared (IR) spectroscopy is a powerful, cost-efficient, and easy tool used to qualitatively and quantitatively identify pure organic and inorganic compounds; except for a few homonuclear O_2, N_2, Cl_2, and H_2 bonds, all molecular species absorb infrared radiation.[136] The main aim of IR spectroscopic analysis is to determine functional groups by using the similarities between the infrared radiation energies and the energy involved in bond vibrations. Infrared spectroscopy deals with the infrared region of the electromagnetic spectrum with a longer wavelength and lower frequency than visible light. When infrared radiation hits a molecule, bonds in the molecule absorb the energy and respond by vibrating. This manifests as the stretching and bending of bonds or internal rotation around a single bond, which results in a change in bond length or angles as illustrated in Fig. 3.2.

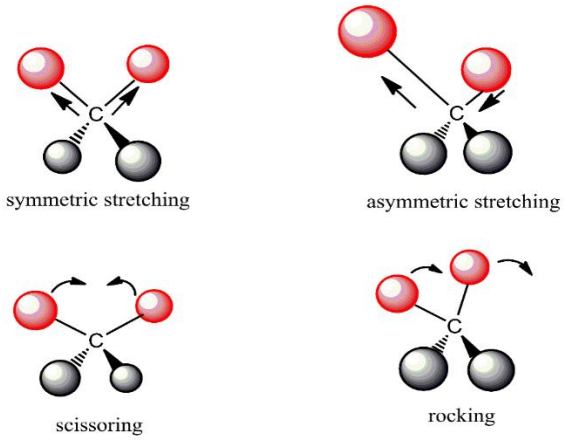

Figure 3.2: Types of molecular vibrations.[137]

Fundamental vibrations that produce a net change in dipole moment may result in IR activity. The greater the change in dipole, the stronger the intensity of the band on an IR spectrum.

[136] D.A. Skoog, D.M West, F.J. Holler, S.R Crouch. *Fundamentals of Analytical Chemistry, 8th Ed.*, Thomson Brooks/Cole, California, **2004**.
[137] L.G. Wade, *Organic Chemistry*, *5th Ed.*, Pearson Education Inc., **2003**.

Stretching vibrations involve the continuous change in interatomic distances along the axis of the bond between two atoms and is divided into two groups. Higher energy (4000-1250 cm^{-1}) is required, and it appears at a shorter wavelength.

a. Symmetric (in phase) stretching involves interatomic distances between two atoms increasing/decreasing.

b. Asymmetric (out of phase) stretching involves interatomic distances between two atoms changing in alternate/opposite directions.

Bending vibrations involve a change in the angle between two atoms and it too can be divided into two groups. Less energy (1400-666 cm^{-1}) is required, and it appears at a longer wavelength.

1. In-plane bending (atoms are in the same plane):
    a. Scissoring, where the two atoms move away/closer towards each other.
    b. Rocking, which is the change in the angle between a group of atoms.
2. Out of plane bending:
    a. Wagging that's due to the change in an angle between the plane of a group of atoms.
    b. Twisting is the change in angle between the planes of two groups of atoms.

Coupling is the result of interaction between vibrations when vibrating bonds are joined to a single, central atom and meet the following requirements:

1. The vibrations must be of the same symmetrical species for interaction to occur.
2. There needs to be a common atom between two vibrating bonds for stretching vibration.
3. There needs to be a common bond between vibrating groups for bending vibrations.

3.5 X-Ray Crystallography

The most common states of matter are solid, liquid, gas, and plasma. The solid states can be divided into crystalline or non-crystalline. Crystalline solids contain atoms, molecules, or ions arranged in an orderly repeating 3D pattern. There are various types of crystalline structures, i.e. 14 Bravais lattices, grouped into 7 crystal systems resulting in a total of 230 various space

groups.[138] X-ray crystallography is a technique used to determine the atomic and molecular structure of a solid crystal, along with visualizing the structure of a protein. The atoms/ molecules in the crystal are periodically arranged in 3 dimensions. By determining the structure of the crystal, which is a geometric arrangement of the atoms in a crystal, more properties and characteristics can be determined i.e. metal-ligand interaction. A crystal exposed to X-rays diffracts the beams into various directions, which crystallographers use to produce a 3D picture of the density of electrons within the crystal. The position of the atoms in the crystal can then be determined from the electron density. Electrons surrounding the molecule diffract as the X-rays hit them, producing a pattern known as an X-ray diffraction pattern. The diffraction patterns are processed to determine the crystal packing symmetry and size of the repeating units that form the crystal.

The intensity of the diffraction spots can be used to determine the "Structure Factor" from which a map of electron density can be calculated.

3.5.1 X-Ray Diffraction

X-ray diffraction (XRD) is a non-destructive analytical technique used for the structure determination and fingerprinting of materials in the solid state. This technique provides information about the internal lattice of a crystalline substance. Bond lengths, angles, and the unit cell dimensions can also be discovered. This generated data is then used to interpret and refine the crystal structure. The concept of X-ray diffraction is best described through Bragg's law, which is described in Par. 3.5.2.[139] A lattice is defined by the vectors x, y, and z such that there is a periodic arrangement of a point in space, so the structure looks the same when viewed from any other point. A unit cell forms the basic building blocks of the crystal structure and is the smallest group of atoms whose 3D repetition at regular arrangements produce the crystalline lattice. The unit cell comprises of the sides x, y, and z and respective angles (α, β, and γ). Miller indices, described by the hkl values, represent the reciprocal space that originates from the set of hkl planes in real space. By determining the point of origin and a set of lattice points that lie on the plane and all planes parallel to it, the hkl planes can be determined to

[138] T. Hahn, *International Tables for Crystallography, Volume A. 5th Ed.*, Kluwer Academic Publishers, Netherlands, **2002**.
[139] S.W. Wallwork, *Introduction to the Calculations of Structure Factors*, University College Cardiff Press, **2001**.

simplify the orientation and position of a plane within a lattice is specified. These lattice planes reflect X-rays and in turn conform to Bragg's law, although in principle the X-rays are actually interacting with the electrons of an atom. The lattices created by the diffracted X-rays are known as the reciprocal lattices which can be indexed; the intensity values can be assigned hkl values according to each diffraction spot with a specific intensity.

3.5.2 Bragg's law

The scattering of X-rays is dependent on the number of electrons in an atom. Bragg's law is used to define the relationship between the X-ray of incident (θ) onto the crystal surface and its angle of reflection.[140] The interaction of crystals with the X-ray produces these interferences. From Fig. 3.3 it's evident that the parallel lattice planes cause X-rays to diffract within the atom.[141] Bragg's law is used to correct the differences in phases that exist because of X-ray reflected from different planes. Only certain θ values of the reflections add up in this phase, producing strong diffracted beams that can be collected synchronically by a distant detector.

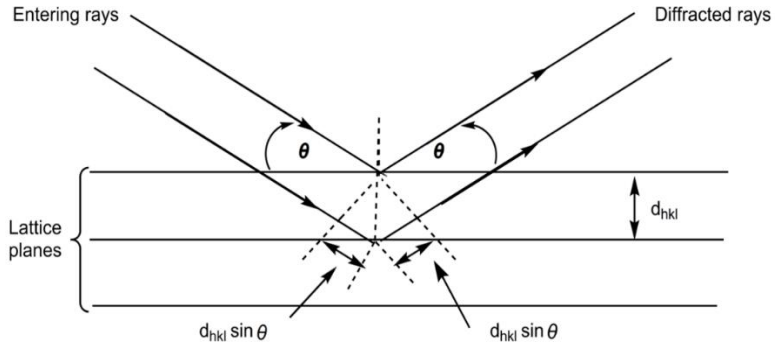

Figure 3.3: Bragg's assembly of X-Ray diffraction.

The distance between two lattice planes is represented by the inter-planar spacing $d_{hkl.}$[142] To observe maximum intensity in the diffraction pattern the Eq. 3.3 is used. [143]

$$n\lambda = 2d\sin\theta \qquad \text{..Eq. 3.3}$$

λ = Wavelength of the X-ray

[140] K.J. Laider, J.H. Meiser, B.C. Sanctuary, *Physical Chemistry 4th Ed.*, Houghton Mifflin Company, New York, **2003**.
[141] W.L. Bragg, *The Crystalline State, The Macmilan Company*, **1934**.
[142] J.M. Buerger, *X-Ray Crystallography*, Academic Press, London, **1971**.
[143] W.L. Bragg, *The Crystalline State: Volume 1,* The MacMillian Company, New York, **1934**.

d = Spacing of the crystal layers (Path difference)

θ = Incident and reflected angle (Between incident ray and scattered plane)

n = Integer number

3.5.3 Structure Factor

The structure factor F_{hkl} indicates the overall scattering of all the atoms within the unit cell relative to the single electron and can be calculated from a known structure, as expressed by Eq. 3.4.

$$F_{hkl} = \sum_{j=1}^{n} f_j \exp[i2\pi(hx_j + ky_j + lz_j)] \quad \text{..Eq. 3.4}$$

f_j is the value of the individual scattering factors of each j atom and $(x_j + y_j + z_j)$ are coordinates of each atom in the unit cell.

$$F_{hkl} = \sum_{j=1}^{n} f_j \cos[i2\pi(hx_j + ky_j + lz_j)] \quad \text{..Eq. 3.5}$$

The structure factor can be expressed in relation to the electron density ρ in the unit cell (Eq. 3.6).

$$F_{hkl} = \int \rho\,(x,y,z) e^{2\pi(hxn+kyn+lzn)} dV \quad \text{..Eq. 3.6}$$

Only the intensities of hkl reflections are measured. The intensity, $I_{hkl,}$ is proportional to the magnitude squared of the corresponding structure factor F_{hkl} and is quantitatively given in the Eq. 3.7 and 3.8 below.

$$I_o(hkl) \propto |F_o(hkl)|^2 \quad \text{..Eq. 3.7}$$

$$I = KLP|F_{hkl}|^2 \quad \text{..Eq. 3.8}$$

K is the proportionality constant, L and P are functions depending on experimental conditions.

Various methods have been developed with the aim of determining the phase structure factor.

3.5.3.1 Direct Methods

From the measured X-ray intensities, the direct method estimates the initial and expanding phases, using a mathematical formula such as the triple phase relation, the Sayre equation and the Tangent formula.[144] This method is sufficient for compounds that only contains light atoms.

3.5.3.2 Patterson Function

The Patterson function is more applicable to compounds containing heavier atoms in the unit cell. This method is based on various vectors between electron densities at two points within the unit cell (x, y, z) and (x+u, y+v, z+w). The Patterson function is given in Eq. 3.9.

$$P(u,v,w) = V^{-1} \sum h \sum k \sum l \, |F_{hkl}|^2 e^{-2\pi(hu+kv+lw)} \quad \text{..Eq. 3.9}$$

The Patterson function only yields information on where the atom lies relative to each other and not relative to the unit cells origin, resulting in the position of one or two of the heavier atoms within the unit cell.

3.5.4 Least-Square Refinement of a Structure Model

The least square refinement is used to refine the chosen model. The method compares experimental data with modelling data, producing similarities between them. The quality of the model fit is usually given by the *R*-value, where the traditional R_1 value is given in Eq. 3.10.[145]

$$R = \frac{\sum ||Fo|-|Fc||}{\sum |Fo|} \quad \text{..Eq. 3.10}$$

An *R*-value below 0.10 or less is usually acceptable and 0.05 indicates a very good correlation between the fitted experimental data and the model. The weighting factor (*w*) indicates the reliability for different measured data. The weighing factor equation is given as

$$wR^2 = \frac{\sum w(Fo2-Fc2)2}{\sum w(Fo2)2} \quad \text{..Eq. 3.11}$$

The general process of determining a crystal structure can be summarised as follows:

[144] G.M. Sheldrick, *Classical direct methods*, Gottingen, **2008**.
[145] S. Nakagawa, P.C.D Johnson, H. Schielzeth, *J. R. Soc. Interface*, **2017**, 134, 14.

Grow good crystals that are suitable in quality and size for X-ray diffraction.

Collect intensity data

Determine unit cell parameters and space group

Use collected data from X-ray diffractometer to determine heavy atom positions

Refine the structure utilizing structural refinement software

3.6 Chemical Kinetics

Chemical kinetics is concerned with the quantitative determination of the rates of chemical reactions, factors that influence the rates, and the explanation of the rates with reference to the reaction mechanisms of chemical processes. The rate of changing the concentrations of reactants or products in respect to time is followed. Concentration, pressure, temperature, and the solvent are environmental factors that can have an influence on the reaction rate. Kinetic measurements are often carried out through spectrophotometry because molecules have a unique absorption spectrum. Kinetic studies by UV/Vis spectroscopy are described through the Beer-Lambert law[146] illustrating the relationship between concentration and absorbance (Eq. 3.12):

$$\log_{10} \frac{I_o}{I_{trs}} = \varepsilon C l = A \qquad \text{..Eq. 3.12}$$

I_o = Intensity of the incident monochromatic light, I_{trs} = transmitted intensity, ε = extinction coefficient, C = concentration, l = path length through the sample and A = the absorbance.

3.6.1 Reaction Rate and Laws

The rate of a reaction is the change in the number of molecules of reactants or products over time and can be expressed in terms of the reactants or the products of the reaction. From the reaction in Scheme 3.1 below, the rate of the reaction can be expressed as Eq. 3.13 and 3.14.

[146] P.W. Atkins, *Physical Chemistry*, Oxford University Press Inc., Oxford, **1994**.

Scheme 3.1: General expression for rat reaction.

$$\mathbf{A + B} \xrightarrow{\mathbf{k}} \mathbf{C}$$

$$Rate = \frac{-d[A]}{dt} = \frac{-d[B]}{dt} = \frac{-d[C]}{dt} \quad \text{..Eq. 3.13}$$

$$= k[\mathrm{A}]^{\mathrm{m}}[\mathrm{B}]^{\mathrm{n}} \quad \text{..Eq. 3.14}$$

$d[A]$ and $d[B]$ represent the changes in the concentration of the reactants and $d[C]$ the change in the concentration of the product. The reaction proceeds over a period of time, dt. The minus sign is due to the decrease in the concentration as the reactant is being consumed, hence the rate will be a positive quantity. k is the rate constant, and the order of the reaction is represented by the m and n values with regards to the concentration of A and B, whilst the sum of m and n give the total order of the rate law (total reaction). The rate constant is independent of A and B concentrations but may be influenced by the environmental factors mentioned earlier. For a catalytic reaction, the catalyst concentration is kept constant, or one reactant is in excess with respect to the other reactants, hence during a reaction, there is a minuscule change in the concentration of the former.[147]

For a *pseudo* first-order reaction, where the [B] >> [A], the concentration of B will stay constant while the concentration of A varies (Scheme 3.2).

The rate of this reaction can be described with Eq. 3.15.

Scheme 3.2: General expression for pseudo first-order reaction.

$$a[\mathrm{A}]^{\mathrm{m}} + b[\mathrm{B}]^{\mathrm{n}} \underset{k_{-1}}{\overset{k_1}{\rightleftharpoons}} c[\mathrm{C}]$$

$$Rate = k_{obs}[\mathrm{A}]^{\mathrm{m}} - k_{-1}[\mathrm{C}] \text{ where } k_{obs} = k[\mathrm{B}]^{\mathrm{n}} \quad \text{..Eq. 3.15}$$

k_{obs} is the observed rate constant, which can be determined by varying the concentration of B. The equilibrium constant for an equilibrium reaction is given as:

$$K_{eq} = \frac{k_1}{k_{-1}} \quad \text{..Eq. 3.16}$$

[147] J.W. Moore, R.G. Pearson, *Kinetics and Mechanism, 3rd Ed.*, New York, John Wiley & Sons, Inc., **1981**.

k_1 and k_{-1} represent the rate constants for the forward and reverse reactions respectively and are obtained from the graph of k_{obs} *vs.* [L]. From the straight line of this graph, k_1 represents the slope and k_{-1} the intercept, as described in Eq. 3.17.

$$k_{obs} = k_1[L] + k_{-1} \quad \text{..Eq. 3.17}$$

From this expression, the second-order rate constant can be determined by first obtaining k_{obs} at different ligand concentrations.

By integrating the initial rate expression from t = 0 to a random point of time (t), Eq. 3.18 is obtained.

$$\ln \frac{[C]_t}{[C]_o} = -k_{obs}t \text{ or, } [C]_t=[C]_o e^{-k_{obs}t} \quad \text{..Eq. 3.18}$$

$[C]_t$ and $[C]_o$ are the concentration changes of the reactants at time = 0 and t respectively. Through the Beer-Lambert law, expressing the absorbance with regard to the concentration allows Eq. 3.19 to be derived.

$$A_{obs} = A_\infty - (A_\infty - A_o)e^{-k_{obs}t} \quad \text{..Eq. 3.19}$$

A_t = absorbance after time t and A_∞ = absorbance at infinite time (when the reaction is complete). Absorbance *vs.* time data can be used in a least-square fit to give k_{obs} for the reaction. The half-life ($t_{½}$) for a first-order reaction, meaning the time required for reactant concentration to decay by 50%, will be:

$$t_{½} = \frac{l_n}{k_{obs}} = \frac{0.693}{kobs} \quad \text{..Eq. 3.20}$$

3.7 Synthesis and Spectroscopic Characterisation

This section describes the synthesis and spectroscopic characterization of all compounds in this MSc-study containing the reactant quantities, yields, infrared (IR) data and nuclear magnetic resonance (NMR) characterization. For the NMR characterization, it should be noted that the superscripts given represent the number of the atom given in the line drawing of the respective Figure in each synthesis schematic of the functionalized ligands and co-ordinated compounds prepared during the study. Some of the complexes described in this chapter were also further characterized by means of single crystal X-ray crystallography, and kinetics will be discussed

in more detail in the chapters to come. The reader is referred to earlier parts above (Par.3.1 to 3.6) for the theory and principles of the spectroscopic techniques.

All the chemicals used for synthesis and characterization of the ligands and complexes were of analytical grade and were purchased from Sigma-Aldrich, South Africa unless otherwise stated. Reagents were used as received, without purification. All preparations were carried out in the air, except when indicated otherwise. All infrared spectra were recorded as neat samples on a Bruker Tensor 27 Standard System spectrophotometer with a laser range of 4000-370 cm-1. The UV/Vis spectra were collected and recorded on a Varian Carey 50 Conc UV/Visible spectrometer equipped with a Julabo F12-mV temperature cell regulator in a 1.000 $\pm$ 0.001 cm quartz cuvette cell. NMR spectroscopic data were obtained on Bruker Avance 300 MHz and 400 MHz spectrometers. Chemical shifts are reported in ppm and given relative to TMS for each spectrum.

3.7.1 Synthesis and Spectroscopic Characterisation of 4-R-PhonyH compounds

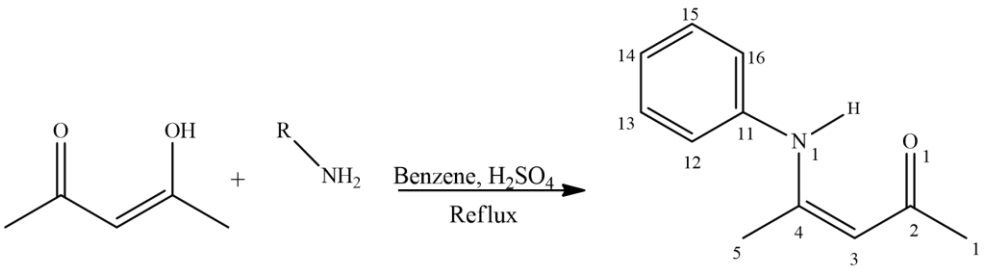

Figure 3.4: General reaction scheme of βenaminoketone ligand synthesis along with the general numbering of the uncoordinated ligand prepared.

3.7.1.1 Synthesis of Z-4-(Methylamino)pent-3-en-2-one (HNMe-acac)

A solution of acetylacetone (5.02 g, 0.05 mol), methylamine (1.55 g, 0.05 mol), and 2 drops H_2SO_4 (conc.) in benzene (60ml) were refluxed for 16 hours in a Dean-Stark trap. The solvent was then removed with a rotary evaporator before recrystallizing with acetone to obtain a yellow solid product in 3.95 g (69.7 %) yield.

IR (ATR): $\nu_{NO(Asym)}$ 1377 cm^{-1}. ^{1}H NMR (300.13 MHz, C_6D_6, 25°C): 1.3 (s, 5H) 1.9 (s, 1H) 2.1 (d, 11H) 4.8 (s, 3H) 10.8 (s, 1NH). ^{13}C NMR (75.48 MHz, C_6D_6, 25°C): 17.7 (s, 1C) 28.3 (s, 11C) 29.0 (s, 5C) 94.7 (s, 3C) 162.9 (s, 4C) 193.0 (s, 2C)

3.7.1.2 Synthesis of Z-4-(4-Methylphenyl)amino)pent-3-en-2-one (4-CH_3-PhonyH)

A solution of acetylacetone (5.01 g, 0.05 mol), 4-methylaniline (5.36 g, 0.05 mol) and 2 drops H_2SO_4 (conc.) in benzene (60 ml) were refluxed for 48 hours in a Dean-Stark trap. The solvent was then removed with a rotary evaporator before recrystallizing with acetone. Yellow crystals suitable for single crystal XRD was obtained in 6.24 g (66.0 %) yield.

IR (ATR): $\nu_{NO(Asym)}$ 1354 cm^{-1}. ^{1}H NMR (300 MHz, C_6D_6, 25°C): 1.5 (s, 5H) 1.9 (s, 1H) 2.0 (s, 114H) 4.9 (s, 3H) 6.6 (d, 12H; 16H) 6.7 (m, 13H; 15H) 12.9 (s, 1NH). ^{13}C NMR (75.48 MHz, C_6D_6, 25°C): 19.0 (s, 1C) 20.3 (s, 5C) 28.8 (s, 114C) 97.3 (s, 3C) 124.2 (d, 13C; 15C) 129.9 (d, 12C; 16C) 134.4 (s, 14C) 136.4 (s, 11C) 159.2 (s, 4C) 195.0 (s, 2C)

3.7.1.3 Synthesis of Z-4-((4-Fluorophenyl)amino)pent-3-en-2-one (4-F-PhonyH)

A solution of acetylacetone (5.01 g, 0.05 mol), 4-fluoroaniline (5.56 g, 0.05 mol) and 2 drops H_2SO_4 (conc.) in benzene (60 ml) were refluxed for 48 hours in a Dean-Stark trap. The solvent was then removed with a rotary evaporator before recrystallizing with acetone. Yellow-brown crystals suitable for single crystal XRD was obtained in 8.21 g (84.9 %) yield.

IR (ATR): $\nu_{NO(Asym)}$ 1357 cm^{-1}. ^{1}H NMR (300 MHz, C_6D_6, 25°C): 1.4 (s, 1H) 2.0 (s, 5H) 4.9 (s, 3H) 6.6 (d, 12H; 16H) 6.5 (d, 13H; 15H) 12.9 (s, 1NH). ^{13}C NMR (75.48 MHz, C_6D_6, 25°C): 18.8 (s, 1C) 29.2 (s, 5C) 96.6 (s, 3C) 115.0 (d, 13C; 15C) 126.1 (d, 12C; 16C) 134.8 (s, 11C) 158.7 (s, 14C) 159.0 (s, 4C) 195.7 (s, 2C)

3.7.1.4 Synthesis of Z-4-((4-Bromophenyl)amino)pent-3-en-2-one (4-Br-PhonyH)

A solution of acetylacetone (5.02 g, 0.05 mol), 4-bromoaniline (8.62 g, 0.05 mol) and 2 drops H_2SO_4 (conc.) in benzene (60 ml) were refluxed for 48 hours in a Dean-Stark trap. The solvent was then removed with a rotary evaporator before recrystallizing with acetone to obtain a brown solid product in 10.94 g (85.9 %) yield.

IR (ATR): $\nu_{NO(Asym)}$ 1350 cm^{-1}. ^{1}H NMR (300 MHz, C_6D_6, 25°C): 1.4 (s, 5H) 1.99 (s, 1H) 4.9 (s, 3H) 6.3 (d, 12H; 16H) 7.0 (d, 13H; 15H) 12.7 (s, 1NH). ^{13}C NMR (75.48 MHz, C_6D_6, 25°C):

18.9 (s, 1C) 29.2 (s, 5C) 98.2 (s, 3C) 117.8 (s, 14C) 125.3 (d, 12C; 16C) 131.8 (d, 13C; 15C) 138.0 (s, 11C) 158.0 (s, 4C) 178.2 (s, 2C)

3.7.2 Synthesis of [Rh(N,O-bid)(CO)$_2$] Complexes

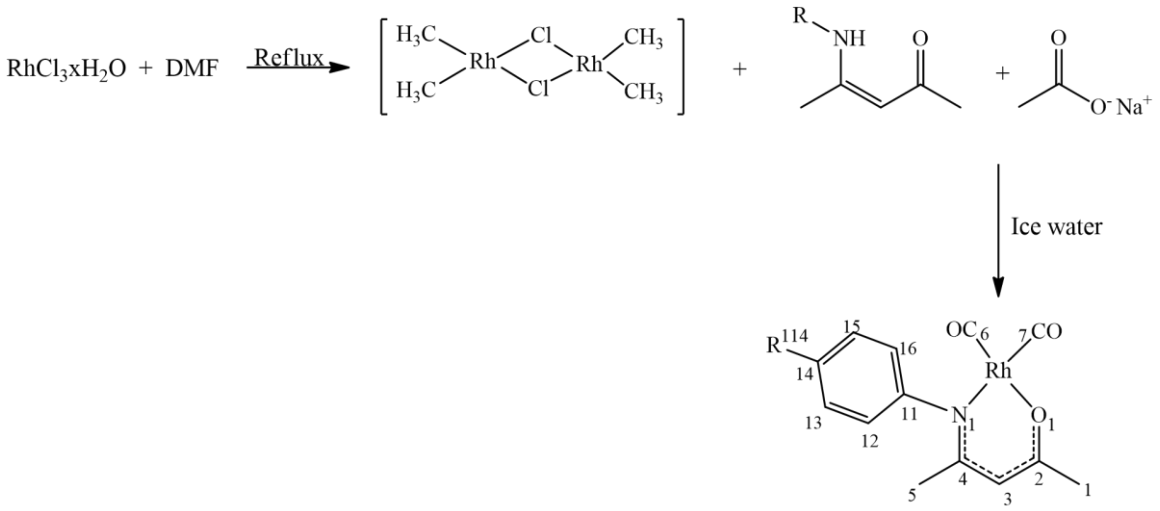

Figure 3.5: General reaction scheme of rhodium dicarbonyl complexes, along with the general numbering of the coordinated complex prepared**.**

3.7.2.1 Synthesis of Dicarbonyl-[Z-4-(Methylamino)pent-3-en-2-onato]-Rhodium(I) [Rh(NMe-acac)(CO)$_2$]

[RhCl(CO)$_2$]$_2$ was prepared by heating RhCl$_3$·3H$_2$O (0.032 g, 0.12 mmol) in 5ml DMF under reflux for 30 minutes. The red solution turned yellow due to the formation of the [RhCl(CO)$_2$]$_2$ dimer. Z-4-(Methylamino)pent-3-en-2-one (0.04 g, 0.37 mmol) and NaOAc (0.031 g, 0.37 mmol) was added to the DMF solution of [RhCl(CO)$_2$]$_2$ while stirring. The red-purple product was then precipitated by ice-water, followed by filtration. Bright purple powder in 0.02 g (83.7 %) yield was obtained.

IR (ATR): $\nu_{CO(asym)}$ 1977 cm^{-1}, $\nu_{CO(sym)}$ 2048 cm^{-1}. ^{1}H NMR (300 MHz, CDCl$_3$, 25°C) 1.4 (s, 5H) 2.0 (s, 1H) 2.2 (s, 11H) 5.0 (s, 3H). ^{13}C NMR (75.48 MHz, CDCl$_3$, 25°C) 18.8 (s, 1C) 29.3 (s, 11C) 23.2 (s, 5C) 96.6 (s, 3C) 134.8 (s, 2C) 145.5 (s, 4C) 195.8 (d, 6C; 7C)

3.7.2.2 Synthesis of Dicarbonyl-[Z-4-(4-Methylphenyl)amino)pent-3-en-2-onato]-Rhodium(I) [Rh(4-CH_3-Phony)$(CO)_2$]

$[RhCl(CO)_2]_2$ was prepared by heating $RhCl_3 \cdot 3H_2O$ (0.035 g, 0.12 mmol) in 5ml DMF under reflux for 30 minutes. The red solution turned yellow due to the formation of the $[RhCl(CO)_2]_2$ dimer. Z-4-(p-tolylamino)pent-3-en-2-one (0.048 g, 0.25 mmol) and NaOAc (0.02 g, 0.25 mmol) was added to the DMF solution of $[RhCl(CO)_2]_2$ while stirring was added to the DMF solution of $[RhCl(CO)_2]_2$. The yellow product was then precipitated by ice-water, followed by filtration and recrystallization with DCM. Yellow crystals suitable for single crystal XRD was obtained in 0.036 g (84.1 %) yield.

IR (ATR): $\nu_{CO(asym)}$ 1988 cm^{-1}, $\nu_{CO(sym)}$ 2057 cm^{-1}. ^1H NMR (300 MHz, $CDCl_3$, 25°C) 1.6 (s, 5H) 2.0 (s, 1H) 2.2 (s, 114H) 5.3 (s, 3H) 6.9 (d, 12H; 16H) 7.0 (d, 13H, 15H). ^{13}C NMR (75.48 MHz, $CDCl_3$, 25°C) 20.5 (s, 114C) 22.9 (s, 5C) 29.6 (s, 114C) 98.6 (s, 3C) 123.6 (d, 13C; 15C) 129.5 (d, 12C; 16C) 135.1 (s, 14C) 166.2 (s, 11C) 162.6 (s, 4C) 181.3 (s, 2C) 206.3 (d, 6C; 7C)

3.7.2.3 Synthesis of Dicarbonyl-[Z-4-(4-Fluorophenyl)amino)pent-3-en-2-onato]-Rhodium(I) [Rh(4-F-Phony)$(CO)_2$]

$[RhCl(CO)_2]_2$ was prepared by heating $RhCl_3 \cdot 3H_2O$ (0.033 g, 0.12 mmol) in 5 ml DMF under reflux for 30 minutes. The red solution turned yellow due to the formation of the $[RhCl(CO)_2]_2$ dimer. Z-4-((4-fluorophenyl)amino)pent-3-en-2-one (0.091 g, 0.47 mmol) and NaOAc (0.038 g, 0.47 mmol) was added to the DMF solution of $[RhCl(CO)_2]_2$ while stirring was added to the DMF solution of $[RhCl(CO)_2]_2$. The bright purple product was then precipitated by ice-water, followed by filtration and recrystallization with DCM. Brown crystals suitable for single crystal XRD was obtained in 0.04 g (91.6 %) yield.

IR (ATR): $\nu_{CO(asym)}$1990 cm^{-1}, $\nu_{CO(sym)}$ 2059 cm^{-1}. ^1H NMR (300 MHz, $CDCl_3$, 25°C) 1.7 (s, 5H) 2.1 (s, 1H) 5.3 (s, 3H) 7.0 (d, 12H; 16H) 7.0 (d, 13H; 15H). ^{13}C NMR (75.48 MHz, $CDCl_3$, 25°C) 22.6 (s, 1C) 29.2 (s, 5C) 98.6 (s, 3C) 121.3 (d, 12C; 16C) 132.9 (d, 13C; 15C) 147.1 (s, 11C) 163.2 (s, 14C) 146.9 (s, 4C) 189.0 (s, 2C) 194.3 (d, 6C; 7C)

3.7.2.4 Synthesis of Dicarbonyl-[Z-4-(4-Bromophenyl)amino)pent-3-en-2-onato]-Rhodium(I) [Rh(4-Br-Phony)$(CO)_2$]

$[RhCl(CO)_2]_2$ was prepared by heating $RhCl_3 \cdot 3H_2O$ (0.101 g, 0.38 mmol) in 5 ml DMF under reflux for 30 minutes. The red solution turned yellow due to the formation of the $[RhCl(CO)_2]_2$

dimer. Z-4-((4-bromophenyl)amino)pent-3-en-2-one (0.11 g, 0.44 mmol) was added to the DMF solution of $[RhCl(CO)_2]_2$. The green-grey product was then precipitated out ice-water, followed by filtration. A grey powder in 0.13 g (87.2 %) yield.

IR (ATR): $\nu_{CO(asym)}$ 1990 cm^{-1}, $\nu_{CO(sym)}$ 2057 cm^{-1}. ^{1}H NMR (300 MHz, $CDCl_3$, 25°C) 2.2 (s, 5H) 2.3 (s, 1H) 5.4 (s, 3H) 6.5 (d, 12H; 16H,) 7.3 (d, 13H; 15H). ^{13}C NMR (75.48 MHz, $CDCl_3$, 25°C) 22.5 (s, 1C) 23.9 (s, 5C) 98.4 (s, 3C) 118.7 (s, 14C) 127.5 (d, 12C; 16C) 132.4 (d, 13C; 15C) 145.7 (s, 11C) 158.6 (s, 4C) 180.3 (s, 2 C) 195.4 (d, 6C; 7C)

3.7.3 Synthesis of [Rh(N,O-bid)(CO)(PR_3)] Complexes

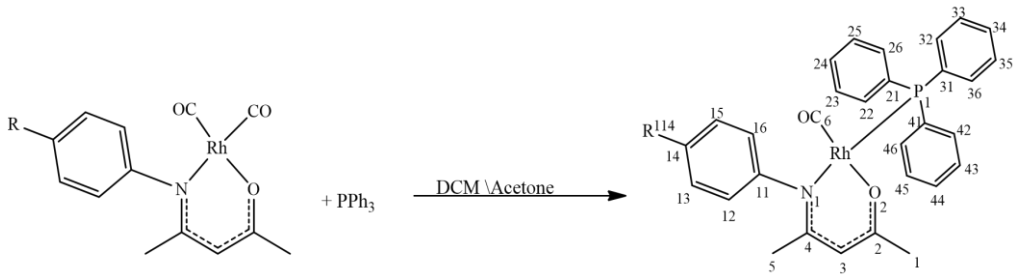

Figure 3.6: General reaction scheme of rhodium carbonyl triphenylphosphine complexes, along with the general numbering of the coordinated complex prepared.

3.7.3.1 Synthesis of Carbonyl-[Z-4-(Methylamino)pent-3-en-2-onato]-Triphenylphosphine-Rhodium(I) [Rh(NMe-acac)(CO)(PPh_3)]

To a 5 ml DCM solution of $[Rh(NMe\text{-}acac)(CO)_2]$ (0.025 g, 0.094 mmol), PPh_3 (0.024 g, 0.094 mmol) was added resulting in evolution of gas whilst solution was being stirred. The solution was left to crystallize obtaining a solid purple product in 0.047 g (100 %) quantitative yield.

IR (ATR): ν_{CO} 1956 cm^{-1}. ^{1}H NMR (300 MHz, CD_2Cl_2, 25°C) 2.2 (s, 5C) 3.3 (s, 1C) 3.8 (s, 11C) 5.2 (s, 3H) 7.7 (m, arom). ^{13}C NMR (300 MHz, C_6D_6, 25°C) 18.3 (s, 1C) 30.2 (s, 11C) 23.6 (s, 5C) 95.2 (s, 3C) 131.7 (s, 2C) 143.1 (s, 4C) 191.3 (s, 6C). ^{31}P NMR (400MHz, CD_2Cl_2, 25°C): δ 42.23 (d, $J_{Rh\text{-}P}$ 156.48Hz)

3.7.3.2 Synthesis of Carbonyl-[Z-4-(4-Methylphenyl)amino)pent-3-en-2-onato]-Triphenylphosphine-Rhodium(I) [Rh(4-CH_3-Phony)(CO)(PPh_3)]

To a 5 ml acetone solution of $[Rh(4\text{-}CH_3\text{-}Phony)(CO)_2]$ (0.035 g, 0.102 mmol), PPh_3 (0.034 g, 0.102 mmol) was added resulting in evolution of gas whilst solution was being stirred. The

solution was left to crystallize obtaining yellow crystals suitable for single crystal XRD in 0.036 g (98.8 %) yield.

IR (ATR): ν_{CO} 1983 cm^{-1}. ^{1}H NMR (300 MHz, C_6D_6, 25°C) 1.9 (s, 5H) 2.6 (s, 1H) 2.8 (s, 114H) 5.6 (s, 3H) 6.9 (d, 12H; 16H) 7.2 (d, 13H; 15H) 7.6 (m, arom). ^{13}C NMR (300 MHz, C_6D_6, 25°C) 19.9 (s, 1C) 28.2 (s, 5C) 30.0 (s, 114C) 97.2 (s, 3C) 125.9 (d, 13C; 15C) 131.2 (s, 12C; 16C) 135.9 (s, 14C) 161.2 (s, 4C) 77.3 (s, 2C) 194.2 (s, 6C). ^{31}P NMR (400MHz, CD_2Cl_2, 25°C): δ 42.85 (d, J_{Rh-P} 152.12 Hz)

3.7.3.3 Synthesis of Carbonyl-[Z-4-(4-Fluorophenyl)amino)pent-3-en-2-onato]-Triphenylphosphine-Rhodium(I) [Rh(4-F-Phony)(CO)(PPh_3)]

To a 5 ml acetone solution of [Rh(4-F-Phony)(CO)2] (0.09 g, 0.25 mmol), PPh3 (0.067 g, 0.25 mmol) was added resulting in evolution of gas whilst solution was being stirred. The solution was left to crystallize obtaining brown crystals suitable for single crystal XRD in 0.15 g (100%) quantitative yield.

IR (ATR): ν_{CO} 1965 cm^{-1}. ^{1}H NMR (300 MHz, C_6D_6, 25°C) 2.2 (s, 5H) 3.2 (s, 1H) 5.6 (s, 3H) 7.1 (d, 12H; 16H) 7.2 (d, 13H; 15H) 7.9 (m, arom). ^{13}C NMR (300 MHz, C_6D_6, 25°C) 24.9 (s, 1C) 30.4 (s, 5C) 99.6 (s, 3C) 120.2 (d, 12H; 16H) 129.7 (d, 13H; 15H) 139.0 (s, 11C) 169.0 (s, 14C) 124.3 (s, 4C) 192.0 (s, 2C) 194.8 (s, 6C). ^{31}P NMR (400MHz, CD_2Cl_2, 25°C): δ 42.89 (d, J_{Rh-P} 154.12 Hz)

3.7.3.4 Synthesis of Carbonyl-[Z-4-(4-Bromophenyl)amino)pent-3-en-2-onato]-Triphenylphosphine-Rhodium(I) [Rh(4-Br-Phony)(CO)(PPh_3)]

To a 5 ml acetone solution of [Rh(4-Br-Phony)$(CO)_2$] (0.051 g, 0.12 mmol), PPh_3 (0.033 g, 0.12 mmol) was added resulting in evolution of gas whilst solution was being stirred. The solution was left to crystallize obtaining a solid dark brown product in 0.081 g (99.9 %) quantitative yield.

IR (ATR): ν_{CO} 1968 cm^{-1}. ^{1}H NMR (300 MHz, C_6D_6, 25°C) 2.5 (s, 5H) 2.8 (s, 1H) 5.7 (s, 3H) 6.9 (d, 12H; 16H) 7.5 (d, 13H; 15H) 7.9 (m, arom). ^{13}C NMR (300 MHz, C_6D_6, 25°C) 22.9 (s, 1C) 24.2 (s, 5C) 98.7 (s, 3C) 119.2 (s, 14C) 138.0 (d, 12C; 6C) 143.63 (d, 13C; 15C) 143.0 (s, 11C) 151.4 (s, 4C) 184.2 (s, 2C) 193.0 (s, 6C). 31P NMR (400MHz, CD2Cl2, 25◦C): δ 42.91 (d, JRh-P 160.74 Hz)

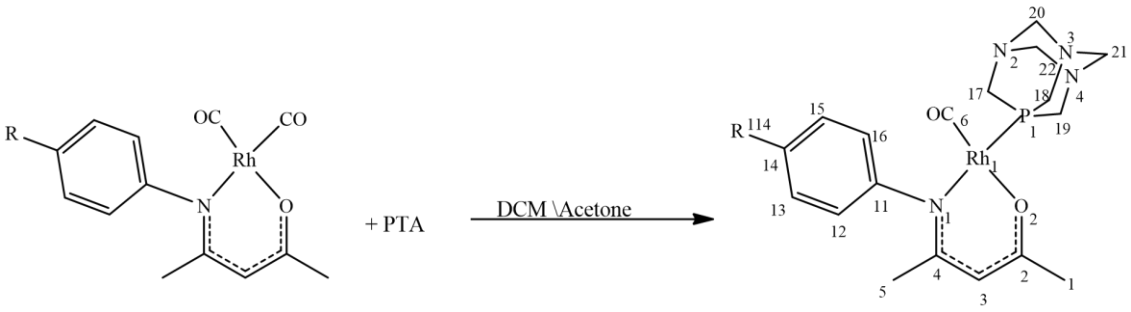

Figure 3.7: General reaction scheme of rhodium carbonyl-1,3,5-triaza-7-phosphaadamantane complexes, along with the general numbering of the coordinated complex prepared.

3.7.3.5 Synthesis of Carbonyl-[Z-4-((4-Methylphenyl)amino)pent-3-en-2-onato]-PTA-Rhodium(I) [Rh(4-CH_3-Phony)(CO)(PTA)]

To a 5 ml acetone solution of [Rh(4-CH_3-Phony)$(CO)_2$] (0.025 g, 0.074 mmol), PTA (0.11 g, 0.072 mmol) was added resulting in evolution of gas whilst solution was being stirred. The solution was left to evaporate. A yellow-brown powder was obtaining in 0.035 g (99.9 %) quantitative yield

IR (ATR): ν_{CO} 1993 cm^{-1}. ^{1}H NMR (300 MHz, C_6D_6, 25°C) 2.0 (s, 5H) 2.2 (s, 1H) 2.3 (s, 114H) 2.4 (s, 17H; 22H; 19H) 3.3(s, 18H; 20H; 21H) 5.9 (s, 3H) 7.2 (d, 12H; 16H) 7.2 (d, 13H; 15H). ^{13}C NMR (300 MHz, C_6D_6, 25°C): 19.6 (s, 1C) 21.3 (s, 5C) 24.5 (s, 114C) 4.7 (s,_17C; 22C; 19C) 81.3 (s, 3C) 82.5 (s, 18C; 20C; 21C) 123.4 (d, 13C; 15C) 130.0 (d, 12C; 16C) 136.9 (s, 14C) 164.7 (s, 4C) 187.1 (s, 2C) 19.8 (s, 6C). ^{31}P NMR (400MHz, CD_2Cl_2, 25°C): δ -36.32 (d, J_{Rh-P} 143.5 Hz)

3.7.3.6 Synthesis of Carbonyl-[Z-4-(4-Fluorophenyl)amino)pent-3-en-2-onato]-PTA-Rhodium(I) [Rh(4-F-Phony)(CO)(PTA)]

To a 5 ml acetone solution of [Rh(4-F-Phony)$(CO)_2$] (0.037 g, 0.074 mmol) PTA (0.015 g, 0.073 mmol) was added resulting in evolution of gas whilst solution was being stirred. The solution was left to evaporate. A light brown powder was obtained in 0.035 g (98.8 %) quantitative yield.

IR (ATR): ν_{CO} 2011 cm^{-1}. ^{1}H NMR (300 MHz, C_6D_6, 25°C) 2.4 (s, 5H) 379.3 (s, 1H) 2.4 (s, 17H; 22H; 19H) 3.3 (s, 18H; 20H; 21H) 5.8 (s, 3H) 7.3 (d, 12H; 16H) 7.4 (13H; 15H). ^{13}C NMR (300 MHz, C_6D_6, 25°C) 19.9 (s, 1C) 24.6 (s, 5C) 44.8 (s, 17C; 22C; 19C) 82.4 (s, 18C; 20C; 21C) 86.3 (s, 3C) 116.9 (d, 13C; 15C) 124.0 (d, 12C; 16C) 161.0 (14C) 165.7 (s, 4C) 187.0 (s, 2C) 194.7 (s, 6C). ^{31}P NMR (400MHz, CD_2Cl_2, 25°C): δ -36.54 (d, J_{Rh-P} 144.2 Hz)

3.8 Evaluation of Synthesis

A range of substituted 4-(phenylamino)pent-3-2-one (N,O-bidH) compounds were synthesised where the various electron withdrawing and donating groups were positioned on the *para* position of the N-phenyl moiety. The synthesised ligands are soluble in both polar and non-polar solvents and were found to be stable in air over a period of several months. The dicarbonyl-[4-(phenylamino)pent-3-en-2-onato]-rhodium(I) [Rh(N,O-bid)$(CO)_2$] complexes that were subsequently synthesised dissolve easily in polar solvents. All the ligands and dicarbonyl complexes were obtained in typical 60-80 % yields.

Carbonyl-[4-(phenylamino)pent-3-en-2-onato]-triphenylphosphine-rhodium(I) [Rh(N,O-bid)(CO)(PPh_3)] complexes were synthesized in virtual quantitative yields to form crystals of high quality that were suitable for crystallographic studies. Carbonyl-[4-(phenylamino)pent-3-en-2-onato]-1,3,5-triaza-7-phosphaadamantane-rhodium(I) [Rh(N,O-bid)(CO)(PTA)] complexes were synthesised in qualitative yield but the no crystals were obtained. The [Rh(N,O-bid)(CO)(PTA)] products are soluble in water and are stable in air for a period of several months.

4 X-RAY CRYSTALLOGRAPHIC STUDY OF FUNCTIONALIZED DICARBONYL-[4-R-(PHENYLAMINO) PENT-3-EN-2-ONATO]-RHODIUM(I) TRIPHENYL PHOSPHINE COMPLEXES

4.1 INTRODUCTION

It was indicated in Chapter 1 that an aim of this MSc project is to design a model catalyst for methanol carbonylation which can be evaluated in future and in turn potentially be applied to the synthesis/improvement of new and/or existing catalysts. Fulfilment of this aim requires the understanding of the molecular structure and the effect of the ligands surrounding the metal centre have on the structure and behaviour of the complex. Fundamental catalysis research thus also requires laboratory techniques such as infrared (IR) spectroscopy, nuclear magnetic resonance (NMR) spectroscopy and X-ray diffraction (XRD), in particular single crystal techniques.

This chapter focuses on analysing the structural properties through the latter XRD technique and comparing the electronic influences from the electron withdrawing and donating ligands coordinated to the metal centre. In particular, the effect of these on structural properties such as bond angles and distances of [Rh(N,O-bid)(CO)(PPh_3)] complexes (where N,O-bid = 4-(phenylamino)pent-3-en-2-onate). The structures reported in this chapter are the [Rh(4-CH_3-Phony)(CO)(PPh_3)] and [Rh(4-F-Phony)(CO)(PPh_3)] complexes, and will be compared to an isostructural complex.[128] Note that although a primary aim of this MSc study is to prepare and characterise *water-soluble* catalyst models using *e.g.* PTA as tertiary phosphine ligand, the latter complexes are notoriously difficult to crystallise and therefore the corresponding PPh_3 analogues were synthesised and studied as closely-related models.

Fig. 4.1 below illustrates the numbering scheme used in the [Rh(N,O-bid)(CO)(PPh_3)] complexes; electron withdrawing and donating groups are represented by the R on the *para* position of the N-phenyl moiety of the N,O-bid ligand. Variation in crystal packing modes of

the complex containing an electron withdrawing *vs*. donating group on the *para* position (R) of the N-phenyl moiety will also be addressed. Moreover, the dihedral angle, defined as the angle between the planes through the phenyl ring on the N,O-bid ligand and the N_1-C_4-C_2-C_3-O_1 moieties, will also be included in discussions.

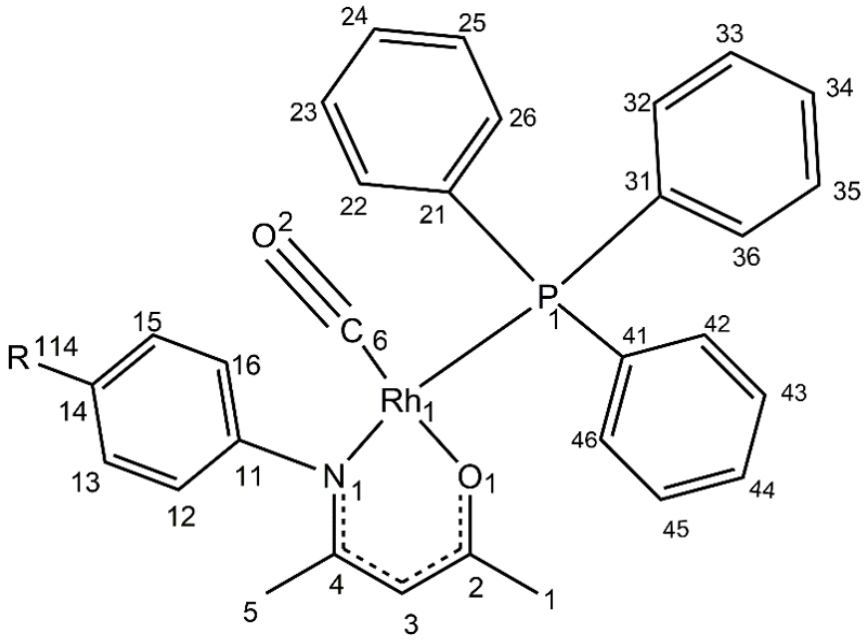

Figure 4.1: Schematic representation of [Rh(N,O-Bid)(CO)(PPh_3)] illustrating the numbering system used throughout this chapter. For the numbering in the phenyl rings, the first digit refers to the ring number and the second number refers to the position of the C-atom in the phenyl ring. R represents the electron withdrawing/donating group attached at the N-phenyl ring.

4.2 EXPERIMENTAL

The reflection data was collected on a Bruker X8 ApexII 4K diffractometer[148] equipped with graphite monochromated Mo Kα (λ = 0.71073 Å) radiation φ and ω scans collected at T = 100(2) K. After completion of the first 50 frames, the data collections were repeated for analysis of any decay of the crystal, which indicated no significant decomposition during the data collection. Frame integrations were performed using SAINT-Plus and XPREP software packages which also included data reduction.149 The data was treated for absorption effects

[148] Bruker, APEX2 (Version 1.0-27), Bruker AXS Inc., Madison, Wisconsin, USA, **2005**.
[149]Bruker, SAINT-Plus, Version 7.12 (including XPREP), Bruker AXS Inc., USA, Madison, Wisconsin, **2004**.

using the multi-scan technique SADABS[150] and the structure was solved with SHELXL using the full-matrix least-squares refinement in Olex-2.[151,152,153] All non-hydrogen atoms were refined anisotropically. Aromatic H atoms were positioned geometrically and allowed to ride on their parent atoms, with U_{iso}(H) = 1.2 U_{eq} (parent) of the parent atom with a C-H distance of 0.96 Å. The methyl and methane H atoms were placed in geometrically idealized positions and constrained to ride on its parent atoms with U_{iso}(H) = 1.5 U_{eq}(C) and U_{iso}(H) = 1.2 U_{eq} (C) and at distances of 0.96 Å and 0.97 Å respectively. The methyl hydrogen atoms were placed in geometrically idealized positions and constrained to ride on its parent atoms with U_{iso}(H) = 1.2 U_{eq}(C) and at a distance of 0.98 Å. All crystal structure graphics were constructed using the program DIAMOND 3.2.[154] Visual Crystal Structure Information System software[155] with 50% probability displacement ellipsoids for non-hydrogen atoms.

4.3 RESULTS

A summary of the general crystal data and refinement parameters for the two Rh(I) complexes reported in this study are given in Table 4.1. Supplementary data for the atomic coordinates, bond distances and angles and anisotropic displacement parameters and torsion angles are given in Appendixes Table A and B for [Rh(4-CH_3-Phony)(CO)(PPh_3)] and [Rh(4-F-Phony)(CO)(PPh_3)] respectively.

[150] Bruker, SADABS, Version **2004**/1, Bruker AXS Inc., USA, Madison, Winsconsin, **1998**.
[151] O.V. Dolomanov, L.J. Bourhis, R.J. Gildea, J.A.K. Howard, H. Pushmann, *J. Appl. Cryst.*, **2009**, 42, 339.
[152] G.M. Sheldrick, *Acta. Cryst.,* A64, **2008**, 112.
[153] A. Altomare, G. Cascarano, C. Giaovazzo, A. Guagliardi, M.C. Burla, G. Polidori, M. Camalli, *J. Appl. Cryst.*, **1994**, 27, 435.
[154] H. Putz, K. Brandenburg, DIAMOND, release 3.1b,crystal Impact GbR, Bonn, Germany, **2005**.
[155] H. Putz, K. Brandenburg, "Crystal and Molecular Structure Visualization" GbR, Kreuzherrenstr, 102, 53227 Bonn, Germany.

Table 4.1: Summary of the X-Ray crystallographic data and refinement parameters for [Rh(4-CH_3-Phony)(CO)(PPh_3)] and [Rh(4-F-Phony)(CO)(PPh_3)].

Property	**[Rh(4-CH_3-Phony)(CO)(PPh_3)]**	**[Rh(4-F-Phony)(CO)(PPh_3)]**
Empirical formula	$C_{31}H_{29}NO_2PRh$	$C_{30}H_{26}NO_2FPRh$
Formula weight	581.43	585.40
Temperature(K)	100(2)	100(2)
Crystal system	Triclinic	Monoclinic
Space group	$P\bar{1}$	$P2_1/c$
a(Å)	10.097(3)	12.525(5)
b(Å)	12.975(3)	20.145(6)
c(Å)	13.031(4)	10.537(5)
α(°)	115.528(9)	90
B(°)	94.403(2)	90
γ(°)	106.491(6)	90
Volume(Å^3)	1437.5(7)	2658.6(5)
Z	2	4
Density$_{calc.}$(g.cm^{-1})	1.343	1.463
μ/mm^{-1}	0.676	0.737
F(000)	596	1192.0
Crystal size(mm^3)	0.644 × 0.451 × 0.107	0.442 × 0.406 × 0.092
Radiation(Å)	0.71069	0.71069
Theta range(°)	3.56 to 56.74	7.66 to 55.99
Index ranges	h = -13 to 13	h = -16 to 16
Reflections collected	26411	48334
Independent reflections	6894	6404
R_{int}	0.0244	0.0318
Completeness to θ_{max} (%)	99.4	100
Data/restraints/parameters	6894/0/328	6404/0/327
Goodness-of-fit on F^2	1.054	1.095
Final *R* indexes [$I \geq 2\sigma(I)$]	R_1 = 0.0290	R_1 = 0.0260
Final R indexes (all data)	R_1 = 0.0340	R_1 = 0.0357
$\rho_{max\ and}\ \rho_{min}$ (e.Å^{-3})	0.44 and -0.38	0.34 and -0.38

4.4 CRYSTAL STRUCTURE OF [RH(4-CH_3-PHONY)(CO)(PPh_3)]

[Rh(4-CH_3-Phony)(CO)(PPh_3)] crystallises as a distorted square-planar complex in the triclinic $P\bar{1}$ space group with 2 molecules in the unit cell, and it consists of a Rh(I) metal centre which is coordinated by a mono-anionic bidentate N,O-enaminoketonato ligand (see Figs. 4.2 and 4.5). PPh_3 is coordinated *trans* to the nitrogen atom of the bidentate ligand while a carbon monoxide occupies the position *trans* to the bidentate oxygen atom.

The phenyl ring linked to the nitrogen of the bidentate ligand has an electron donating CH_3 group attached at the *para* position and the carbonyl ligand lies *cis* to the PPh_3. The complex was prepared according to the procedure described in Par. 3.7.3.2. [Rh(4-CH_3-Phony)(CO)(PPh_3)], where Phony$^-$ = 4-(phenylamino)pent-3-en-2-onate. The molecular structure is represented in Fig. 4.2, while important bond distances and angles are reported in Table 4.2 and positional and thermal parameters are given in Table A of the Appendix.

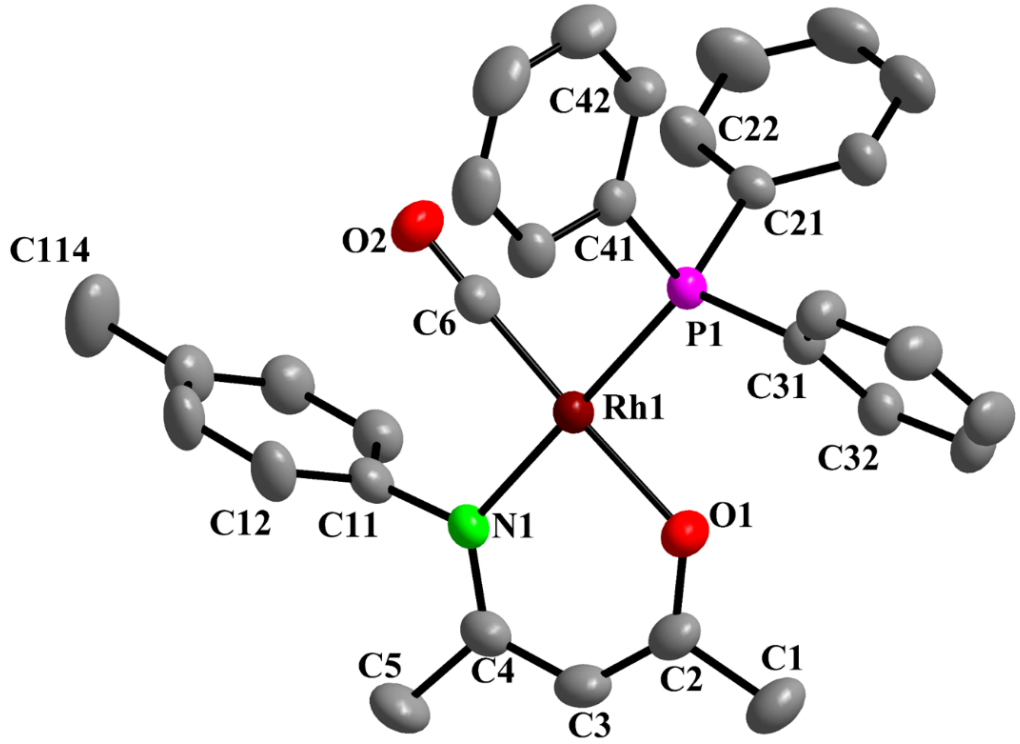

Figure 4.2: DIAMOND[155] view of [Rh(4-CH_3-Phony)(CO)(PPh_3)], where Phony = 4-(phenylamino)pent-3-en-2-onate (50% probability displacement ellipsoids). Selected hydrogen atoms and labels have been omitted for clarity. For the C atoms in the phenyl ring, the first digit refers to the ring number and the second number refers to the position of the C-atom in the phenyl ring.

Table 4.2: Selected bond distances (Å) and angles (°) for [Rh(4-CH_3-Phony)(CO)(PPh_3)].

Atoms	**Distances (Å)**	**Atoms**	**Angles (°)**
N_1-Rh_1	2.087(2)	O_1-Rh_1-N_1	89.33(8)
O_1-Rh_1	2.020(2)	O_1-Rh_1-P_1	90.72(5)
P_1-Rh_1	2.269(5)	C_6-Rh_1-P_1	86.53(7)
C_6-Rh_1	1.809(2)	C_6-Rh_1-N_1	93.46(9)
C_6-O_2	1.151(3)	O1-Rh1-C6	177.13(8)
C_{111}-N_1	1.151(3)	N1-Rh(I)-P1	179.54(5)
C_4-N_1	1.313(3)	Dihedral angle[a]	86.209(6)
C_2-O_1	1.281(3)	θ_E[b]	164.16(3)
N_1-- O_1 (Bite distance)	2.889(4)	$\nu_{(CO)}$ (cm^{-1})	1983[c]

[a] Dihedral angle between the N-C-C-C-O plane and the N-phenyl ring.

[b] The effective cone angle as defined in Par. 2.3.4.

[c] The carbonyl stretching frequency characterised in Par 3.7.3.2.

No classic hydrogen interactions were observed for [Rh(4-CH_3-Phony)(CO)(PPh_3)], with the shortest intermolecular C-H$\cdots$O distance being 2.692 Å between H_{11B} and O_2.

An intermolecular agostic C-H$\cdots$Rh interaction of distance 2.987 Å and C-H-Rh angle 153.43 ˚ was observed, as illustrated in Fig. 4.4 and described in Table 4.3. This interaction possibly compensates for the absence of other types of hydrogen interactions.

A plane constructed through O_1, N_1, C_6, and P_1 indicates that the complex is distorted square-planar, with the Rh(I) atom being displaced from the plane by -0.0089(2) Å. The angles between O_1-Rh_1-C_6 and N_1-Rh_1-P_1 are 177.13(8) ˚ and 179.54(5) ˚ respectively which account for the slight displacement of the Rh atom from the plane.

The dihedral angle between the N-C-C-C-O plane and the N-phenyl ring is 86.209(6) °, thus close to 90 ° and almost perpendicular, and underlines the steric interaction experienced by the

N-phenyl ring. Fig. 4.3 illustrates the packing style of [Rh(4-CH_3-Phony)(CO)(PPh_3)] along the c-axis, while Fig. 4.4 indicates the agostic Rh···H interaction.

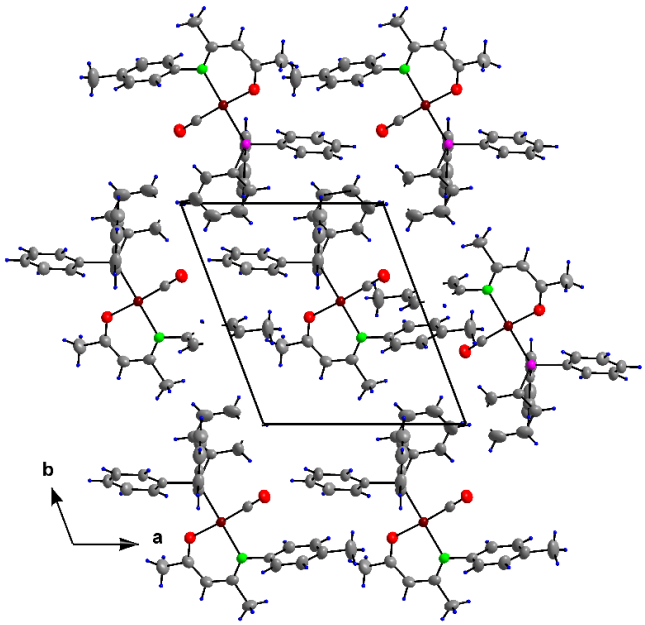

Figure 4.3: View of [Rh(4-CH_3-Phony)(CO)(PPh_3)] along the c-axis illustrating the packing style.

From the packing it is clear that the methyl groups are positioned on opposite sides of two molecules, with an inversed head-to-tail orientation. The packing appears to minimise the steric hindrance upon the rhodium(I) metal. No other interactions were observed which may be due to the steric bulk of triphenylphosphine.

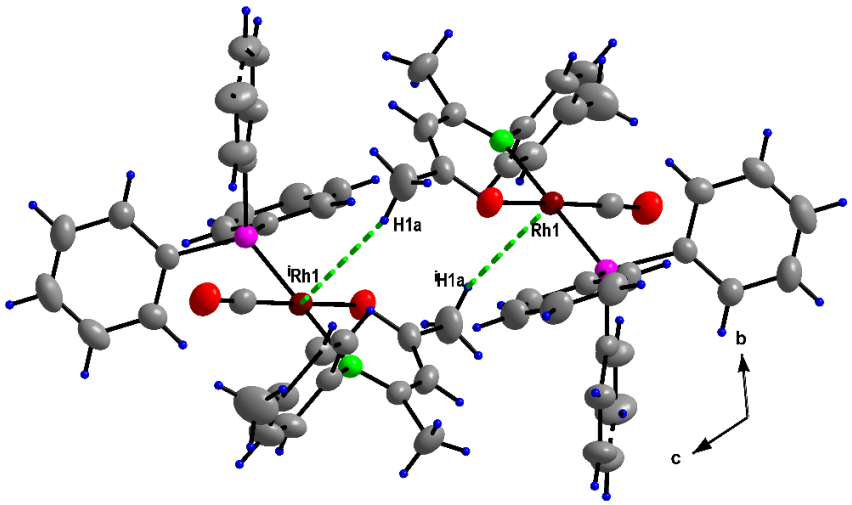

Figure 4.4: Partial unit cell of [Rh(4-CH_3-Phony)(CO)(PPh_3)] showing the agostic Rh···H interaction in dashed yellow lines. The symmetry operator is given in Table 4.

Table 4.3: Hydrogen interactions for [Rh(4-CH_3-Phony)(CO)(PPh_3) (Å and °)

D-X-A	**D_{D-X}** (Å)	**D_{X-A}** (Å)	**D_{D-A}** (Å)	**< D-X-A (°)**
$C_1 – H_{1A}$-Rh^i_1	0.96	2.987	3.870	153.43

i) Symmetry operator: 1-x; 1-y; 1-z

4.5 CRYSTAL STRUCTURE OF [RH (4-F-PHONY)(CO)(PPH_3)]

[Rh(4-F-Phony)(CO)(PPh_3)] crystallises in the monoclinic $P2_1/c$ Space Group with $Z = 4$, as a distorted square-planar complex which consists of a Rh(I) metal centre coordinated by a mono-anionic bidentate N,O-enaminoketonato ligand. The PPh_3 is coordinated *trans* to the nitrogen atom of the N,O-bid ligand with a carbon monoxide in the fourth position. The molecular structure is represented in Fig.4.5.

The [Rh(4-F-Phony)(CO)(PPh_3)] complex, where $Phony^-$ = 4-(phenylamino)pent-3-en-2-onate, was prepared according to the procedure described in Par. 3.7.3.3. The N-phenyl ring moiety of the bidentate ligand has an electron withdrawing F group at the *para* position and the carbonyl ligand lies *cis* to the PPh_3. Important bond distances and angles are reported in Table 4.4 and positional and thermal parameters for the atoms are given in Table B of the Appendix. The [Rh(4-F-Phony)(CO)(PPh_3)] molecule is isostructural to [Rh(4-CH_3-Phony)(CO)(PPh_3)] and may be visually compared in Fig. 4.2 and 4.5, although the crystals are not isomorphous as such.

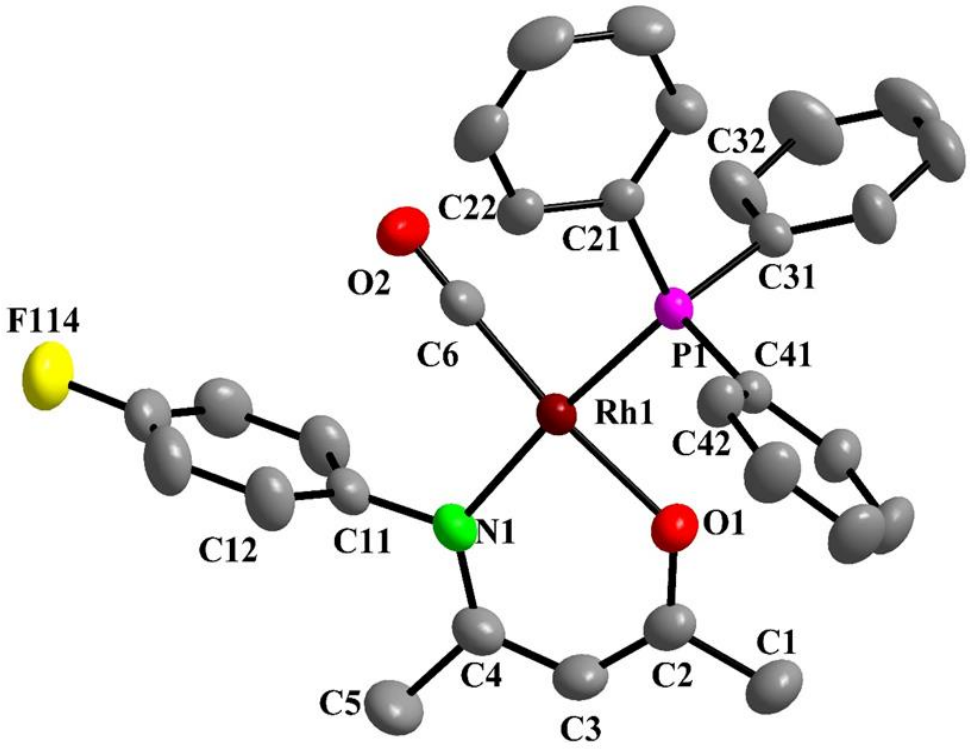

Figure 4.5: DIAMOND[155] view of [Rh(4-F-Phony)(CO)(PPh_3)], where Phony = 4-(phenylamino)pent-3-en-2-onate (50% probability displacement ellipsoids). Selected hydrogen atoms and labels have been omitted for clarity. For the C atoms in the phenyl ring, the first digit refers to the ring number and the second number refers to the position of the C-atom in the phenyl ring.

Table 4.4: Selected bond distances (Å) and angles (°) for [Rh(4-F-Phony)(CO)(PPh_3)]

Atoms	**Distances (Å)**	**Atoms**	**Angles (°)**
N_1-Rh_1	2.082(2)	O_1-Rh_1-N_1	89.34(8)
O_1-Rh_1	2.029(2)	O_1-Rh_1-P_1	90.72(6)
P_1-Rh_1	2.268(4)	C_6-Rh_1-P_1	86.47(8)
C_6-Rh_1	1.801(2)	C_6-Rh_1-N_1	93.46(9)
C_6-O_2	1.157(3)	O_1-Rh_1-C_6	172.71(8)
C_{111}-N_1	1.435(3)	N_1-Rh_1-P_1	172.83(5)
C_4-N_1	1.312(3)	Dihedral angle[a]	88.896(5)
C_2-O_1	1.278(3)	θ_E [b]	150.75(4)
N_1-O_1	2.889(4)	$\nu_{(CO)}$ (cm^{-1})	1965[c]

[a] Dihedral angle between the N-C-C-C-O plane and the N-phenyl ring.

[b] The effective cone angle as defined in Par. 2.3.4.

[c] The carbonyl stretching frequency characterised in Par 3.7.3.3.

No classic hydrogen interactions were observed for [Rh(4-F-Phony)(CO)(PPh_3)], with the shortest intermolecular C-H$\cdots$O distance being 2.550 Å for H_{35} and O_2.

An intermolecular agostic C-H$\cdots$Rh interaction of distance 3.171 Å and angle 13.34 ° was observed, as illustrated in Fig. 4.7 and described in Table 4.5. This interaction seemingly compensates somewhat for the lack of other types of interactions. A plane constructed through O_1, N_1, C_6, and P_1 indicates that the complex is distorted square-planar, with the Rh(I) atom displaced from the plane by -0.0085(3) Å. The angles between O_1-Rh_1-C_6 and N_1-Rh_1-P_1 are 172.71(8) ° and 172.83(5) ° respectively, which accounts for the slight displacement of the Rh atom from the plane.

Fig. 4.6 illustrates the packing style of [Rh(4-CH_3-Phony)(CO)(PPh_3)] along the a-axis. Fig. 4.7 illustrates the agostic Rh$\cdots$H interaction.

The dihedral angle between the N-C-C-C-O plane and the N-phenyl ring is 88.896(5)°, again close to 90°, as found in [Rh(4-CH_3-Phony)(CO)(PPh_3)] described above, which underlines the steric interaction experienced by the N-phenyl ring.

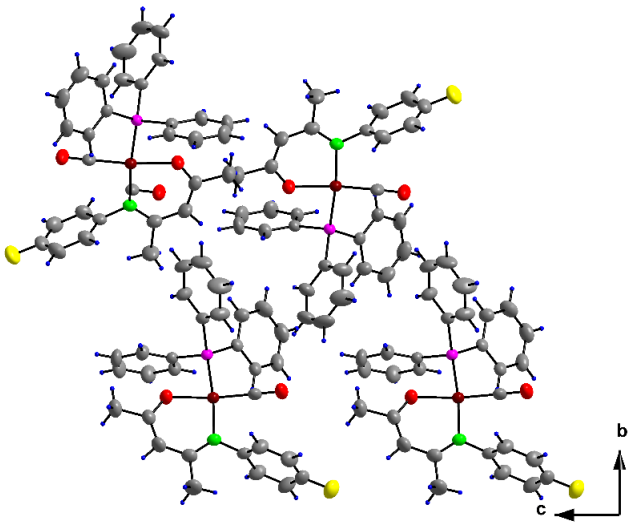

Figure 4.6: View of [Rh(4-F-Phony)(CO)(PPh3)] along the a-axis illustrating the packing style.

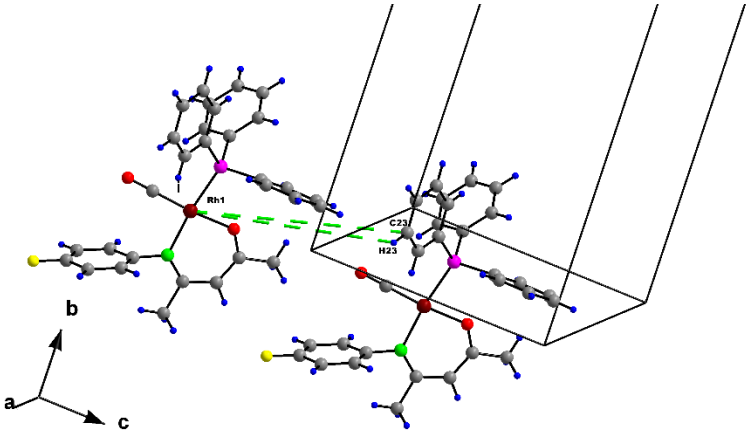

Figure 4.7: Partial unit cell of [Rh(4-CH_3-Phony)(CO)(PPh_3)] showing the agostic Rh···H interaction in dashed green lines. The symmetry operator is given in Table 4.3.

Table 4.5: Hydrogen bonds for [Rh(4-F-Phony)(CO)(PPh_3)] (Å and °)

D-X-A	**D_{D-X}** (Å)	**D_{X-A}** (Å)	**D_{D-A}** (Å)	**< D-X-A (°)**
C_{23} – H_{23}- Rh_1	3.653	3.171	0.93	13.34

i) Symmetry operator: 1+x; y; -1+z

The head-to-tail pattern observed for this [Rh(4-F-Phony)(CO)(PPh_3)] complex is clear from Fig. 4.6, whereby the triphenylphosphine ligands face each other but there is no interaction between them.

4.6 DISCUSSION

The two compounds reported here, [Rh(4-CH_3-Phony)(CO)(PPh_3)] and [Rh(4-F-Phony)(CO)(PPh_3)], are isostructural. They possess different unit cell parameters (Table 4.1) and an RMS overlay value of 0.242 Å which can be attributed to their different electron withdrawing and donating properties. The overlay structure in Fig. 4.8 indicate that principle structural differences lie at the phenyl rings of the phosphines, and there are slight deviations between the CO ligands and the 4-CH_3 and F substituents at the para position of the N-phenyl rings.

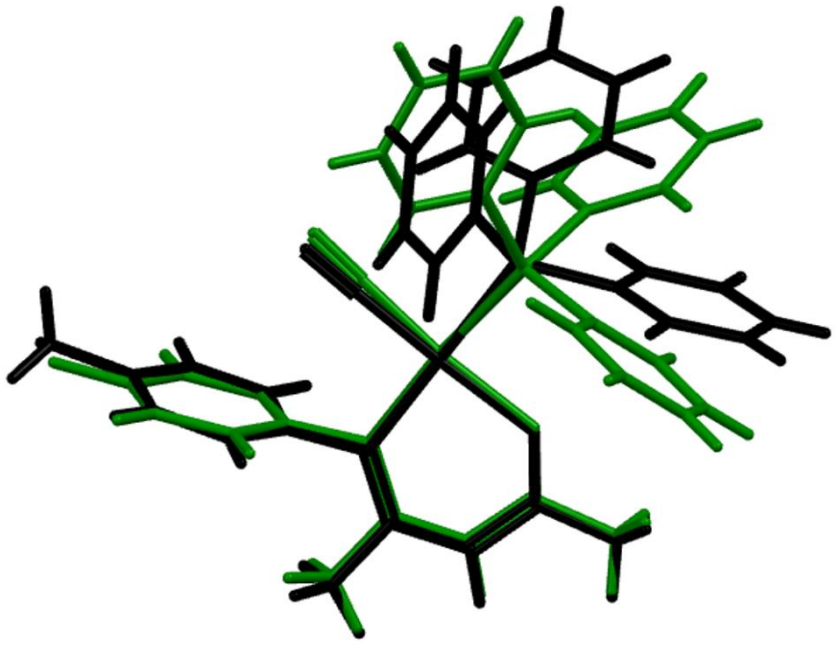

Figure 4.8: Overlay figures of [Rh(4-CH_3-Phony)(CO)(PPh_3)] (black) and [Rh(4-F-Phony)(CO)(PPh_3)] (green). RMS value = 0.242 Å

The solid-state cell volume of [Rh(4-F-Phony)(CO)(PPh_3)] (2658.6(5) $Å^3$) is much larger than that of [Rh(4-CH_3-Phony)(CO)(PPh_3)] (1437.5(7) $Å^3$) as required by the triclinic and

monoclinic crystal systems and the number of molecules in the unit cells, respectively. However, when normalised, the relative solid-state molecular volumes (664 vs. 719 $Å^3$ for the two complexes respectively), clearly illustrate the relative larger volume required by the methyl substituent *vs*. that of the fluoro compound.

Intermolecular C-H···Rh agostic interactions are observed in both [Rh(4-CH_3-Phony)(CO)(PPh_3)] and [Rh(4-F-Phony)(CO)(PPh_3)].

Table 4.6 compares the three isostructural [Rh(N,O-bid)(CO)(PPh_3)] complexes, similar to those shown in Fig. 4.9 (no's. III and V, this study; compared to IV) but having different electronic withdrawing and donating groups on the *para* position of the phenyl ring coordinated to the N atom.

The three [Rh(4-R-Phony)(CO)(PPh_3)] complexes are isostructural and chemically similar. The studied complexes all display no classic hydrogen bonds but agostic interactions were observed. It is clear that the solid-state properties as reported within the two complexes analysed in this dissertation are very similar to the [Rh(4-Cl-Phony)(CO)(PPh_3)] complex.[128]

The absence of significant intermolecular hydrogen interactions, other than the intermolecular agostic ones, were noted in [Rh(N,O-bid)(CO)(PPh_3)] complexes. These complexes have different electron withdrawing and donating groups and are correlated in Table 4.6. The bite angles (N_1-Rh_1-O_1) all lie within the 89° range. A noticeable decrease in the effective Tolman angle θ_E value between the various electron withdrawing and donating groups is observed in the order of 4-CH_3>4-Cl>4-F from Table 4.6. A similar correlation seems prevalent between the effective Tolman angle and the J_{Rh-P}: as the effective Tolman angle decreases the J_{Rh-P} increases.

Table 4.6: Summary of important distances (Å) and angles (°) for synthesised complexes vs. a similar complex[9] from literature.

	[Rh(4-CH_3-Phony)(CO)(PPh_3)]	**[Rh(4-F-Phony)(CO)(PPh_3)]**	**[Rh(4-Cl-Phony)(CO)(PPh_3)]**[128]
Rh_1-N_1(Å)	2.087(2)	2.082(2)	2.080(2)
Rh_1-O_1(Å)	2.020(2)	2.029(2)	2.034(2)
Rh_1-P_1(Å)	2.269(5)	2.268(4)	2.2627(8)
Rh_1-C_6(Å)	1.809(2)	1.801(2)	1.814(3)
N_1-Rh_1-O_1(°)	89.33(8)	89.34(8)	89.04(9)
O_1-Rh_1-P_1(°)	90.72(5)	90.72(6)	90.75(6)
P_1-Rh_1-C_6(°)	86.53(7)	86.47(8)	86.56(9)
C_6-Rh_1-N_1(°)	93.46(9)	93.46(9)	93.7(1)
N_1-Rh_1-P_1(Å)	179.54(5)	172.83(5)	178.39(7)
O_1-Rh_1-C_6(Å)	177.13(8)	172.71(8)	176.61(1)
Dihedral angle[a] (°)	86.209(6)	88.896(5)	83.76(9)
θ_E [b](°)	164.16(3)	150.75(4)	154.89(3)
H···Rh	2.987	3.171	2.90
ν_{CO}(cm^{-1})[c]	1983.9	1965.6	1986.2
δ^{31}P(ppm)[d]	42.8	42.2	44.4
J_{Rh-P} (Hz)[e]	152.1	156.4	155.7

[a] Dihedral angle between the N-C-C-C-O plane and the N-phenyl ring.

[b] The effective cone angle, as defined in Table 4.2 and Table 4.4.

[c] The carbonyl stretching frequency characterised in Par 3.7.3.2 and Par 3.7.3.3.

[d] Chemical shift characterised in Par 3.7.3.2 and Par 3.7.3.3.

[e] Coupling constant characterized in 3.7.3.2 and Par 3.7.3.3.

The two structures reported in this MSc dissertation are further compared to other [Rh(N,O-Bid)(CO)(PPh3)] complexes reported in literature (as illustrated in Fig. 4.9) and are discussed next, see also Table 4.7.

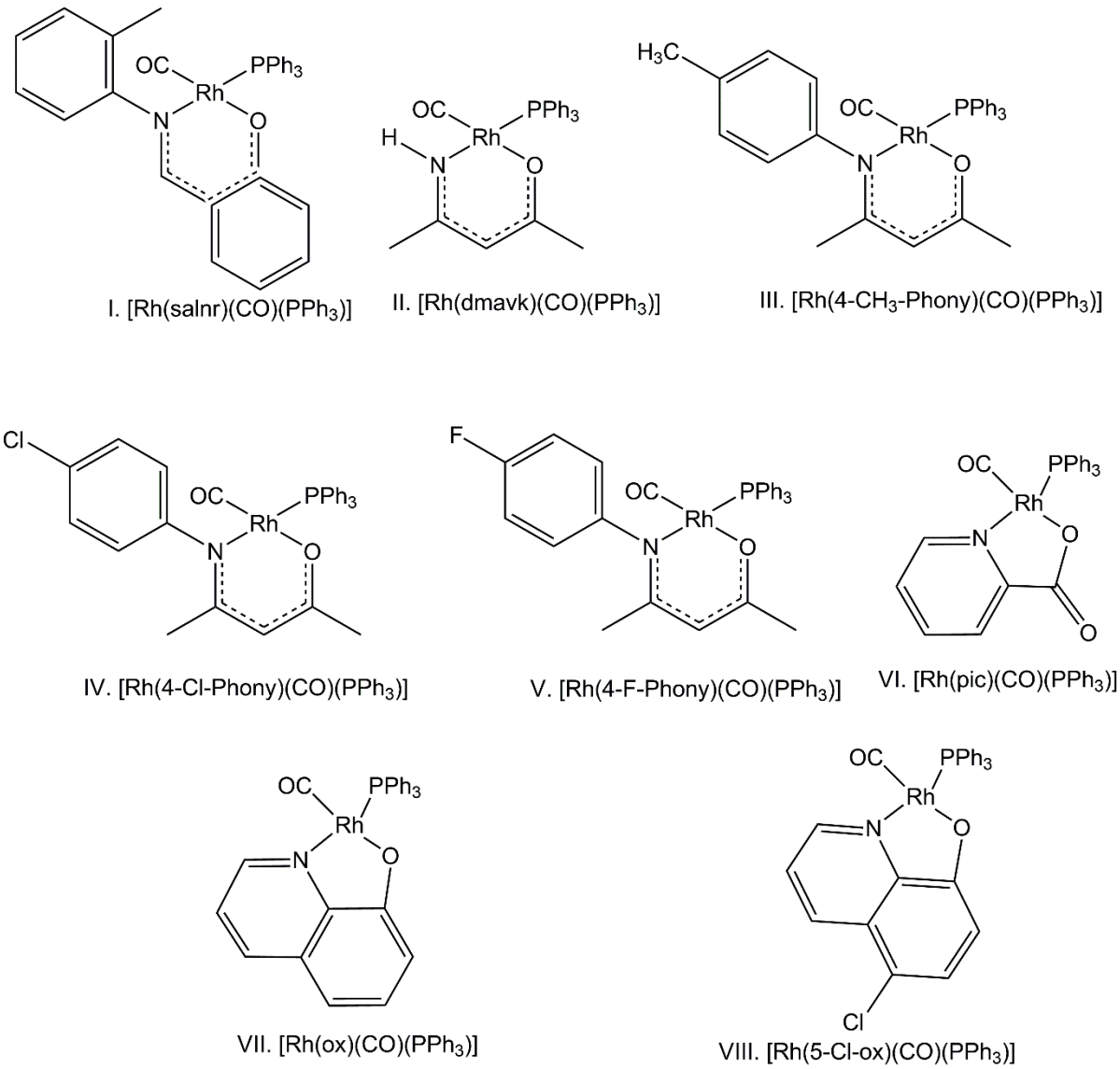

I. [Rh(salnr)(CO)(PPh$_3$)] II. [Rh(dmavk)(CO)(PPh$_3$)] III. [Rh(4-CH$_3$-Phony)(CO)(PPh$_3$)]

IV. [Rh(4-Cl-Phony)(CO)(PPh$_3$)] V. [Rh(4-F-Phony)(CO)(PPh$_3$)] VI. [Rh(pic)(CO)(PPh$_3$)]

VII. [Rh(ox)(CO)(PPh$_3$)] VIII. [Rh(5-Cl-ox)(CO)(PPh$_3$)]

Figure 4.9: Structures of complexes [Rh(N,O-Bid)(CO)(PPh$_3$)] complexes with N,O-Bid = salnr,[162] dmavk,[159,157] 4-CH$_3$-Phony,[a] 4-Cl-Phony,[158] 4-F-Phony,[a] pic,[160,161] quin,[160] ox, [161,162] and 5-Cl-ox.[161,162]

Table 4.7: Correlation between Rh-P bond distances and NMR parameters of [Rh(N,O-Bid)(CO)(PPh_3)] complexes.

No.	L,L'-Bid-PR_3[a]	N[b]	O	Ring size	Bite angle (°)	Rh-P distance (Å)	δ ^{31}P (ppm)	$^1J_{Rh-P}$ (Hz)
I	salnr-PPh_3 [156]	N	O	6	88.7	2.281(2)		
II	dmavk-PPh_3 [157,158]	N	O	6	87.4	2.275(1)	41.5	148.0
III	4-CH_3-Phony-PPh_3[c]	N	O	6	89.33(8)	2.269(5)	42.8	152.1
IV	4-Cl-Phony-PPh_3[158]	N	O	6	89.04(9)	2.267(8)	44.4	155.7
V	4-F-Phony-PPh_3[c]	N	O	6	89.34(8)	2.268(4)	42.2	156. l
VI	pic-PPh_3 [160,161]	N	O	5	78.9	2.262(2)	40.2	161.9
VII	ox-PPh_3[159,160]	N	O	5	80.0	2.261(2)	41.4	161.1
VII	5-Cl-ox-PPh_3[161]	N	O	5		2.248(1)	-	166.0

Notes:[a] L,L'-Bid ligands: 4-CH_3-PhonyH = 4-(4-methylphenylamino)pent-3-en-2-one; 4-F-PhonyH = 4-(4-fluorophenylamino)pent-3-en-2-one; 4-Cl-PhonyH = 4-(4-hlorophenylamino)pent-3-en-2-one; 5-Cl-oxH = 5-chloro-8-hydroxyquinoline; dmavkH = dimethylaminovinylketone; oxH = 8-hydroxyquinoline; picH = picolinic acid; salnrH = N-*o*-tolylsalicylaldiminato;

[b] P atom *trans* to N atom.

[c] From this study.

Table 4.7 compares Rh-P bond distances and NMR parameters of [Rh(N,O-Bid)(CO)(PPh_3)] complexes. A correlation between the Rh-P, J_{Rh-P} and δ ^{31}P shows that as the Rh-P bond distance increases, the coupling constant and the chemical shift decreases.

It is clear that the [Rh(N,O-bid)(CO)(PPh_3)] complexes obtained in this study behave very similar than corresponding complexes reported in the literature, making the inclusion of the two structures reported herein, relevant in the broader context of these model catalyst Rh(I) complexes.

[156] J.G. Leipoldt, S.S. Basson, E.C. Grobler, A. Roodt, *Inorg. Chim. Acta.*, **1985**, 99, 13.
[157] M.R. Galding, T.G. Cherkasova, L.V. Osetrova, Y.S. Varshavsky, *J. Organomet. Chem.*, **2001**, 628, 195.
[158] J.L. Damoense, W. Purcell, A. Roodt, J.G. Leipoldt, *Rhodium Express*, **1994**, 5,10.
[159] D.E. Graham, G.J. Lamprecht, I.M. Potgieter, A. Roodt, J.G. Leipoldt, *Transition Met. Chem*., **1991**, 16, 193.
[160] G.J.J. Steyn, A. Roodt, A.J.G. Leipoldt, *Rhodium Express*, **1993**, 1, 25.
[161] J.M. Janse van Rensburg, A. Muller, A. Roodt, *Acta Cryst*., **2007**, E63, m3015–m3016.

4.7 Conclusion

Two model complexes have been synthesised and crystallised, and successfully characterised by single crystal X-ray diffraction as reported in this chapter. The electron donating [Rh(4-CH_3-Phony)(CO)(PPh_3)] and electron withdrawing [Rh(4-F-Phony)(CO)(PPh_3)] complexes were studied and characterised, and were found to be stable in solution and solid state. This might be attributed to the N-substituted phenyl ring in the bidentate ligand which crystallises almost perpendicular to the square plane, exerting a steric interaction and as such preventing for example reaction with molecular oxygen.

The two complexes crystallized iso-structurally and both do not display significant intermolecular interactions. Despite the difference in the electronic properties of the atom on the para position of the N-phenyl group, large differences between the bond distances and angles were not observed. Instead, the differences at the phenyl rings of the phosphine ligands were the most significant. An important conclusion form this is that some adjustments in future may be done on this position without significantly influencing the metal center.

Preliminary kinetic studies of CO substitution from [Rh(4-CH_3-Phony)$(CO)_2$] by PTA as entering ligand has been investigated and are reported in the next chapter, along with a preliminary comparison of iodomethane oxidative addition to [Rh(4-CH_3-Phony)(CO)(PTA)] and [Rh(4-CH_3-Phony)(CO)(PPh_3)].

5 KINETICS AND EQUILIBRIUM STUDY OF CARBONYL SUBSTITUTION BY TERTIARY PHOSPHINES IN [Rh (4-CH_3-PHONY)$(CO)_2$] AND IODOMETHANE OXIDATIVE ADDITION TO [RH(4-CH_3-PHONY)(CO)(PR_3)] COMPLEXES

5.1 INTRODUCTION

Kinetic investigations supply researchers with insight into the mechanism by which chemical modifications occur. In particular, various homogeneous catalysis systems are based on rhodium metal complexes in the presence of tertiary phosphines as catalyst precursors, wherein the rates at which the processes take place has a direct influence on the effectivity of the system.[162,163,164,165,166] Important information regarding the intimate mechanism of rhodium systems exists that can be used to reveal important information leading to the designing and optimising of new catalyst species. Thus, this study deals with the preliminary kinetic investigation of the reactions between two types of "bench-marking" reactions, well-known to occur in many catalytic cycles: [167,168] (a) substitution of carbon monoxide from [Rh(4-CH_3-Phony)$(CO)_2$] by PTA to yield [Rh(4-CH_3-Phony)(CO)(PTA)], and (b) iodomethane (MeI)

[162] B. Moasser, W.L. Gladfelter, D.C. Roe, *Organometallics*, **1995**, 14, 3832.
[163] A. Van Rooy, E.N. Orji, P.G.J. Kramer, P.W.N.M. Van Leeuwen, *Organometallics*, **1995**, 14, 34.
[164] H. Yamashita, B.L. Roan, T. Sakakura, M. Tanaka, *J. Mol. Catal.*, **1993**, 81, 255.
[165] A.M. Trzeciak, T. Glowiak, R. Grzybek, J.J. Ziolkowski, *J. Chem. Soc. Dalton. Trans.*, **1997**, 1831.
[166] A.M. Trzeciak, E. Wolszczak, J.J. Ziolkowski, *New. J. Chem.*, **1996**, 20, 365.
[167] S. Polovina, M. Vojtech, I. Dejanovi, A. Grujic, M. Stijepovic, *ACS*, **2018**, 32, 6378.
[168] T. Bligaard, R.M. Bullock, C.T. Campbell, J.G. Chen, B.C. Gates, R.J. Gorte, C.W. Jones, W.D. Jones, J.R. Kitchin, S.L. Scott, *ACS Catal.*, **2016**, 6, 2590.

oxidative addition to [Rh(4-CH_3-Phony)(CO)(PPh_3)] and [Rh(4-CH_3-Phony)(CO)(PTA)]. Illustrations of these complexes are seen in Fig. 5.1.

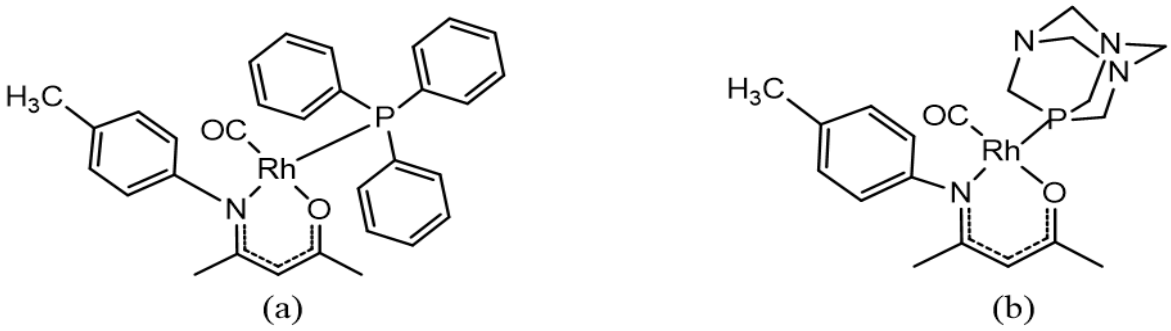

Figure 5.1: Diagram of (a) [Rh(4-CH_3-Phony)(CO)(PPh_3)] and (b) [Rh(4-CH_3-Phony)(CO)(PTA)] investigated in this study.

This insight can in turn be used to provide more fundamental knowledge for future design of a potential model water-soluble homogeneous rhodium(I) catalyst. By understanding the effect of the electron donating methyl group in the *para* position of the N-phenyl ring of the ligand that was reacted with the rhodium(I) dicarbonyl chlorido dimer to form [Rh(4-CH_3-Phony)$(CO)_2$], the design of a catalyst becomes more viable.

In this chapter [Rh(4-CH_3-Phony)(CO)(PPh_3)] and [Rh(4-CH_3-Phony)(CO)(PTA)] are investigated through preliminary kinetic studies. The rate of substituting the CO in [Rh(4-CH_3-Phony)$(CO)_2$] with PTA to form [Rh(4-CH_3-Phony)(CO)(PTA)] complex was studied, along with the oxidative addition of iodomethane to [Rh(4-CH_3-Phony)(CO)(PPh_3)] and [Rh(4-CH_3-Phony)(CO)(PTA)]. The substitution of d^8 square-planar metal complexes offers the opportunity to investigate the reactivity of a metal centre within metal complexes containing different coordinated ligands.

The oxidative addition mechanism of iodomethane to [Rh(4-CH_3-Phony)(CO)(PPh_3)] and [Rh(4-CH_3-Phony)(CO)(PTA)] are discussed in this section as obtained from literature and based thereupon, the rate reaction that could be compared to the data found from the substitution reaction of [Rh(4-CH_3-Phony)$(CO)_2$] with PTA.

5.2 EXPERIMENTAL

All reagents used were of analytical grade and used as purchased from Sigma-Aldrich, South Africa, unless otherwise stated. The rhodium metal complexes were synthesised, characterised and purified as described in Par. 3.7.1. [Rh(4-CH_3-Phony)$(CO)_2$], [Rh(4-CH_3-Phony)(CO)(PPh_3)], and [Rh(4-CH_3-Phony)(CO)(PTA)] complexes were prepared as described as in Par. 3.7.2.2; 3.7.3.2, and 3.7.3.5.

The FT-IR spectra were recorded as liquid samples in dichloromethane in a NaCl cell on a Bruker Tensor 27 spectrometer in the range of 2200-1650 cm^{-1}, where the rhodium species lie. The IR spectrometer was equipped with a temperature cell regulator (accurate within 0.3°C). The kinetic measurements were conducted on an infrared Digilab FTS 2000 Fourier transform spectrometer using a He-Ne laser at 632.3 nm.

The ^{31}P NMR spectra were obtained on a 400 MHz Bruker spectrometer operating at the ^{31}P frequency of 161.98 MHz. The ^{31}P chemical shifts are reported relative to 85 % H_3PO_4 (0 ppm) external standard. The NMR was locked and shimmied with CD_2Cl_2, but all kinetic measurements were conducted in dichloromethane unless otherwise indicated.

UV-Vis measurements were conducted on a Varian Carey 50 Conc. spectrometer in a 1.00 cm quartz cuvette cell equipped with a Julabo F12-mV temperature cell regulator accurate within 0.1°C. The substitution reaction of the rhodium(I) dicarbonyl species with PTA and the iodomethane oxidative addition to rhodium(I) tertiary phosphines complexes was investigated through UV/Vis.

All the kinetic experiments were performed under *pseudo* first order conditions and the data was conducted by means of Microsoft Office Professional Plus 2010 and MicroMath Scientist for Windows.[169]

5.3 TREATMENT OF DATA

All the reactions conducted in this study were performed under *pseudo* first-order conditions, where [L] >> [Rh]. The observed *pseudo* first-order rate constants for the substitution and oxidative addition reactions were obtained from fitting experimentally obtained data as a function of time. The incorporation of the Beer-Lambert law with the first order exponential

[169] MicroMath Scientist for Windows, Version 2.01, Copyright © **1986-1995**, MicroMath, Inc.

yields the following equation for the analysis of absorbance change vs. time in the simple-first order reactions.

$$A_t = A_\infty(A_\infty - A_o)e^{k_{obs}t} \quad \text{..Eq. 5.1}$$

A_t and A_o are the absorbances at time t and o, A_∞ is the absorbance at completion of the reaction and k_{obs} is the pseudo first order rate constant of the reaction determined from the least-square fit of absorbance *vs.* time.

The substitution and oxidative addition reactions in this study were conducted at various PTA and CH_3I concentrations. The observed *pseudo* first order rate constant data were plotted against [PTA] and [MeI]. The graphs of k_{obs} *vs.* [L] are used to obtain k_1 and k_{-1} in a straight line, as described in Eq. 5.2. k_1 and k_{-1} represent the rate constants for the forward (slope) and reverse (intercept) reactions respectively.

$$k_{obs} = k_1[L] + k_{-1} \quad \text{..Eq. 5.2}$$

From this expression, the second order rate constant (Eq. 5.3) can be determined by first obtaining k_{obs} at different ligand concentrations. Eq. 5.4 is used to determine the equilibrium constant (K_1).

$$k_1 = \frac{k_{obs}}{[PTA]} \quad \text{..Eq. 5.3}$$

$$K_1 = \frac{k_1}{k_{-1}} \quad \text{..Eq. 5.4}$$

5.4 RESULTS AND DISCUSSION

5.4.1 GENERAL REACTION MECHANISM FOR SUBSTITUTION STUDIES

Rhodium(I) dicarbonyl complexes of the form [Rh(L,L'-bid)(CO_2)] are well known for undergoing substitution reactions with tertiary phosphines as entering nucleophiles with the corresponding loss of one carbonyl ligand.[170,171,172] The general carbonyl substitution reaction of (N,O-enaminoketonato) dicarbonyl rhodium(I), [Rh(N,O-bid)($CO)_2$] with water soluble,

[170] F. Bonati, G. Wilkinson, *J. Chem. Soc.*, **1964**, 3156.
[171] S. Serron, J. Huang, S.P. Nolan, *Organometallics*, **1998**, 17, 534.
[172] F.R. Hartley, *Supported Metal Complexes*, D. Reidel Publishing Company, The Netherlands, Dordrecht, **1985**, 223.

non-sterically demanding, 1,3,5-triaza-7-phosphaadamantane, is therefore considered in this study as illustrated in Fig. 5.2.

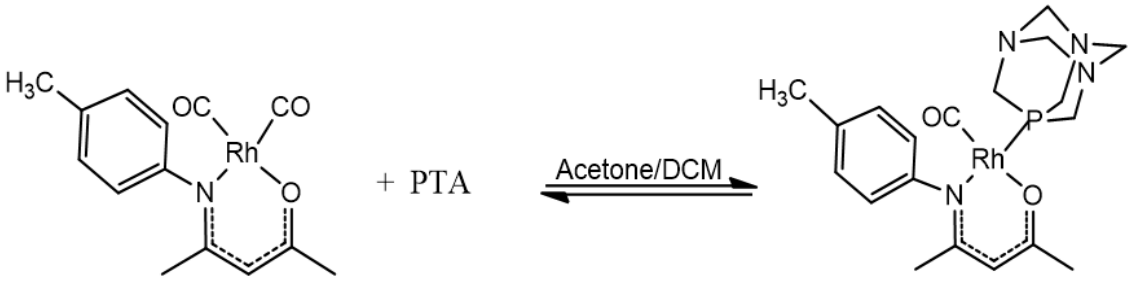

Figure 5.2: General carbonyl substitution reaction of [Rh(4-CH_3-Phony)$(CO)_2$] by PTA.

As discussed in Par 2.4.4.1, square planar substitution reactions by entering nucleophiles may follow a direct or solvent associative pathway.[173] The pathways are illustrated in Fig. 5.3 where the species are numbered as follows: 1. [Rh(4-CH_3-Phony)$(CO)_2$] is the reactant, 2. [Rh(4-CH_3-Phony)(CO)(PTA)] is the substituent product and 3. [Rh(4-CH_3-Phony)(CO)(S)] a potential parallel solvent complex.

Scheme 5.1: Schematic representation of the square planar substitution reaction with parallel direct substitution and solvent assisted pathways.

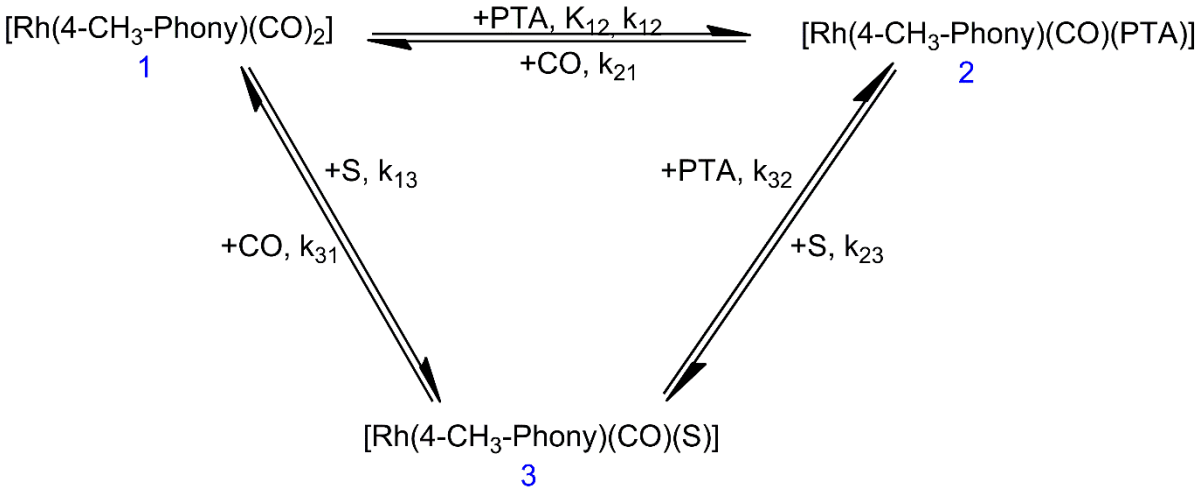

The liberated CO ligand, when substituted, is important in the substitution process under certain conditions, hence it has been incorporated in Eq. 5.5. The reaction in Scheme in Fig. 5.1 can be used to derive an expression that describes the relationship between the pseudo first-order

[173] L.I. Elding, A.B. Gröning, O. Gröning, *J. Chem. Soc., Dalton Trans.*, **1981**, 1093.

rate constant k_{obs}, and the concentrations of the various species in solution under conditions where an appreciable (but not very large) equilibrium (K_{eq}) exists as seen in Eq. 5.5.[174]

$$k_{obs} = k_{12}([PTA] + \frac{[CO]}{K_{eq}}) + \frac{\frac{k_{13}k_{32}}{K_{eq}k_{31}}[CO] + k_{13}\frac{k_{32}}{k_{31}}[PTA]}{[CO]+\frac{k_{32}}{k_{31}}[PTA]} \quad \text{..Eq. 5.5}$$

K_{eq}, in Equation 5.5 represents the equilibrium constant for the formation of the final product [Rh(4-CH_3-Phony)(CO)(PTA)]. The rate of the forward (k_{12}) reaction divided by the rate of the reverse (k_{21}) reaction is used to define the equilibrium constant, with the direct and solvent assisted pathways in Equilibrium, giving equation 5.6.[13]

$$K_{eq} = \frac{k_{12}}{k_{21}} = \frac{k13\ k32}{k31\ k23} \quad \text{..Eq. 5.6}$$

The simplified two-term rate law (Eq. 5.7) is encountered in square planar reactions as a result of having a K_{eq} that is very large.[175,176,177,178]

$$k_{obs} = k_{12}[PTA] + k_{13} \quad \text{..Eq. 5.7}$$

If the observed rate constant under these conditions is plotted against [PTA], a linear relationship will be observed where the slope is indicated as the k_{12} term and the intercept as the k_{13} constant (solvent pathway).

The second-order rate constant (Eq. 5.8) describes the substitution pathway related to the reaction of [Rh(4-CH_3-Phony)$(CO)_2$] and PTA, that (assuming non-equilibrium conditions in a non-coordinating solvent; thus a negligible k_{13} step) depends mainly on the entering ligand as evident from Scheme 5.1 and Eq. 5.7.

$$k_{12} = \frac{k_{obs}}{[PTA]} \quad \text{..Eq. 5.8}$$

Under equilibrium conditions (small K_{eq} values) the concentration of the leaving group, CO in this case, can contribute significantly to the overall rate and the full equation (Eq. 5.5) describing the observable rate is obeyed.

[174] J.Y. Seguin, M. Zador, *Inorg. Chim. Acta.*, **1976**, 20, 203.
[175] D.J.A. De Waal, W. Robb, *Inorg. Chim. Acta.*, **1978**, 26, 91.
[176] H.B. Gray, R.J. Olcott, *Inorg. Chem.*, **1962**, 1, 481.
[177] R.G. Pearson, H.B. Gray, F. Basolo, *J. Am. Chem. Soc.*, **1960**, 82, 787.
[178] S. Otto, A. Roodt, *J. Organomet. Chem.*, **2006**, 691, 4626.

The equilibrium constant of the reaction, $K_{eq,}$ may be calculated from spectroscopic measurements, i.e. UV/Vis and NMR, but can also be obtained kinetically.

5.4.2 PRELIMINARY SUBSTITUTION STUDY

The CO substitution from [Rh(4-CH_3-Phony)$(CO)_2$] by PTA (1,3,5-triaza-7-phosphaadamantane) in dichloromethane was investigated in a preliminary study and evaluated at 25 °C using both ^{31}P NMR and standard UV/Vis and IR techniques. As indicated, the PTA ligand was chosen because of its unique water-soluble properties, which should yield a corresponding water-soluble complex, and may in principle be used in water, a "green" solvent. Apart from this, PTA also has other unique properties with respect to its structure and cone angle, see Par. 2.3.4.

From this study the mechanism of substitution could be validated and determined whether it was *via* the direct or solvent pathway. In addition to the validation of the mechanism, the substitution process needed to be evaluated in order to determine the *rate constant* which could provide insight regarding the reactivity of the compound with specific nucleophiles.

5.4.2.1 ^{31}P NMR study of the CO substitution from [Rh(4-CH_3-Phony)$(CO)_2$] by PTA

Four different experiments were conducted as described below to evaluate the possible equilibrium present in Scheme 5.1 and estimate the rate of substitution and product formation.

(I) Fig. 5.3 illustrates the ^{31}P spectrum of free PTA in DCM solution, displaying a singlet at -102 ppm, see (B). Similarly, in spectrum (A) the ^{31}P spectrum of [Rh(4-CH_3-Phony)(CO)(PTA)] (synthesis see Par. 3.7.3.5) is given, displaying a characteristic doublet due to the first-order coupling with Rh, at -36.3ppm, $^1J(^{103}Rh\text{-}^{31}P)$ = 143.5 Hz. The latter is emphasized in insert (i).

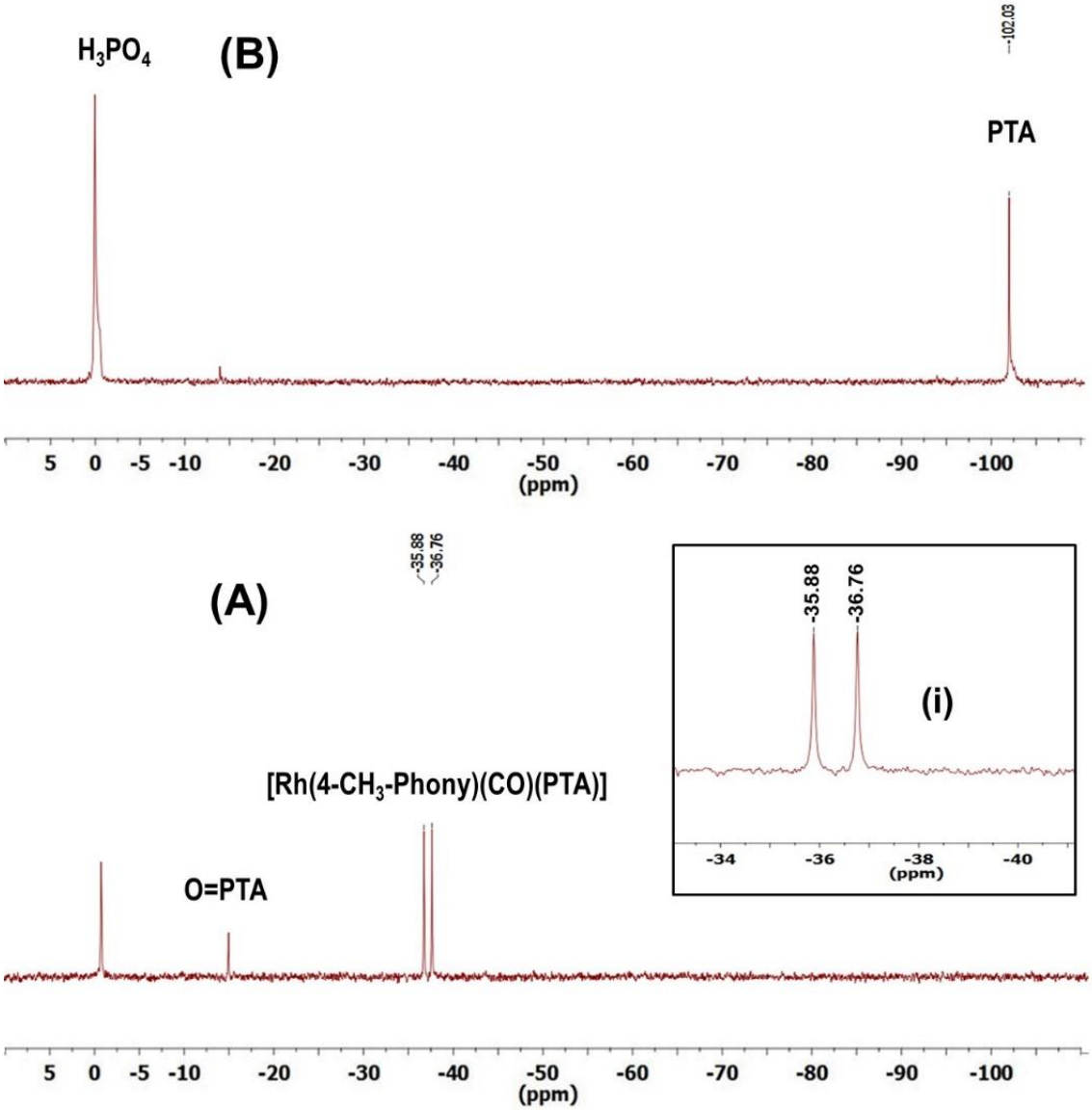

Figure 5.3: (A) ^{31}P-NMR spectrum of free PTA in CD_2Cl_2; [PTA] = 0.6 x 10^{-3} M; (B) ^{31}P-NMR spectrum of [Rh(4-CH_3-Phony)(CO)(PTA)] = 1.42 x 10^{-2} M, from synthesis, see Par 3.7.3.5. Insert (i) Expanded signal for [Rh(4-CH_3-Phony)(CO)(PTA)].

(II) Next, as illustrated in Fig. 5.4, the possible presence of an equilibrium in the formation of the [Rh(4-CH_3-Phony)(CO)(PTA)] complex is evaluated (Scheme 5.1), where

- Spectrum (A) illustrates the 1:1 mixture of free PTA and [Rh(4-CH_3-Phony)$(CO)_2$], clearly showing the seemingly quantitative formation of the [Rh(4-CH_3-Phony)(CO)(PTA)] complex.

- Following this, the liberated CO was removed by bubbling N_2 directly through the solution in the NMR tube, and then collecting the spectrum, see Fig. 5.4 (B).
- Finally, CO was again bubbled through the mixture within the NMR tube and the spectrum collected, see Fig. 5.4 (C).

It is clear that the initial reaction was seemingly quantitative, and the equilibrium indicated in Scheme 5.1 lies far towards the [Rh(4-CH_3-Phony)(CO)(PTA)] complex. However, some indication of the presence of very broad signals at -60 to -70 ppm (see Fig. 5.4 (B) and (C)) suggest that there might be also more complex dynamics present.

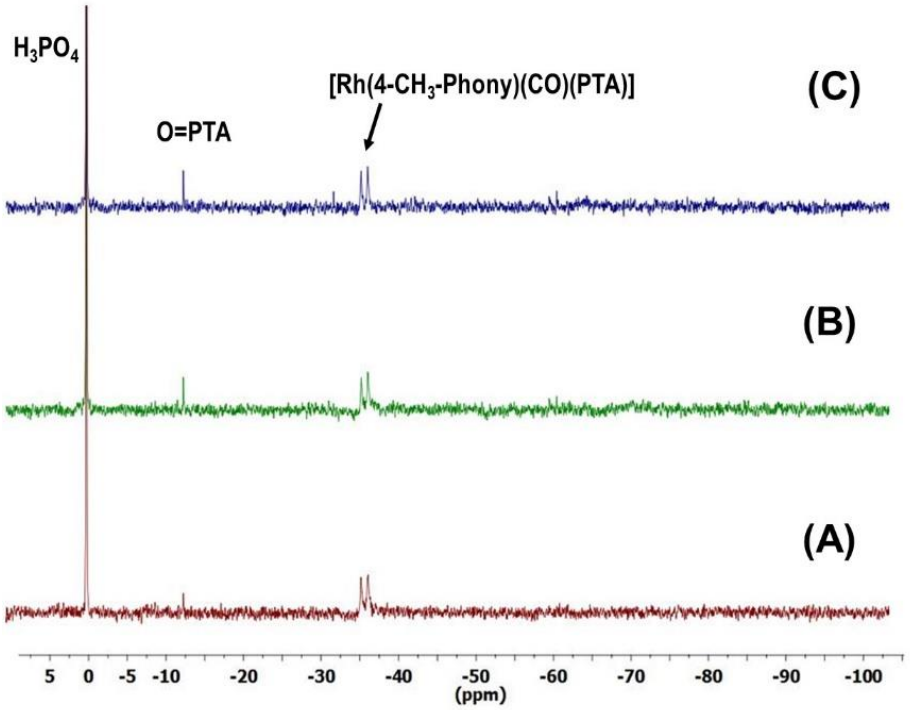

Figure 5.4: ^{31}P-NMR spectra for the formation of [Rh(4-CH_3-Phony)(CO)(PTA)], through the CO substitution reaction of [Rh(4-CH_3-Phony)$(CO)_2$] = 0.02 M and [PTA] = 0.02M, in $CDCl_3$ at 25 °C under (A) atmospheric conditions (red); (B) a nitrogen saturated solution (Green); (C) a CO saturated solution (blue).

(III) Thirdly, as illustrated in Fig. 5.5, evaluation of the reaction dynamics for the formation of the [Rh(4-CH_3-Phony)(CO)(PTA)] complex was investigated by ^{31}P NMR (mechanism in Scheme 5.1).

Thus, a 4:1 [PTA]:[Rh] ratio was evaluated, see Fig. 5.5 (A), and it is clear that two new signals (Spectrum 1: one *unresolved* at -58 ppm (i); i.e. no formal first-order coupling to the Rh; and another at -62 ppm (ii) *resolved* signal which increases with time) are observed.

Furthermore, a broadening of the signals attributable to the [Rh(4-CH_3-Phony)(CO)(PTA)] (-36 ppm (iii)) and to free PTA (-100 ppm (iv)) complex is observed.

This complicates the system significantly and might be indicative of:

- A fast exchange between the PTA (-100 ppm) and the [Rh(4-CH_3-Phony)(CO)(PTA)] complex (-36 ppm), see Fig. 5.5 (iii) and (iv) respectively.
- But then also an "unreactive" intermediate (possibly even the five-coordinate [Rh(4-CH_3-Phony)(CO)$(PTA)_2$] complex) might be present (ii; spectra 2-5).
- A typical broadening of the new signal at ca. -58 ppm (i), indicative of fast exchange (Spectrum 1) is observed. However, if this is the *average* signal in a very fast exchange mode between the PTA (-100 ppm) and the [Rh(4-CH_3-Phony)(CO)(PTA)] complex (-36 ppm), then the two individual broadened signals due to the latter must have been *absent*.

Thus overall, there is evidence for *two* new species formed: the broadened signal at -58 ppm and the resolved signal at -62 ppm.

On top of that, the broadening of the two signals of free PTA (-100 ppm) and the [Rh(4-CH_3-Phony)(CO)(PTA)] complex (-36 ppm) emphasizes the additional dynamics in the system.

As already indicated, it significantly complicates the system and the decision was made not to attempt to analyse this further in the MSc study in detail, since it will require a large fraction of a full academic year, and not appropriate on MSc level.

(IV) Nevertheless, finally, another experiment wherein an even higher [PTA]:[Rh] ratio =10:1 was employed, was evaluated, see Fig. 5.5 (B). Surprisingly, the addition of a larger amount of PTA "simplifies" the spectra, showing a fast line-broadened signal at ca -61ppm, and a slightly broadened signal of free PTA at -102 ppm. It thus indicates all Rh species in a fast exchange mode.

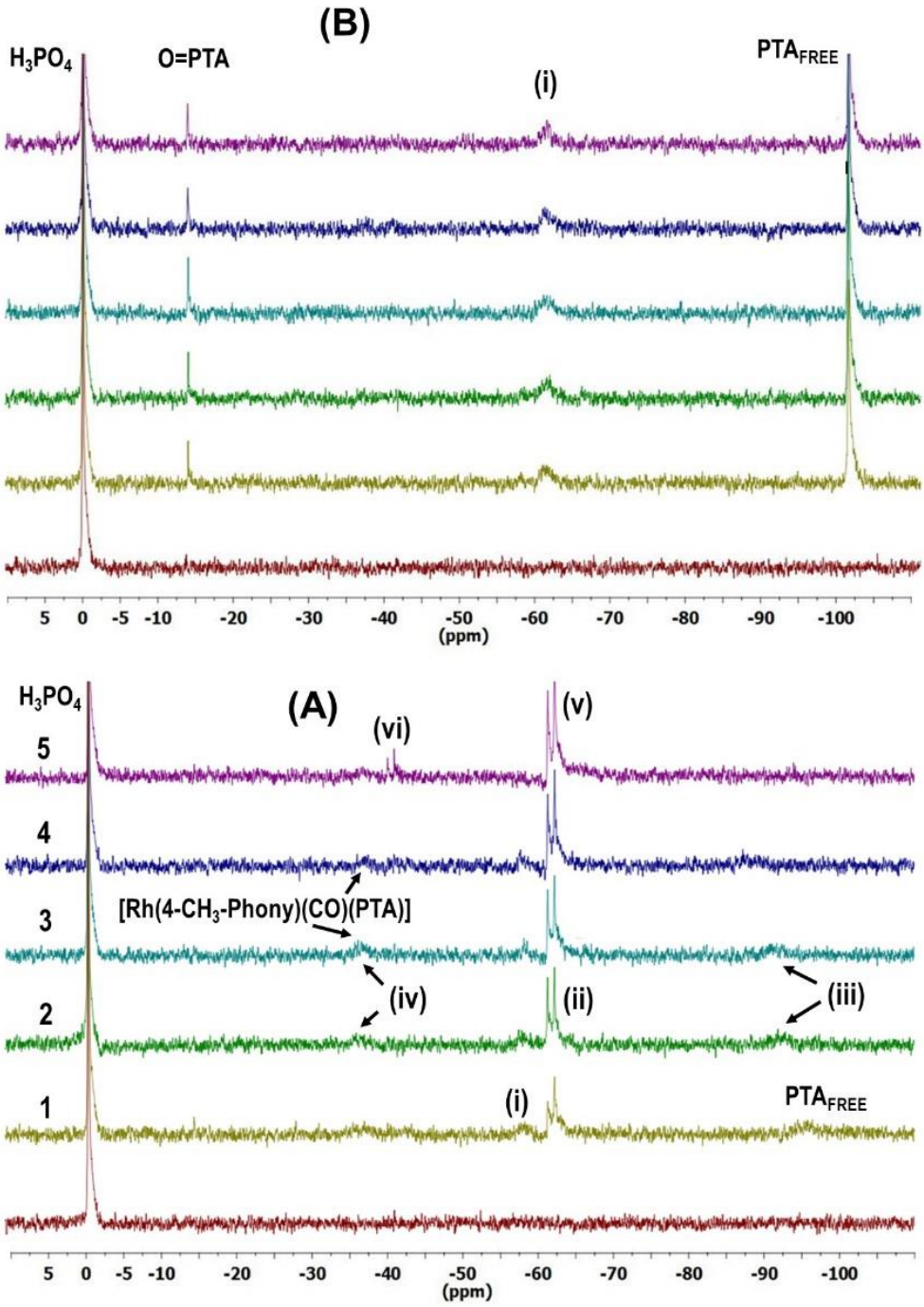

Figure 5.5: (A) Successive ^{31}P-NMR spectra for the formation of [Rh(4-CH_3-Phony)(CO)(PTA)], through the substitution reaction of Rh(4-CH_3-Phony)$(CO)_2$] = 0.02 M and [PTA] = 0.085 M, in DCM at 25 °C; Δt = 99s. (B) Successive ^{31}P-NMR spectra for the formation of [Rh(4-CH_3-Phony)(CO)(PTA)], through the substitution reaction of Rh(4-CH_3-Phony)(CO)(PTA)] = 0.02 M and [PTA] = 0.244 M in DCM at 25 °C, Δt = 99 s.

The exchange rates observed from these line-broadenings are in the range of 10 to -100 ppm and are reasonably compatible with that observed under special conditions, see UV/vis kinetics as described below.

As indicated, since it would have required significant additional time and the system was significantly more complicated as initially anticipated, the decision was made not to attempt to analyse this further in the MSc study in detail.

It was nevertheless opted to at least investigate the kinetics using a more general UV/vis approach, and the preliminary study is reported below.

5.4.2.2 UV/Vis study of the CO substitution from [Rh(4-CH_3-Phony)$(CO)_2$] by PTA

The UV/vis spectral change for the CO substitution reaction from [Rh(4-CH_3-Phony)$(CO)_2$] by PTA in dichloromethane as a solvent is illustrated in Fig. 5.6.

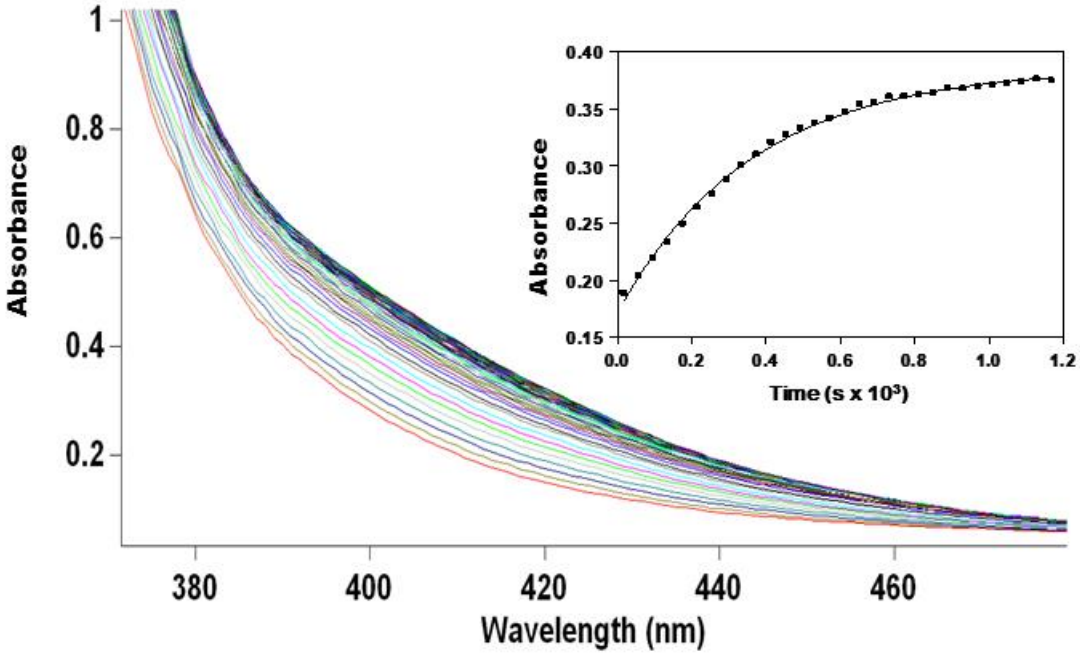

Figure 5.6: Characteristic UV/Vis spectra for the substitution reaction between [Rh(4-CH_3-Phony)$(CO)_2$] and PTA in dichloromethane as solvent as 25 °C. [Rh] = 3.36 x 10^{-4} M, [PTA] = 4.04 x 10^{-2} M, λ = 424 nm.

The k_{obs} values obtained from the reaction between [Rh(4-CH_3-Phony)$(CO)_2$] and various [PTA] concentrations are presented in Fig. 5.7. It is clear that Eq. 5.7 is obeyed.

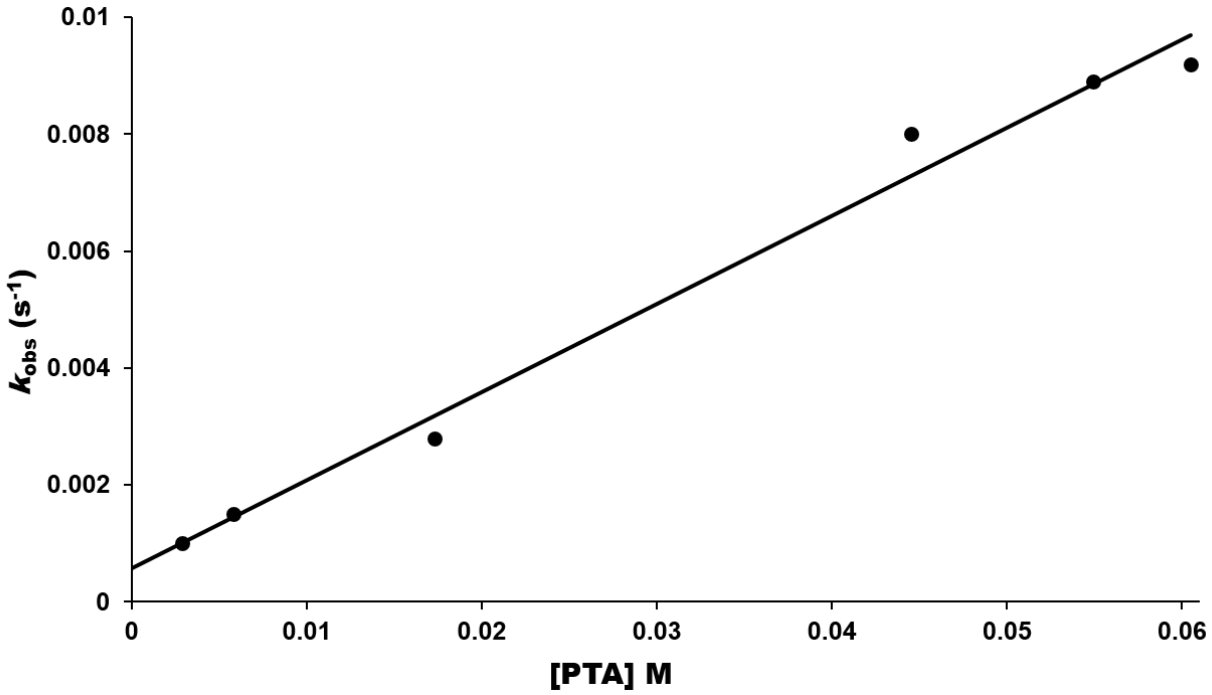

Figure 5.7: Dependence of the observed pseudo first-order rate constant on [PTA] for carbonyl substitution in [Rh(4-CH_3-Phony)$(CO)_2$]. [Rh]= 3.3602 x 10^{-4} M, [PTA] = 3 x 10^{-3} to 6.0 x 10^{-2} M at 25°C found in dichloromethane for this study using UV/Vis. λ = 424 nm.

Table 5.1: UV/Vis kinetic data obtained from the carbonyl substitution in [Rh(4-CH_3-Phony)$(CO)_2$] with [PTA] at 25°C in dichloromethane[a]

	[Rh(4-CH_3-Phony)(CO)(PTA)]
k_1 **(M^{-1} s^{-1})**	0.1506(3)
k_{-1} **(s^{-1})**	0.0006(1)
K_1 **(M^{-1})**	251(120)

[a] Eqs. 5.7 and 5. 8 used

The UV/Vis kinetic study for the formation of the assumed [Rh(4-CH_3-Phony)(CO)(PTA)] complex shows a linear dependency between the observed rate constant and the PTA concentration (Eq. 5.7). The small intercept k_{-1} value obtained indicates a direct mechanism with no appreciable solvent dependent pathway, while the large equilibrium constant (K_1) indicates that the formation of the product is clearly favoured.

5.4.3 General reaction Mechanism for Oxidative Addition studies

As indicated, rhodium complexes make up some of the most widely propagated homogeneous catalysts[179,180,181] Examples include carbonylation of methanol to produce acetic acid, hydroformylation of alkenes to produce aldehydes and olefin hydrogenation by Wilkinson's catalyst [Rh(Cl(PPh_3)$_3$].[182,183] In the carbonylation of methanol an electron-rich rhodium(I) centre is required for the rate-determining oxidative addition reaction. The nature of the ligands around the metal centre controls the catalytic reactivity of rhodium(I) complexes, thus manipulating the electro-steric properties of these ligands to alter/manipulate the reaction rates of essential steps in homogeneous catalyst.[184,185] The oxidative addition general mechanism for iodomethane to [Rh(L,L'-Bid)(CO)(PR_3)] complexes has been established previously.[121,122,123,124,125,126,127,128] Fig. 5.8 illustrates the formation of rhodium alkyl and acyl species.[186] The oxidative addition of iodomethane to the rhodium(I) complex (**A**) leads to the formation of an alkyl (**D**) species. Migratory insertion of the CO ligand into the Rh-methyl bond to form the acyl species (**C**). The solvent dependent pathway may also be observed, as indicated in Fig. 5.8.

[179] D.E. Webster, *Plat. Met. Rev.*, **1969**, 13, 104.
[180] P. Kvintovics, B. Heil, L. Marko, *ACS*, **1979**, 173, 26.
[181] I. Arribas, M. Rubio, P. Kleman, A. Pizzano, *J. Org. Chem.*, **2013**, 78, 3997.
[182] P.M. Maitlis, A. Haynes, G.J. Sunley, M.J. Howard, *J. Chem. Soc., Dalton Trans*., **1996**, 2187.
[183] H.W. Bohen, B. Cornils, *Adv. Catal*., **2002**, 47, 1.
[184] A. Brink, A. Roodt, G. Steyl, H.G. Visser, *Dalton Trans.*, **2010**, 39, 5572.
[185] A. Brink, A. Roodt, H.G. Visser, *Cryst. Rev.*, **2011**, 17, 241.
[186] B. Breit, *Angew. Chem. Int.*, **2005**, 44, 6816.

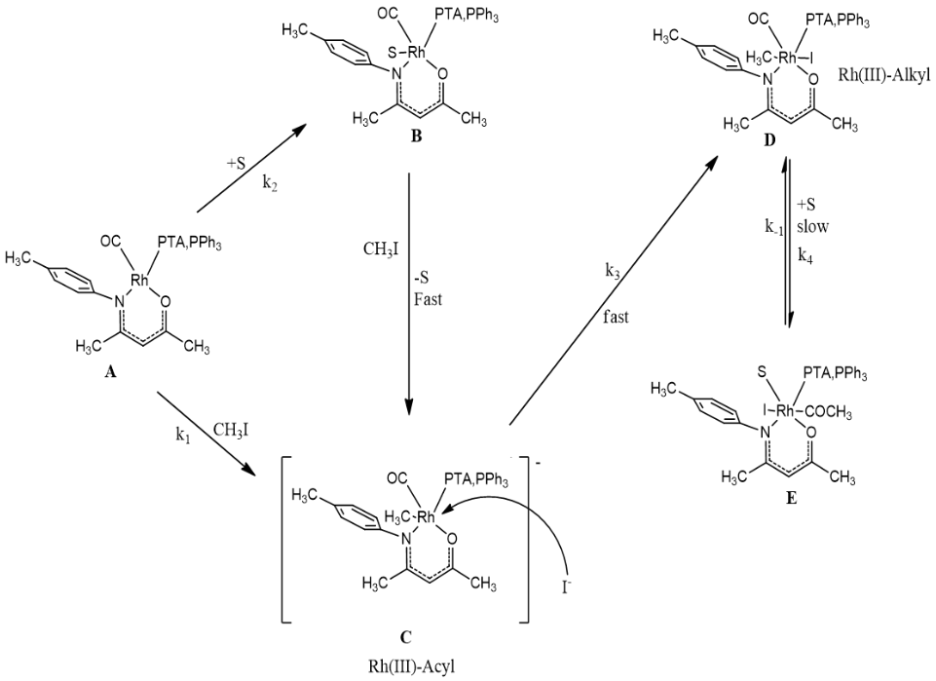

Figure 5.8: Proposed general reaction mechanism of [Rh(4-CH_3-Phony)(CO)(PTA)] and [Rh(4-CH_3-Phony)(CO)(PPh_3)] complexes with iodomethane (CH_3I). S= solvent molecule.

5.4.4 PRELIMINARY IODOMETHANE OXIDATIVE ADDITION STUDIES

In this study, the oxidative addition of iodomethane to the [Rh(4-CH_3-Phony)(CO)(PTA)] and [Rh(4-CH_3-Phony)(CO)(PPh_3)] complexes indicated the disappearance of Rh(I) and the formation Rh(III) alkyl product. No acyl product was observed through the FT-IR and ^{31}P NMR spectra. This may be due to the slow formation rate of acyl species related to the oxidative addition step. Fig. 5.9 and 5.10 illustrate the disappearance of the Rh(I) complex at $\nu_{(CO)}$ = 1966 cm^{-1} with the simultaneous growth of the Rh(III) at $\nu_{(CO)}$ = 2058 cm^{-1} upon the addition of iodomethane.

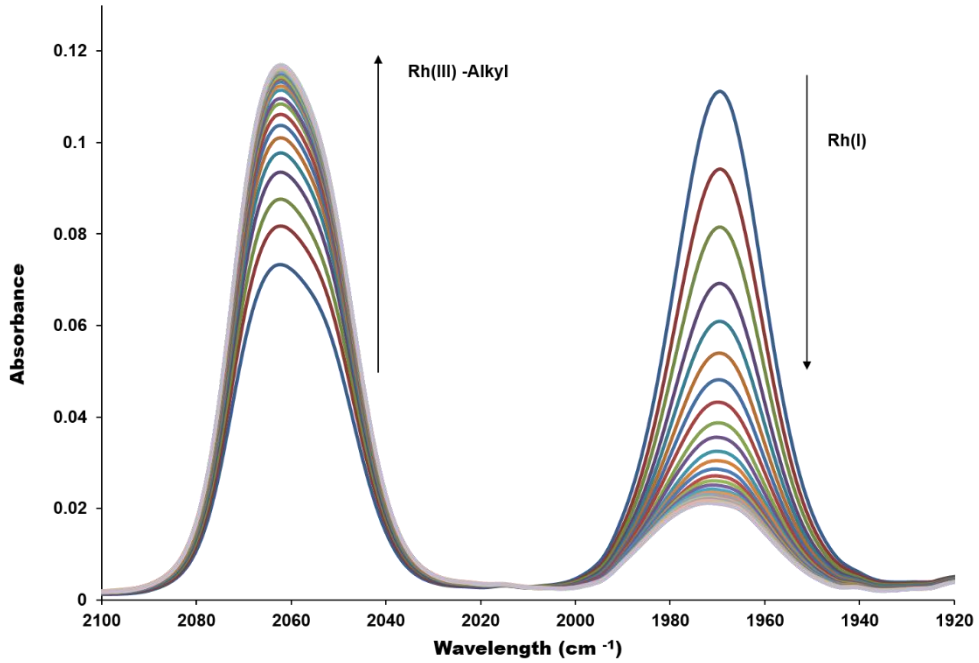

Figure 5.9: Representative IR scans for oxidative addition of iodomethane to [Rh(4-CH_3-Phony)(CO)(PTA) in dichloromethane at 25 ˚C. [Rh(4-CH_3-Phony)(CO)(PTA)] = 1.506 x 10^{-3} M, [MeI] = 0.1 M.

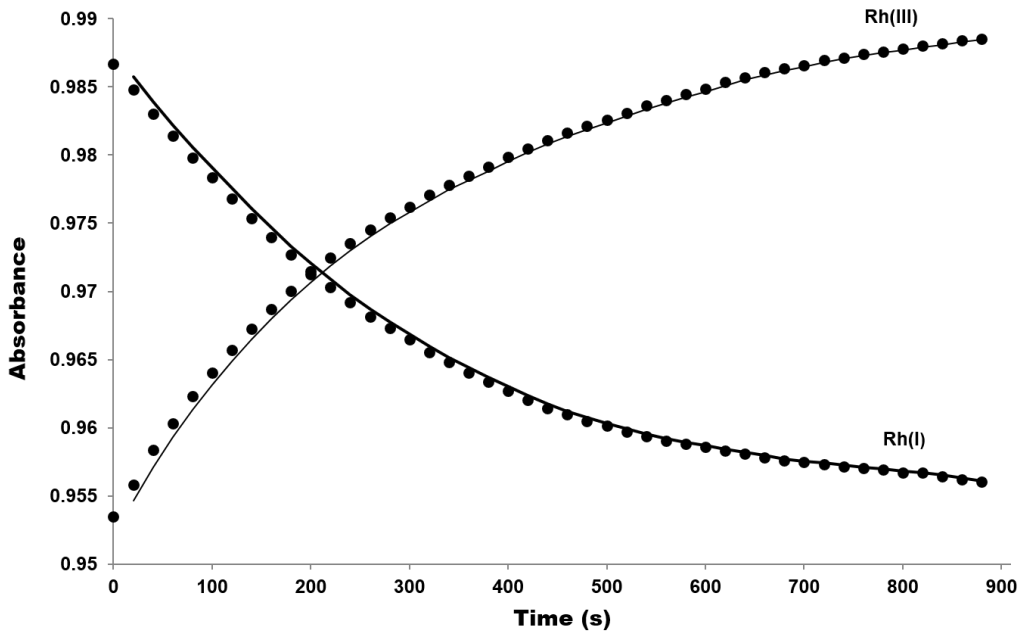

Figure 5.10: Disappearance of Rh(I) (k_{obs} = 0.0169(3) s^{-1} species with the simultaneous growth of Rh(III) (k_{obs} = 0.0166(4) s^{-1}) alkyl species. [Rh(4-CH_3-Phony)(CO)(PTA)] = 1.506x10^{-3} M, [MeI] = 0.1 M at 25 ˚C.

A similar trend was observed for the [Rh(4-CH_3-Phony)(CO)(PPh_3)] complex. The absence of the corresponding acyl product was confirmed by ^{31}P NMR investigation as shown in Fig. 5.11, Fig. 5.12, with the rate date reported in Table 5.2.

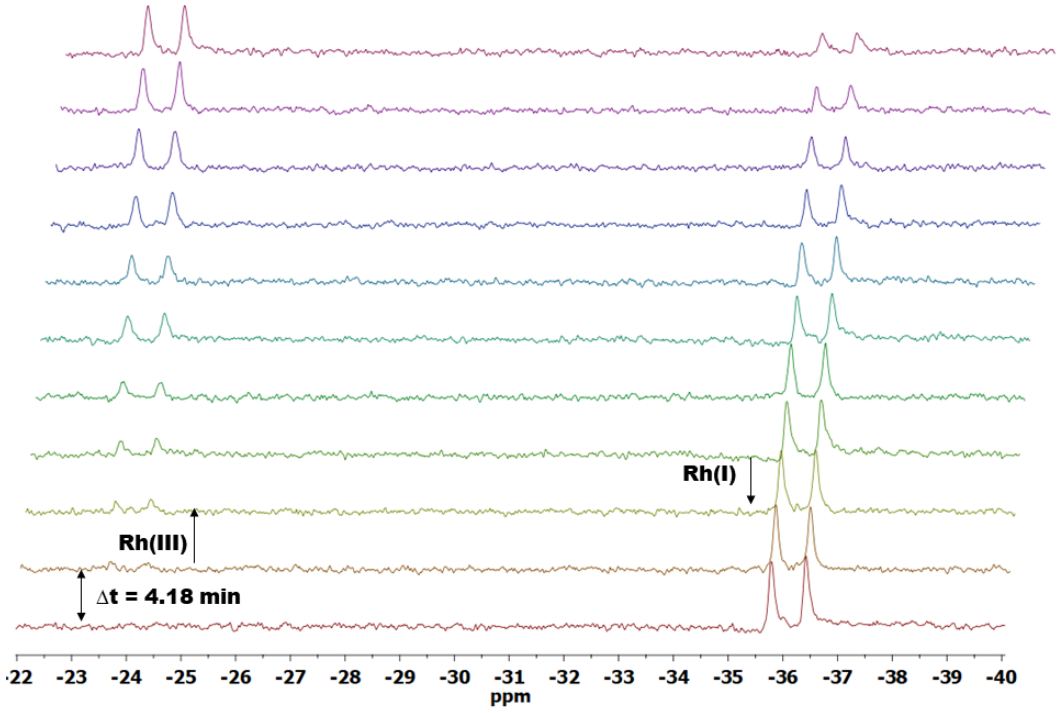

Figure 5.11: Successive ^{31}P NMR spectra for the disappearance of Rh(I) species and the simultaneous formation of the Rh(III) alkyl species for the reaction of [Rh(4-CH_3-Phony)(CO)(PTA)] with iodomethane in dichloromethane at 25° C; [Rh] = 0.02 M, [MeI] = 0.54 M.

Fig. 5.11 illustrates the observed ^{31}P NMR spectra for the iodomethane oxidative addition to [Rh(4-CH_3-Phony)(CO)(PTA)] in dichloromethane at 25 °C. Spectra show the disappearance of the Rh(I) peak at -36.6 ppm and the formation of the Rh(III) alkyl peak at -24.3 ppm. The spectra are referenced internally to 85 % H_3PO_4 (δ = 0 ppm). The total peaks are plotted against time for 16 spectra. [However, only 11 have been plotted above to illustrate the increase of peaks (number of scans = 8 scans)]. The chemical shift, coupling constant and observed rate constant data are reported in Table 5.3.

Fig. 5.12 illustrates the observed ^{31}P NMR spectra for the iodomethane oxidative addition to [Rh(4-CH_3-Phony)(CO)(PPh_3)] in dichloromethane at 25 ˚C. Spectra show the disappearance of the Rh(I) peak at 42.8 ppm and the formation of the Rh(III) alkyl peak at 23.2 ppm. The spectra are referenced internally to 85 % H_3PO_4 (δ = 0 ppm). The total peaks are plotted against time for 250 spectra, however, only 11 have been plotted here to illustrate the increase of peaks (number of scans = 32 scans). The chemical shift, coupling constant and observed rate constant data is displayed in Table 5.3.

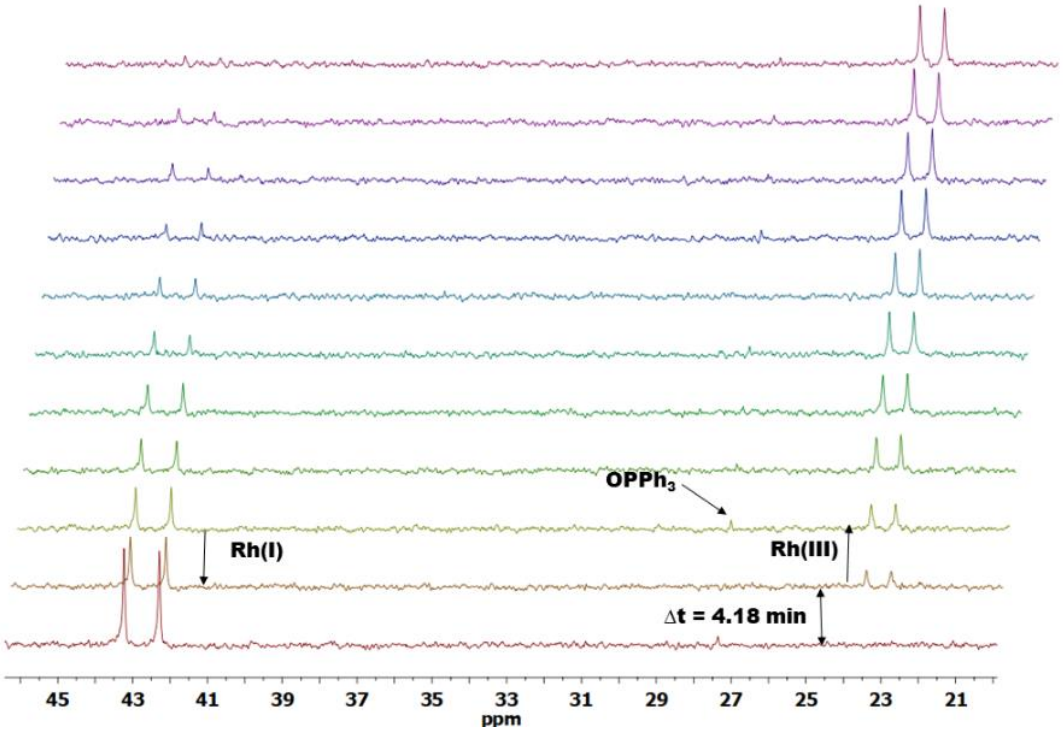

Figure 5.12: Successive ^{31}P-NMR spectra for the disappearance of Rh(I) species and the simultaneous formation of the Rh(III) alkyl species for the reaction of [Rh(4-CH_3-Phony)(CO)(PPh_3)] with iodomethane in dichloromethane at 25˚ C; [Rh] = 0.02 M, [MeI] = 0.006 M.

Table 5.2: IR kinetic data for the oxidative addition of iodomethane to the complex [Rh(4-CH_3-Phony)(CO)(PR_3)] in dichloromethane at 25 °C. [Rh] = 0.01 M and [MeI] = 0.05 M, 0.1 M, and 0.3 M.

[MeI] M		$\nu_{(CO)}$ **(cm^{-1})**		k_{obs} **(s^{-1})**	
		PTA	**PPh_3**	**PTA**	**PPh_3**
0.05	Rh(I)	1966		0.0106(5)	
	Rh(III) Alkyl	2057		0.0103(4)	
0.1	Rh(I)	1966	1966	0.0169(3)	0.0166(3)
	Rh(III) Alkyl	2058	2064	0.0166(4)	0.016(2)
0.2	Rh(I)	1970	1969	0.0272(3)	0.02577(4)
	Rh(III) Alkyl	2057	2059	0.0244(2)	0.0253(2)
0.3	Rh(I)		1967		0.0372(3)
	Rh(III) Alkyl		2062		0.0372(2)

Table 5.3: Summary of the chemical shifts, coupling constants and k_{obs} data from Fig. 5.11 and 5.12 for rhodium species present during the iodomethane oxidative addition to complexes [Rh(4-CH_3-Phony)(CO)(PTA)] and [Rh(4-CH_3-Phony)(CO)(PPh_3)] respectively

	Chemical shift (ppm)		**Coupling constant $^1J_{Rh-P}$ (Hz)**		**k_{obs} (x 10^{-3} s^{-1})**	
Species	PTA	PPh_3	PTA	PPh_3	PTA	PPh_3
Rh(I)	-36.6	42.8	144.3	156.2	4.12(5)	15.3(3)
Rh(III) alkyl	-24.3	23.2	115.3	111.4	0.92(3)	7.95(1)

Next, the kinetics were studied in more detail using UV/vis, of which a typical reaction is illustrated in Fig. 5.13.

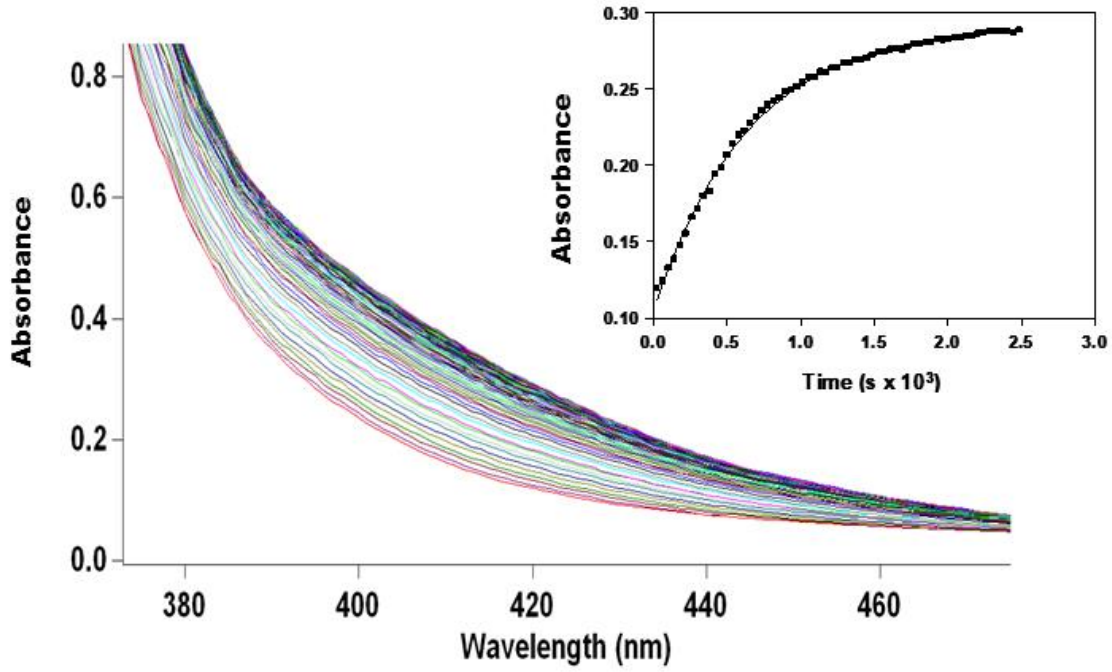

Figure 5.13: Typical UV/Vis spectra change for the reaction between iodomethane and [Rh(4-CH_3-Phony)(CO)(PPh_3)] in dichloromethane at 25 ˚C, [Rh] = 3.36 x 10^{-4} M, λ = 413 nm, [MeI] = 0.054 M.

The overall spectral changes for the oxidative addition are evaluated through UV/Vis, representing both the disappearance of Rh(I) and the formation of Rh(III) alkyl species. Fig. 5.14 illustrates a plot of the observed rate constant vs. the iodomethane concentration for the [Rh(4-CH_3-Phony)(CO)(PTA)] and [Rh(4-CH_3-Phony)(CO)(PPh_3)] complexes in dichloromethane at 25 ˚C.

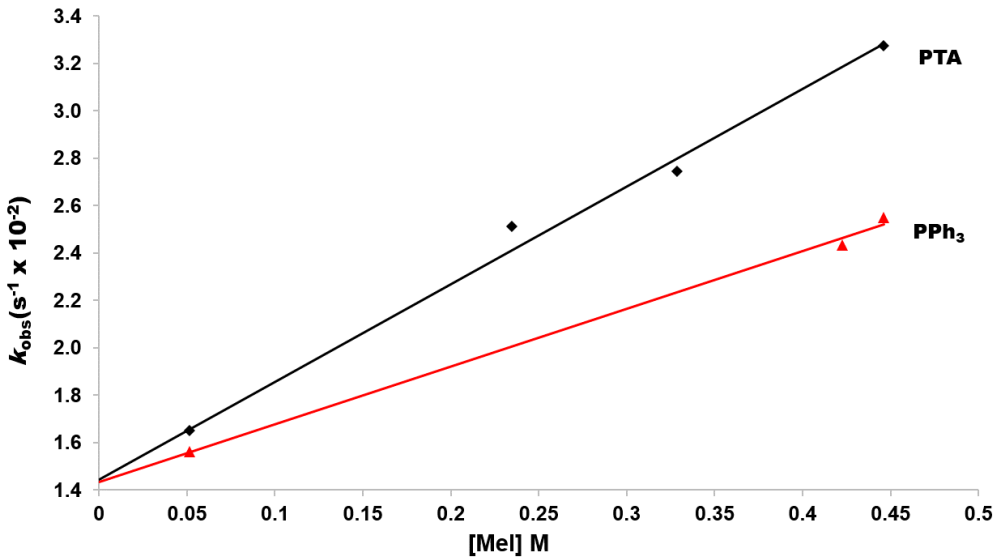

Figure 5.14: Plot of the observed rate constant *vs*. iodomethane concentration for the iodomethane oxidative addition to complexes [Rh(4-CH_3-Phony)(CO)(PTA)] and [Rh(4-CH_3-Phony)(CO)(PPh_3)] in dichloromethane at 25 °C; [Rh] = 3.36 x 10^{-4} M and [MeI] = 0.052 - 0.44 M.

Although not discussed in detail here, more elaborate background has been given in Chapter 2 (see Par. 2.4.4.2), in particular with respect to rate laws which operate.

For the purpose of this preliminary study, however, a simple forward two-term rate law, as described by pathway A to D in Fig. 5.8, yielding Eq. 5.7, is assumed for the iodomethane oxidative addition reported here.

The oxidative addition of MeI through UV/Vis kinetic studies for the two rhodium(I) complexes clearly indicates a linear dependency between the observed rate constant and the iodomethane concentration as predicted by Eq. 5.7. This data could then be used to determine the forward and reverse rate constants, as well as an estimation of the equilibrium constant (Table 5.4).

Table 5.4: UV/Vis **k**inetic data obtained for the iodomethane oxidative addition to [Rh(4-CH_3-Phony)(CO)(PTA)] and [Rh(4-CH_3-Phony)(CO)(PPh_3)] in Dichloromethane at 25°C. [Rh] = 3.36 x 10^{-4} M and [MeI] = 0.052 -0.44M.

Species	k_1 ($M^{-1}.s^{-1}$)	k_{-1}(s^{-1})	K_1 (M^{-1})	$^1J_{Rh-P}$ (Hz)
[Rh(4-CH_3-Phony)(CO)(PTA)]	0.039(2)	0.015(3)	2.81(2)	142.5
[Rh(4-CH_3-Phony)(CO)(PPh_3)]	0.024(2)	0.014(1)	1.7(4)	152.1

5.5 CONCLUSION

The study of the CO substitution reaction from [Rh(4-CH_3-Phony)$(CO)_2$] by PTA indicates that the formation of [Rh(4-CH_3-Phony)(CO)(PTA)] complex proceeds principally *via* the direct pathway and that the reaction goes to completion based on the large K_1. Based on equilibrium studies in ^{31}P NMR substitution studies it is fair to say that the forward reaction is favoured, but upon further investigation it is evident that there is a more complex dynamics present.

Successive ^{31}P NMR studies of 4:1 [PTA]:[Rh] indicated that the system was more complex as fast exchange, new species and possible a five-coordinate [Rh(4-CH_3-Phony)(CO)$(PTA)_2$] complex may exist.

It is clear that a more elaborate investigation is required to attempt to answer some of the questions raised from this preliminary substitution study.

Results from the oxidative addition of iodomethane to [Rh(4-CH_3-Phony)(CO)(PTA)] and [Rh(4-CH_3-Phony)(CO)(PPh_3)] as summarised in Table 5.2 indicate that the rate of Rh(I) disappearance for both studied rhodium species at different MeI concentrations is fairly similar to the rate of Rh(III) alkyl formation. The observed rate constants for the oxidative addition at different [MeI] show an increase. This implies that the observed rate is directly proportional to the concentration of MeI.

The observed iodomethane oxidative addition rate constants for the [Rh(4-CH_3-Phony)(CO)(PTA)] vs the [Rh(4-CH_3-Phony)(CO)(PPh_3)] complexes further imply that there is not a significant electronic variation introduced on the metal centre in spite of the variation of the steric and electronic parameters of the two tertiary phosphines, PTA vs PPh_3.

The coupling constants between the two different species indicate a directly proportional relationship to the observed rate constant. And correlates with the observation seen in the FT-IR results in that Rh(I) disappears fast and the formation of Rh(I) alkyl species is slower.

The equilibrium constant value (K_1) of the PTA species is far greater than that of the PPh_3 species, indicating that the PTA species favours formation to the final product. Moreover, the kinetic studies indicate that the application of the PTA species data will be applicable in the design of a catalyst as it favours the formation of the product.

Likewise, as for the preliminary CO substitution study reported above, a much more elaborate oxidative addition study is required for elucidating more aspects identified herein.

In spite of these inherent complicating aspects observed in this preliminary studies, the solution behaviour of the novel PTA complexes shows promise to be further investigated in future and to contribute more to the basic knowledge of the potentially water-soluble [Rh(4-CH_3-Phony)(CO)(PTA)] as model catalyst.

6 EVALUATION OF STUDY

6.1 INTRODUCTION

This study was aimed at synthesising and investigating a model water-soluble rhodium(I) complex that could be used as a potential homogeneous catalyst precursor in Carbonylation processes.

6.2 SYNTHESIS AND CRYSTALLOGRAPHY

Four ligand derivatives of 4-(phenylamino)pent-3-en-2-one (PhonyH) were synthesized and characterised through NMR, and infrared spectroscopy. These enaminoketonato ligands, containing an N-Phenyl ring, were selected and synthesised with electron withdrawing/ donating groups the *para* position, to ensure small steric effects and subtle evaluation of electronic effects. The successful preparation of substituted dicarbonyl-[4-(phenylamino)pent-3-en-2-onato]-rhodium(I) ([Rh(N,O-bid)$(CO)_2$]) complexes were next achieved, as confirmed via characterization using NMR and infrared spectroscopy. The [Rh(N,O-bid)$(CO)_2$] complexes served as the precursors for the substitution of one CO ligand by tertiaryphosphines, PR_3 (PR_3 = PPh_3 and PTA), as again confirmed by NMR and infrared spectroscopy. Although four carbonyl-[4-(phenylamino)pent-3-en-2-onato]-triphenylphosphine-rhodium(I) ([Rh(N,O-bid)(CO)(PPh_3)]) complexes were successfully synthesized, only [Rh(4-CH_3-Phony)(CO)(PPh_3)] and [Rh(4-F-Phony)(CO)(PPh_3)] were characterized additionally with X-ray crystallography. The two complexes were found to be isostructural and both displayed similar intermolecular interactions despite their electronic differences due to substituents on the *para* position of the N-phenyl. Carbonyl-[4-(phenylamino)pent-3-en-2-onato]-1,3,5-triaza-7-phosphaadamantane-rhodium(I) ([Rh(N,O-bid)(CO)(PTA)]) complexes that were synthesized were found to be soluble in water and stable in air.

Overarchingly it can be stated that success was achieved to obtain a water-soluble complex which can be further explored in future for actual catalytic properties.

6.3 KINETIC STUDIES

6.3.1 PRELIMINARY SOLUTION STUDY OF THE CO SUBSTITUTION FROM [RH(4-CH_3-PHONY)$(CO)_2$]

Evaluation of the electronic environment experienced by the rhodium(I) centre was studied through preliminary substitution kinetics and discussed in Chapter 5. An exploratory investigation of a square-planar CO substitution from [Rh(4-CH_3-Phony)$(CO)_2$] by PTA as ligand was presented. Based on UV/Vis kinetic studies that showed a large equilibrium constant (K_1), the reaction could be studied under non-equilibrium conditions which favoured the formation of the product. However, the reaction that theoretically seemed "simple" was indeed more complicated as concluded from ^{31}P NMR studies due to fast exchange, a seemingly "unreactive" intermediate and evidence of a new species. Hence, it was decided to not analyse this further in the MSc study although excellent preliminary results were obtained which allows one to build on it in future.

6.3.2 PRELIMINARY IODOMETHANE OXIDATIVE ADDITION TO [RH(4-CH_3-PHONY)(CO)(PPH_3)] AND [RH(4-CH_3-PHONY)(CO)(PPH_3)]

Preliminary iodomethane oxidative addition was conducted on [Rh(4-CH_3-Phony)(PPh_3)] and [Rh(4-CH_3-Phony)(PTA)] in order to evaluate the influence and differences of the two tertiaryphosphine rhodium(I) complexes on the bench-mark reaction associated with homogeneous catalysis. Through time-resolved IR and NMR investigations, it was found that for both species there was a rapid decrease of rhodium(I) with simultaneous formation of a rhodium(III) alkyl species. There was no detection of a rhodium(III) acyl species under the conditions employed. The observed rates for [Rh(4-CH_3-Phony)(PPh_3)] and [Rh(4-CH_3-Phony)(PTA)] complexes were comparable despite the variation of the steric and electronic parameters of the two tertiary phosphines, PTA *vs.* PPh_3. The equilibrium constant value (K_1) of the PTA species favours formation to the final product when compared to PPh_3. Hence the application of the PTA species data will be applicable in the design of a catalyst as it favours the formation of the product and is water-soluble.

6.4 FUTURE WORK

Research which may be classified under the broad concept of 'green chemistry' should be a focal aspect in all future. Based on the results obtained from this study, further investigation, to expand on the current knowledge of the coordination modes and the kinetic behaviours of these rhodium(I) systems, include:

Further investigation regarding substitution kinetic studies i.e. fast exchange, "unreactive" intermediate and evidence of a new species and effects of additional subtle changes thereupon.

Further investigation in the coordination of these systems using a wider range of water-soluble ligands of the form PR_3 (PR_3 = TPPTS/TPPMS/TPPDP).

Isolation of single crystals of Rh(I)-PTA and Rh(III)-PTA complexes synthesised in this study.

Theoretical computational calculations could aid in understanding the kinetic behaviour.

Evaluate the catalytic activity of these systems in actual carbonylation reactions and exploring also other catalysis such as hydroformylation, methoxy-carbonylation, hydrogenation and homologation reactions.

A APPENDIX

Table A.1: Atomic coordination ($x10^4$) and equivalent isotropic displacement parameters ($Å^2 \times 10^3$) for [Rh(4-CH_3-Phony)(CO)(PPh_3)]. $U_{(eq)}$ is defined as one third of the trace of the orthogonalized U^{ij} tensor.

Atom	***x***	***y***	***z***	**U(eq)**
C1	7637(3)	6478(3)	5320(2)	57.3(7)
C2	6288(2)	6242(2)	4526.9(19)	39.2(5)
C3	5750(3)	7164(2)	4786(2)	42.8(5)
C4	4439(2)	7078.4(19)	4223.6(19)	37.4(5)
C5	4071(3)	8227(2)	4738(2)	53.5(6)
C6	2317(2)	3750(2)	319(2)	36.0(5)
C11	2195(2)	6063.6(18)	2885(2)	34.7(4)
C2	2009(3)	643(2)	2034(2)	44.4(5)
C3	663(3)	6286(2)	1558(3)	50.4(6)
C4	-516(3)	5833(2)	1926(3)	48.9(6)
C15	-309(3)	5491(2)	2776(2)	46.0(6)
C16	1027(3)	5595(2)	3247(2)	40.5(5)
C4	-1986(3)	5686(4)	405(4)	77.7(10)
C21	3168(2)	370.0(18)	1610.7(18)	32.6(4)
C22	1724(3)	153(2)	472(3)	53.5(7)
C23	83(3)	182(3)	1549(3)	68.1(9)
C24	333(4)	-567(3)	1806(3)	62.2(8)
C25	2754(3)	-375(2)	1939(3)	60.0(7)
C26	3672(3)	583(2)	1838(2)	46.4(6)
C31	6102(2)	2675.8(18)	1901.4(19)	31.9(4)
C32	6653(2)	3007(2)	3055(2)	39.4(5)
C33	7969(3)	2953(2)	3364(2)	48.6(6)
C34	8754(3)	2597(2)	2538(2)	50.7(6)

C35	8225(2)	2282(2)	398(2)	47.7(6)
C36	6904(2)	2322(2)	1079(2)	38.8(5)
C41	4052(2)	232.1(19)	-80.5(18)	31.2(4)
C42	3495(3)	903(2)	-903(2)	42.2(5)
C43	3338(3)	551(3)	-2083(2)	57.0(7)
C44	3737(3)	418(3)	-2458(2)	57.6(7)
C45	4296(3)	2635(3)	-1653(2)	49.2(6)
C46	4436(2)	2992(2)	-468(2)	40.4(5)
N1	3555.8(19)	6081.5(15)	3321.6(15)	31.4(4)
O1	5747.9(17)	5160.7(15)	3665.7(4)	42.1(4)
O2	304.7(18)	3286.9(17)	586.2(16)	52.4(4)
P1	4324.9(5)	2674.1(5)	496.5(5)	27.86(1)
Rh1	3920.6(2)	4446.9(2)	2452.1(2)	29.42(6)

Table A.2: Anisotropic displacement parameters ($Å^2×10^3$) for [Rh(4-CH_3-Phony)(CO)(PPh_3)]. The anisotropic displacement factor exponent takes the form $2π^2[h^2a^{*2}U_1+...+2hka×b×U_2]$

Atom	**U_1**	**U_{22}**	**U_{33}**	**U_{23}**	**U_3**	**U_2**
C1	45.7(4)	66.6(18)	44.2(15)	16.6(3)	-5.0(1)	17.9(3)
C2	36.3(1)	44.2(2)	30.6(1)	15.3(10)	3.8(9)	10.2(9)
C3	42.4(2)	35.1(1)	35.9(2)	8.0(9)	4.1(10)	8.2(9)
C4	44.6(2)	30.7(10)	36.3(1)	4.6(9)	2.6(9)	3.5(9)
C5	64.1(17)	32.3(2)	54.8(16)	10.2(1)	3.3(3)	21.0(2)
C6	35.1(1)	34.2(1)	41.7(2)	17.0(9)	1.1(9)	17.5(9)
C11	38.7(1)	27.4(9)	39.8(2)	3.6(9)	1.2(9)	17.0(8)
C12	40.6(2)	49.7(3)	60.8(15)	37.8(2)	17.3(1)	20.7(1)
C13	49.6(4)	56.0(15)	68.1(17)	43.6(4)	4.1(3)	26.6(2)
C14	41.4(3)	49.0(4)	65.5(17)	29.4(3)	4.1(2)	24.4(1)
C15	40.9(2)	50.8(4)	55.6(15)	27.9(2)	20.8(1)	22.2(1)
C16	45.7(3)	40.5(2)	41.6(2)	21.9(10)	15.4(10)	18.5(10)
C117	45.6(16)	108(3)	108(3)	70(2)	15.3(17)	37.6(18)
C21	37.2(1)	27.8(9)	31.2(10)	2.5(8)	10.6(8)	1.0(8)

C22	39.8(3)	48.7(4)	82(2)	37.6(4)	20.9(3)	17.7(1)
C23	46.7(15)	57.0(17)	101(3)	40.3(18)	31.1(16)	10.9(3)
C24	75(2)	41.8(4)	63.7(18)	27.3(3)	23.8(15)	6.0(3)
C25	76(2)	42.3(4)	65.7(18)	34.1(4)	9.3(15)	4.3(3)
C26	48.0(3)	39.5(2)	54.5(15)	25.7(1)	6.6(1)	15(1)
C31	27.8(10)	31.4(10)	37.8(1)	16.4(9)	6.3(8)	2.5(8)
C32	39.3(2)	42.2(2)	41.9(2)	21.8(10)	9.4(10)	18.6(10)
C33	47.0(4)	49.5(4)	45.8(4)	21.2(1)	-4.3(1)	18.3(1)
C34	31.9(2)	50.5(4)	63.2(17)	20.3(3)	0.0(1)	18.9(1)
C35	31.8(1)	51.0(4)	55.4(15)	18.2(2)	1.8(1)	18.8(10)
C36	32.7(1)	42.3(2)	39.1(2)	15.4(10)	7.9(9)	16.3(9)
C41	26.6(9)	37.4(10)	32.6(10)	16.8(9)	7.4(8)	4.7(8)
C42	44.6(3)	40.5(2)	38.6(2)	16.4(10)	8.4(10)	15.2(10)
C43	59.9(17)	58.4(16)	36.6(3)	10.0(2)	6.8(2)	20.1(3)
C44	56.9(16)	89(2)	37.7(4)	32.3(15)	16.0(2)	36.1(16)
C45	46.7(4)	73.6(18)	53.1(15)	44.0(15)	23.2(2)	31.4(3)
C46	37.1(1)	45.2(2)	46.4(3)	25.9(1)	2.4(10)	17.2(10)
N1	34.6(9)	28.7(8)	32.8(9)	4.6(7)	6.9(7)	3.8(7)
O1	38.1(8)	39.6(8)	39.8(9)	1.2(7)	-1.6(7)	16.3(7)
O2	38.7(9)	51.2(10)	54.6(1)	17.9(9)	-7.1(8)	4.3(8)
P1	25.8(2)	28.1(2)	30.9(3)	3.7(2)	6.3(19)	1.55(19)
Rh1	27.98(9)	27.48(9)	32.1(10)	2.70(7)	4.95(6)	1.59(6)

Table A.3: Bond distances (Å) for [Rh(4-CH_3-Phony)(CO)(PPh_3)]

Bond	**Length**	**Bond**	**Length**
C1-C2	1.54(3)	C23-C24	1.369(5)
C2-C3	1.374(3)	C24-C25	1.368(5)
C2-O1	1.281(3)	C25-C26	1.388(4)
C3-C4	1.44(3)	C31-C32	1.390(3)
C4-C5	1.517(3)	C31-C36	1.391(3)
C4-N1	1.33(3)	C31-P1	1.830(2)

C6-O2	1.151(3)	C32-C33	1.388(3)
C6-Rh1	1.809(2)	C33-C34	1.382(4)
C1-C2	1.386(3)	C34-C35	1.375(4)
C11-C16	1.382(3)	C35-C36	1.389(3)
C11-N1	1.151(3)	C41-C42	1.390(3)
C2-C3	1.383(3)	C41-C46	1.386(3)
C3-C4	1.387(4)	C41-P1	1.831(2)
C4-C5	1.382(4)	C42-C43	1.383(4)
C14-C117	1.508(4)	C43-C44	1.383(4)
C15-C16	1.382(3)	C44-C45	1.373(4)
C21-C22	1.386(3)	C45-C46	1.389(3)
C21-C26	1.386(3)	N1-Rh1	2.0866(18)
C21-P1	1.836(2)	O1-Rh1	2.0204(17)
C22-C23	1.381(4)	P1-Rh1	2.2695(9)

Table A.4: Bond angles (˚) for [Rh(4-CH_3-Phony)(CO)(PPh_3)]

Bond	**Angle**	**Bond**	**Angle**
C3-C2-C1	19.1(2)	C33-C32-31	20.0(2)
O1-C2-C1	4.6(2)	C34-C33-32	20.5(2)
O1-C2-C3	26.3(2)	C35-C34-C33	19.9(2)
C2-C3-C4	27.0(2)	C34-C35-36	19.9(2)
C3-C4-C5	15.8(2)	C35-C36-31	20.7(2)
N1-C4-C3	24.0(2)	C42-C41-P1	23.19(17)
N1-C4-C5	20.2(2)	C46-C41-42	18.7(2)
O2-C6-Rh1	178.6(2)	C46-C41-P1	18.15(17)
C2-C1-N1	21.2(2)	C43-C42-41	20.4(2)
C16-C11-C2	19.2(2)	C44-C43-42	20.4(3)
C16-C11-N1	19.5(2)	C45-C44-43	19.7(2)
C3-C2-C1	19.8(2)	C44-C45-46	20.0(2)
C2-C3-C4	21.6(2)	C41-C46-45	20.8(2)
C3-C4-C5	21.8(3)	C4-N1-C11	19.27(18)

C15-C4-C3	17.8(2)	C4-N1-Rh1	25.59(15)
C15-C4-C114	20.4(3)	C11-N1-Rh1	15.1(3)
C4-C15-C16	21.3(2)	C2-O1-Rh1	27.43(15)
C11-C16-C15	20.4(2)	C21-P1-Rh1	15.38(7)
C22-C21-C26	17.7(2)	C31-P1-C21	102.86(10)
C22-C21-P1	19.34(17)	C31-P1-C41	103.22(10)
C26-C21-P1	22.95(18)	C31-P1-Rh1	17.55(7)
C23-C22-C21	21.3(3)	C41-P1-C21	103.66(10)
C24-C23-C22	20.3(3)	C41-P1-Rh1	2.49(7)
C25-C24-C23	19.4(3)	C6-Rh1-N1	93.41(8)
C24-C25-C26	20.7(3)	C6-Rh1-O1	177.3(8)
C21-C26-C25	20.6(3)	C6-Rh1-P1	86.53(7)
C32-C31-C36	18.9(2)	N1-Rh1-P1	179.54(5)
C32-C31-P1	19.28(17)	O1-Rh1-N1	89.33(7)
C36-C31-P1	21.77(17)	O1-Rh1-P1	90.72(5)

Table A.5: Torsion angles (˚) for [Rh(4-CH_3-Phony)(CO)(PPh_3)]

Bond	**Angle**	**Bond**	**Angle**
C1-C2-C3-C4	-173.0(2)	C31-C32-C33-C34	1.4(4)
C1-C2-O1-Rh1	176.98(17)	C32-C31-C36-C35	0.9(3)
C2-C3-C4-C5	176.5(2)	C32-C31-P1-C21	-70.32(19)
C2-C3-C4-N1	-2.5(4)	C32-C31-P1-C41	-177.93(17)
C3-C2-O1-Rh1	-2.1(4)	C32-C31-P1-Rh1	57.62(19)
C3-C4-N1-C11	174.3(2)	C32-C33-C34-C35	-0.6(4)
C3-C4-N1-Rh1	-4.0(3)	C33-C34-C35-C36	0.0(4)
C5-C4-N1-C11	-4.7(3)	C34-C35-C36-C31	-0.1(4)
C5-C4-N1-Rh1	176.99(17)	C36-C31-C32-C33	-1.5(3)
C1-C2-C3-C4	1.1(4)	C36-C31-P1-C21	107.87(19)
C2-C11-C16-C15	-0.9(4)	C36-C31-P1-C41	0.3(2)
C2-C11-N1-C4	89.5(3)	C36-C31-P1-Rh1	-24.19(17)
C2-C11-N1-Rh1	-92.0(2)	C41-C42-C43-C44	0.2(4)
C2-C3-C4-C15	-1.0(4)	C42-C41-C46-C45	-1.3(3)

C2-C3-C4-C17	-179.6(3)	C42-C41-P1-C21	-19.4(2)
C3-C4-C15-C16	-0.1(4)	C42-C41-P1-C31	87.57(19)
C4-C15-C16-C11	1.0(4)	C42-C41-P1-Rh1	-44.74(17)
C16-C11-C2-C3	-0.2(4)	C42-C43-C44-C45	0.1(4)
C16-C11-N1-C4	-95.9(2)	C43-C44-C45-C46	-1.1(4)
C16-C11-N1-Rh1	82.6(2)	C44-C45-C46-C41	1.7(4)
C17-C4-C15-C16	178.6(3)	C46-C41-C42-C43	0.4(3)
C21-C22-C23-C24	2.2(5)	C46-C41-P1-C21	161.35(17)
C22-C21-C26-C25	-1.0(4)	C46-C41-P1-C31	-91.65(18)
C22-C21-P1-C31	173.8(2)	C46-C41-P1-Rh1	36.04(18)
C22-C21-P1-C41	-78.9(2)	N1-C11-C2-C3	174.4(2)
C22-C21-P1-Rh1	44.5(2)	N1-C11-C16-C15	-175.5(2)
C22-C23-C24C25	-2.6(5)	O1-C2-C3-C4	6.0(4)
C23-C24-C25-C26	1.2(5)	P1-C21-C22-C23	179.9(2)
C24-C25-C26-C21	0.6(4)	P1-C21-C26-C25	178.7(2)
C26-C21-C22-C23	-0.4(4)	P1-C31-C32-C33	176.73(18)
C26-C21-P1-C31	-5.8(2)	P1-C31-C36-C35	-177.31(18)
C26-C21-P1-C41	101.4(2)	P1-C41-C42-C43	-178.9(2)
C26-C21-P1-Rh1	-35.3(18)	P1-C41-C46-C45	177.97(18)

B APPENDIX

Table B.1: Atomic coordination ($x10^4$) and equivalent isotropic displacement parameters ($Å^2 \times 10^3$) for [Rh(4-CH_3-Phony)(CO)(PPh_3)]. $U_{(eq)}$ is defined as one third of the trace of the orthogonalized U^{ij} tensor.

Atom	***x***	***y***	***z***	**U(eq)**
C1	3294(2)	3.8(15)	9822(2)	59.0(7)
C2	3234.9(18)	-175.9(1)	8445(2)	41.1(5)
C3	3660(2)	-761.4(2)	8042(2)	49.6(6)
C4	3748.8(18)	-992.6(1)	6784(2)	43.5(5)
C5	4248(3)	-1671.2(3)	6627(3)	68.3(8)
C6	2556.2(19)	319.5(10)	415.9(19)	41.8(5)
C1	364.3(16)	-947.7(9)	4551.8(19)	35.0(4)
C2	2857.1(19)	-354.2(2)	4006(2)	48.8(5)
C3	3021(2)	-1618.6(3)	2807(2)	57.6(6)
C4	3940(2)	-463.2(2)	2188(2)	51.9(6)
C15	4701(2)	-1067.8(2)	2705(2)	54.9(6)
C16	4534.9(18)	-805.6(2)	3897(2)	47.7(5)
C21	594.5(15)	362.9(10)	4839.4(17)	32.1(4)
C22	159.6(17)	856.3(1)	4101.0(18)	39.6(5)
C23	-626.2(19)	993.6(3)	3206(2)	50.1(6)
C24	-968.8(19)	1628.7(15)	3027(2)	55.4(6)
C25	-548(2)	236.4(4)	3748(2)	55.8(6)
C26	225.6(18)	2002.8(1)	4656(2)	43.6(5)
C31	2310.3(16)	1937.5(9)	6246.3(18)	33.8(4)
C32	3216(2)	2027.9(2)	5539(3)	55.2(6)
C33	3744(2)	2627.6(15)	5552(3)	77.3(9)
C34	3383(2)	337.0(3)	6293(3)	66.7(8)
C35	2494(2)	3052.3(2)	7016(3)	61.6(7)

C36	1958(2)	2457.4(1)	6998(2)	49.7(6)
C41	765.1(16)	1090.3(9)	7490.0(17)	32.8(4)
C42	192.7(19)	203.0(1)	8701.5(19)	44.2(5)
C43	577(2)	1088.5(3)	9764(2)	55.6(6)
C44	-443(2)	860.4(4)	9644(2)	59.3(7)
C45	-872(2)	747.4(3)	8463(2)	54.7(6)
C46	-269.7(17)	863.8(1)	7390.9(19)	41.0(5)
F114	4085.1(16)	-172.4(8)	994.1(4)	78.9(5)
N1	3434.1(3)	-655.6(8)	5777.9(15)	34.4(3)
O1	2768.2(3)	256.3(7)	7733.3(3)	43.7(4)
O2	2570.7(19)	380.0(9)	3026.6(15)	66.5(5)
P1	1585.7(4)	160.6(2)	6069.3(4)	28.96(1)
Rh1	2603.5(2)	239.2(2)	5817.3(2)	30.37(6)

Table B.2: Anisotropic displacement parameters ($Å^2×10^3$) for [Rh(4-CH_3-Phony)(CO)(PPh_3)]. The anisotropic displacement factor exponent takes the form $2\pi^2[h^2a^{*2}U_1+...+2hka×b×U_2]$

Atom	**U_1**	**U_{22}**	**U_{33}**	**U_{23}**	**U_3**	**U_2**
C1	71.6(18)	67.7(16)	37.7(1)	3.5(1)	-3.0(1)	7.8(4)
C2	39.9(2)	46.7(3)	36.7(10)	5.8(9)	-1.1(9)	-2.6(9)
C3	58.7(15)	47.6(3)	42.4(1)	8.3(10)	-8(1)	9.7(1)
C4	42.4(2)	37.3(1)	50.7(2)	3.1(9)	-3.5(10)	5.3(9)
C5	90(2)	50.3(15)	64.5(16)	2.0(2)	-8.6(15)	29.7(15)
C6	56.7(4)	28.8(1)	39.9(1)	-0.1(8)	5.6(10)	8.6(9)
C1	34.8(10)	27.5(9)	42.7(10)	-1.9(8)	0.8(8)	4.2(8)
C2	38.3(2)	48.8(3)	59.4(3)	-1.6(1)	5.8(10)	-5.1(10)
C3	54.8(15)	53.5(15)	64.5(15)	-20.0(2)	-4.8(2)	-3.4(2)
C4	68.2(17)	43.9(3)	43.7(2)	-5.8(10)	5.4(1)	16.3(2)
C15	51.9(15)	52.6(4)	60.6(4)	1.3(2)	21.8(2)	2.2(2)
C16	40.5(2)	44.3(3)	58.4(3)	-7.5(10)	7.3(10)	-5.2(10)
C21	32.2(10)	34.2(10)	30.0(9)	3.6(7)	2.9(7)	-3.8(8)
C22	47.6(2)	38.7(1)	32.5(9)	2.4(8)	0.8(9)	-8.1(9)

C23	49.2(4)	65.2(16)	35.8(10)	0.9(10)	-3.9(10)	-19.1(2)
C24	41.3(3)	80.0(19)	44.8(2)	4.4(2)	-1(1)	-5.0(3)
C25	47.1(4)	55.0(15)	65.3(15)	17.0(2)	-8.3(2)	7.6(2)
C26	42.6(2)	38.9(2)	49.3(2)	1.2(9)	-5(1)	0.7(9)
C31	34.7(10)	28.4(9)	38.2(10)	0.4(8)	-4.6(8)	-0.9(8)
C32	47.0(4)	38.6(2)	80.1(17)	-4.1(2)	17.0(2)	-4.7(10)
C33	53.8(17)	55.5(17)	23(3)	4.9(17)	22.5(17)	-17.3(4)
C34	68.7(18)	36.4(3)	95(2)	6.5(3)	-22.4(16)	-18.4(3)
C35	79(2)	35.8(3)	69.8(16)	-3.9(1)	-1.7(15)	-5.2(3)
C36	59.3(15)	37.6(2)	52.2(2)	-1.5(10)	6.0(1)	-5.8(1)
C41	40.1(1)	27.7(9)	30.5(9)	-0.6(7)	3.8(8)	2.7(8)
C42	47.5(3)	48.4(3)	36.5(10)	-4.0(9)	-1.6(9)	-0.7(10)
C43	72.3(18)	65.9(17)	28.8(10)	-5.1(10)	1.8(10)	2.5(4)
C44	69.1(18)	71.5(17)	37.7(1)	2.0(1)	17.6(1)	-7.2(4)
C45	52.3(4)	64.9(16)	47.2(2)	-0.3(1)	1.8(1)	-4.7(2)
C46	44.1(2)	44.3(2)	34.7(10)	-1.4(8)	3.9(9)	-6.8(10)
F114	4.6(15)	71.8(1)	50.3(8)	-16.1(8)	2.2(9)	19.1(10)
N1	33.3(9)	29.3(8)	40.6(8)	-1.9(7)	1.0(7)	2.0(7)
O1	53.0(9)	44.5(9)	33.5(7)	-0.6(6)	-1.6(7)	9.4(7)
O2	2.0(17)	52.8(10)	34.9(8)	4.0(7)	1.9(9)	22(1)
P1	32.8(3)	25.5(2)	28.6(2)	-1.57(17)	1.19(18)	-0.4(19)
Rh1	34.66(9)	26.3(9)	30.32(8)	-0.26(5)	2.03(6)	0.99(6)

Table B.3: Bond distances (Å) for [Rh(4-CH_3-Phony)(CO)(PPh_3)]

Bond	**Length**	**Bond**	**Length**
C1-C2	1.502(3)	C23-C24	1.362(4)
C2-C3	1.363(3)	C24-C25	1.377(4)
C2-O1	1.287(3)	C25-C26	1.383(3)
C3-C4	1.41(3)	C31-C32	1.374(3)
C4-C5	1.52(3)	C31-C36	1.387(3)
C4-N1	1.317(3)	C31-P1	1.818(2)

C6-O2	1.155(3)	C32-C33	1.377(4)
C6-Rh1	1.801(2)	C33-C34	1.368(4)
C1-C2	1.376(3)	C34-C35	1.364(4)
C11-C16	1.378(3)	C35-C36	1.373(3)
C11-N1	1.439(3)	C41-C42	1.400(3)
C2-C3	1.387(3)	C41-C46	1.377(3)
C3-C4	1.362(4)	C41-P1	1.827(2)
C4-C15	1.354(4)	C42-C43	1.383(3)
C4-F114	1.368(3)	C43-C44	1.363(4)
C15-C16	1.380(3)	C44-C45	1.372(3)
C21-C22	1.392(3)	C45-C46	1.383(3)
C21-C26	1.382(3)	N1-Rh1	2.0818(16)
C21-P1	1.835(2)	O1-Rh1	2.0283(17)
C22-C23	1.387(3)	P1-Rh1	2.2684(7)

Table B.4: Bond angles (˚) for [Rh(4-CH_3-Phony)(CO)(PPh_3)]

Bond	Angle	Bond	Angle
C3-C2-C1	20.3(2)	C31-C32-C33	20.6(2)
O1-C2-C1	4.2(2)	C34-C33-C32	20.2(3)
O1-C2-C3	25.5(2)	C35-C34-C33	19.9(2)
C2-C3-C4	27.7(2)	C34-C35C36	20.1(2)
C3-C4-C5	15.9(2)	C35-C36-C31	20.6(2)
N1-C4-C3	24.2(2)	C42-C41-P1	21.38(16)
N1-C4-C5	20.0(2)	C46-C41-C42	18.50(19)
O2-C6-Rh1	177.1(2)	C46-C41-P1	19.85(4)
C2-C11-C16	19.4(2)	C43-C42-C41	20.0(2)
C2-C11-N1	20.47(19)	C44-C43-C42	20.5(2)
C16-C11-N1	20.09(18)	C43-C44-C45	20.1(2)
C11-C2-C3	20.2(2)	C44-C45-C46	20.0(2)
C4-C3-C2	18.6(2)	C41-C46-C45	20.8(2)
C3-C4-F14	18.3(2)	C4-N1-C11	17.64(17)

C15-C4-C3	22.5(2)	C4-N1-Rh1	25.27(4)
C15-C4-F114	19.2(2)	C11-N1-Rh1	16.96(2)
C4-C15-C16	18.7(2)	C2-O1-Rh1	27.68(4)
C11-C16-C15	20.5(2)	C21-P1-Rh1	18.51(7)
C22-C21-P1	19.50(16)	C31-P1-C21	102.49(9)
C26-C21-C22	18.43(19)	C31-P1-C41	105.42(9)
C26-C21-P1	22.01(15)	C31-P1-Rh1	15.84(7)
C23-C22-C21	20.5(2)	C41-P1-C21	102.37(9)
C24-C23-C22	20.2(2)	C41-P1-Rh1	10.61(6)
C23-C24-C25	20.1(2)	C6-Rh1-N1	94.08(8)
C24-C25-C26	20.1(2)	C6-Rh1-O1	172.71(8)
C21-C26-C25	20.7(2)	C6-Rh1-P1	91.61(7)
C32-C31-C36	18.5(2)	N1-Rh1-P1	172.83(5)
C32-C31-P1	18.16(16)	O1-Rh1-N1	89.26(6)
C36-C31-P1	23.25(17)	O1-Rh1-P1	85.59(4)

Table B.5: Torsion angles (˚) for [Rh(4-CH_3-Phony)(CO)(PPh_3)]

Bond	**Angle**	**Bond**	**Angle**
C1-C2-C3-C4	-174.7(2)	C32-C31-C36-C35	1.1(3)
C1-C2-O1-Rh1	175.24(16)	C32-C31-P1-C21	-92.84(19)
C2-C3-C4-C5	-179.2(3)	C32-C31-P1-C41	160.38(18)
C2-C3-C4-N1	1.2(4)	C32-C31-P1-Rh1	37.7(2)
C3-C2-O1-Rh1	-4.3(3)	C32-C33-C34-C35	-0.4(5)
C3-C4-N1-C11	177.7(2)	C33-C34C35-C36	-0.2(4)
C3-C4-N1-Rh1	-6.6(3)	C34-C35-C36-C31	-0.2(4)
C5-C4-N1-C11	-1.9(3)	C36-C31-C32-C33	-1.7(4)
C5-C4-N1-Rh1	173.77(19)	C36-C31-P1-C21	83.0(2)
C11-C2-C3-C4	-0.4(4)	C36-C31-P1-C41	-23.8(2)
C2-C11-C16-C15	-0.1(3)	C36-C31-P1-Rh1	-46.39(17)
C2-C11-N1-C4	89.7(3)	C41-C42-C43-C44	0.6(4)
C2-C11-N1-Rh1	-86.3(2)	C42-C41-C46-C45	-0.3(3)

C2-C3-C4-C15	0.8(4)	C42-C41-P1-C21	-154.04(17)
C2-C3-C4-F4	-178.4(2)	C42-C41-P1-C31	-47.17(19)
C3-C4-C15-C16	-0.8(4)	C42-C41-P1-Rh1	78.76(17)
C4-C15-C16-C11	0.4(4)	C42-C43-C44-C45	-0.6(4)
C16-C11-C2-C3	0.1(4)	C43-C44-C45-C46	0.1(4)
C16-C11-N1-C4	-92.3(2)	C44-C45-C46-C41	0.3(4)
C16-C11-N1-Rh1	91.7(2)	C46-C41-C42-C43	-0.2(3)
C21-C22-C23-C24	1.0(3)	C46-C41-P1-C21	31.97(18)
C22-C21-C26-C25	-0.8(3)	C46-C41-P1-C31	38.84(17)
C22-C21-P1-C31	155.80(16)	C46-C41-P1-Rh1	-95.23(17)
C22-C21-P1-C41	-95.09(17)	F4-C4-C15-C16	178.4(2)
C22-C21-P1-Rh1	26.87(18)	N1-C11-C2-C3	178.1(2)
C22-C23-C24-C25	-1.0(4)	N1-C11-C16-C15	-178.1(2)
C23-C24-C25-C26	0.1(4)	O1-C2-C3-C4	4.9(4)
C24-C25-C26-C21	0.8(4)	P1-C21-C22-C23	177.04(16)
C26-C21-C22-C23	-0.1(3)	P1-C21-C26-C25	-177.86(18)
C26-C21-P1-C31	-27.15(19)	P1-C31-C32-C33	174.4(2)
C26-C21-P1-C41	81.96(18)	P1-C31-C36-C35	-174.7(2)
C26-C21-P1-Rh1	-156.08(15)	P1-C41-C42-C43	-174.24(18)
C31-C32-C33-C34	1.4(5)	P1-C41-C46-C45	173.89(18)